

Fall 12-2016

Effect of Slot Span on Wing Performance

Juan F. Granizo
Embry-Riddle Aeronautical University

Follow this and additional works at: <https://commons.erau.edu/edt>



Part of the [Aerodynamics and Fluid Mechanics Commons](#)

Scholarly Commons Citation

Granizo, Juan F., "Effect of Slot Span on Wing Performance" (2016). *Doctoral Dissertations and Master's Theses*. 301.

<https://commons.erau.edu/edt/301>

This Thesis - Open Access is brought to you for free and open access by Scholarly Commons. It has been accepted for inclusion in Doctoral Dissertations and Master's Theses by an authorized administrator of Scholarly Commons. For more information, please contact commons@erau.edu.

EFFECT OF SLOT SPAN ON WING PERFORMANCE

A Thesis

Submitted to the Faculty

of

Embry-Riddle Aeronautical University

by

Juan F Granizo

In Partial Fulfillment of the

Requirements for the Degree

of

Master of Science in Aerospace Engineering

December 2016

Embry-Riddle Aeronautical University

Daytona Beach, Florida

EFFECT OF SLOT SPAN ON WING PERFORMANCE

by

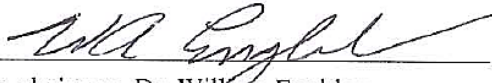
Juan F Granizo

A Thesis prepared under the direction of the candidate's committee chairman, prof. Snorri Gudmundsson, and the candidate's committee co-chairman, Dr. William Engblom, Department of Aerospace and Mechanical Engineering, and has been approved by the members of the thesis committee. It was submitted to the School of Graduate Studies and Research and was accepted in partial fulfilment of the requirements for the degree of Master of Science in Aerospace Engineering.

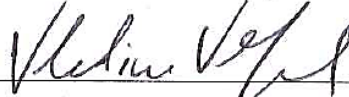
THESIS COMMITTEE



Chairman, Prof. Snorri Gudmundsson



Co-chairman, Dr. William Engblom



Member, Dr. Vladimir Golubev



Graduate Program Coordinator, Dr. Magdy Attia

12-5-2016

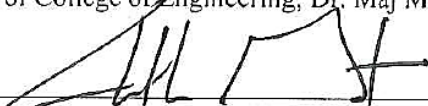
Date



Dean of College of Engineering, Dr. Maj Mirmirani

12/2/2016

Date



Vice Chancellor, Academic Support, Dr. Christopher Grant

12/2/16

Date

Acknowledgements

First and foremost, I thank God for being the source of my energy, knowledge, patience, and blessings that have allowed me to get to this point in my life. I recognize that the goals that I have achieved are because of Him and the people that He has put in my life.

Second, I would like to thank my family for being the source of my inspiration. I am who I am because of them and the values that they have taught me. To my sister and brother who, by their admiration, inspire me to go farther in life. To my father who has never neglected his infinite support and love. And especially to my mother who, through her prayers, has always been by my side.

Third, I am very grateful with my committee chair, Prof. Snorri Gudmundsson, which by his knowledge, guidance, patience, and support made it possible for me to finished this thesis research successfully. He gave me the most valuable advice that a professional engineer could receive, “It is not about being theoretical, it is about being practical.”

Fourth, I would like to extend my gratitude to my committee co-chair, Dr. William Engblom, whose experience and knowledge helped me to performed a successful CFD study. The experience that he shared with me along this process is invaluable.

Finally, I want to express my eternal gratitude to all my friends who support me. They are my refuge in times of adversity.

“Have I not commanded you? Be strong and courageous. Do not be frightened, and do not be dismayed, for the Lord your God is with you wherever you go”

-Joshua 1:9

Table of Contents

Acknowledgements	iii
Table of Contents	v
List of Tables	viii
List of Figures	ix
Symbols	xiii
Abstract	xiv
I. Introduction	1
1.1. Slot Geometry	2
1.2. Slot Position	6
1.3. Stability and Control	11
1.4. Computational Fluid Dynamics – CFD.....	15
II. Review of the Relevant Literature	17
2.1. Fixed Wing Aerodynamic Characteristics	17
2.1.1. Airfoil Theory	17
2.1.2. Finite Wing Theory.....	23
2.2. The Slat Effect.....	31
2.3. Low-Drag Fixed Slot.....	33
2.3.1. The Best Slot Position.....	34

2.3.2.	Effect of the Slot Shape	36
2.3.3.	Effect of the Fix Wing Shape.....	37
2.3.4.	Effect of Moving the Slot Farther Back.....	38
2.4.	Boundary Layer and Flow Separation.....	39
2.4.1.	Reynolds Number	39
2.4.2.	Boundary Layer Transition.....	41
2.4.3.	Flow Separation	42
III.	Methodology	43
3.1.	The Clark – Y Airfoil.....	43
3.2.	Viscous Model Selection.....	45
3.3.	SST Transition.....	47
3.3.1.	Domain Dimension	47
3.3.2.	Mesh Resolution	49
3.3.3.	Solution Convergence.....	51
3.3.4.	Grid Independence	52
3.4.	Plain Wing.....	53
3.5.	Full – Slotted Wing	55
3.6.	Partially – Slotted Wings.....	57
IV.	Results.....	59
4.1.	2-D Plain Airfoil Analysis.....	59

4.2.	Grid Independence Analysis	62
4.3.	Plain Wing Analysis.....	65
4.4.	Full – Slotted Wing Analysis	67
4.5.	Partially – Slotted Wings Analysis.....	69
V.	Analysis	72
5.1.	CFD Prediction.....	72
5.2.	Wing Properties Estimation	73
5.2.1.	Data Trend	74
5.2.2.	Transformation from 2D to 3D.....	77
5.3.	Lift Comparison	81
5.3.1.	Maximum Lift Coefficient.....	81
5.3.2.	Stall Angle	85
5.3.3.	Lift Curve Slope.....	87
5.3.4.	Lift Coefficient at Zero AOA	88
5.3.5.	Angle of Attack at Zero Lift	89
5.4.	Drag Comparison	90
VI.	Validation	91
VII.	Conclusion	95
VIII.	Opportunity for Future Work	97
	References	98

List of Tables

Table 2. 1. Aerodynamic coefficients for 2-D and 3-D bodies.....	20
Table 3. 1. Clark-Y airfoil profile and ordinates [33].	44
Table 3. 2. Number of cells for each mesh density	53
Table 5. 1. Properties form the lift curves of the plain and slotted airfoil, and the plain and full-slotted wing.	77
Table 5. 2. Three-dimensional coefficient estimations for the plain wing.....	78
Table 5. 3. Three-dimensional coefficient estimation for the full-slotted wing.....	78

List of Figures

Figure 1. 1. Zenith STOL series.....	1
Figure 1. 2. Slot geometric parameters.	3
Figure 1. 3. Slot geometry design.	4
Figure 1. 4. Influence of the slot cut-off in the wing performance.	5
Figure 1. 5. Slot position parameters.	6
Figure 1. 6. Lift and drag coefficients for a slotted wing – Variable depth.	8
Figure 1. 7. Lift and drag coefficients for a slotted wing – Variable gap.	9
Figure 1. 8. Lift and drag coefficients for a slotted wing – Variable width.....	10
Figure 1. 9. Use of a slot in combination with a flap.	11
Figure 1. 10. Leading edge slats and flap deflection on an Airbus A310-300.....	12
Figure 1. 11. Rolling moment coefficients of a Clark-Y slotted wing.....	14
Figure 1. 12. Flow separation over the Clark-Y wing.	15
Figure 2. 1. Lift and drag as components of the resultant force R.....	18
Figure 2. 2. Airfoil terminology representation.	19
Figure 2. 3. 2-D lift coefficient curve for the Clark-Y with its terminology.	21
Figure 2. 4. Flow stream-lines around the Clark-Y airfoil at different angles of attack..	22
Figure 2. 5. Drag polar for the Clark-Y with its terminology.....	23
Figure 2. 6. Airflow direction around the wing and wing-tip vortex.....	24
Figure 2. 7. Velocity components of the plane perpendicular to the freestream flow.	25
Figure 2. 8. Representation of the lift orientation with downwash effects.	26
Figure 2. 9. Comparison of 2-D and 3-D lift curve.....	27
Figure 2. 10. Correction factor for the wing stall angle estimation.	29

Figure 2. 11. Flow Separation over a wing by increasing the angle of attack.	30
Figure 2. 12. Stall progression comparison between two different wings.	31
Figure 2. 13. Simplification of a slat by a point-vortex.	32
Figure 2. 14. Velocity distributions over an airfoil alone and airfoil with vortex.	33
Figure 2. 15. Effect of the slot gap on the maximum lift coefficient and the angle where this is obtained for a given slot depth.	35
Figure 2. 16. Changes in the slot geometry.....	36
Figure 2. 17. Changes in the shape of the main wing.	37
Figure 2. 18. Changes in the shape of the slot.	38
Figure 2. 19. Boundary layer visualization.	39
Figure 2. 20. Laminar, transition, and turbulent phases of a free shear flow.....	40
Figure 2. 21. Scaled sections of the boundary layer in an airfoil.....	41
Figure 2. 22. Boundary layer transition from laminar to separated flow.	42
Figure 3. 1. Clark – Y airfoil.....	45
Figure 3. 2. Two-dimensional C-Grid boundary conditions.....	46
Figure 3. 3. C-Grid geometrical constrains.....	48
Figure 3. 4. Comparison of results between an incorrectly dimensioned grid (left) and a correctly dimensioned one (right).	48
Figure 3. 5. Mesh density along the surface of the airfoil.	49
Figure 3. 6. Y+ distribution along the Clark-Y airfoil surface.	50
Figure 3. 7. Convergence history of the lift coefficient for the Clark-Y airfoil.....	51
Figure 3. 8. Grid distribution at the wing-tip.	54
Figure 3. 9. Three dimensional grid. Top view dimensioning.	54

Figure 3. 10. Three-dimensional grid boundary conditions.....	54
Figure 3. 11. Slot geometry (left) and position (right) in reference with the plain Clark-Y airfoil.....	55
Figure 3. 12. Grid distribution at the tip of the slotted Clark-Y wing.	56
Figure 3. 13. Grid over the full-slotted Clark-Y wing.	57
Figure 3. 14. Slot-span ratio definition.	58
Figure 3. 15. Grid over the 50% tip-slotted Clark-Y wing.	58
Figure 4. 1. 2-D lift coefficient versus angle of attack of the Clark-Y airfoil	59
Figure 4. 2. 2-D drag coefficient versus lift coefficient of the Clark-Y airfoil.....	60
Figure 4. 3. 2-D pitching moment coefficient versus angle of attack of the Clark-Y airfoil.	61
Figure 4. 4. 2-D lift coefficient versus AoA. Grid comparison for the Clark-Y airfoil...	62
Figure 4. 5. 2-D drag coefficient versus lift coefficient grid comparison for the Clark-Y airfoil.....	63
Figure 4. 6. 2-D pitching moment coefficient versus AoA. Grid comparison for the Clark-Y airfoil.....	64
Figure 4. 7. Clark-Y wing lift coefficient versus angle of attack.....	65
Figure 4. 8. Clark-Y wing drag coefficient versus angle of attack	66
Figure 4. 9. Full-span slotted wing. Lift coefficient versus angle of attack.....	67
Figure 4. 10. Full-span slotted wing. Drag coefficient versus angle of attack.....	68
Figure 4. 11. Tip-slotted wing, $0.5b_s$. Lift coefficient versus angle of attack.	69
Figure 4. 12. Tip-slotted wing, $0.5b_s$. Drag coefficient versus angle of attack.	70
Figure 4. 13. Lift curves for all slotted wings	71

Figure 5. 1. Trendline for the linear region of the lift coefficient for the two-dimensional airfoils.	75
Figure 5. 2. Lift curve trending curve for all angles of attack.	76
Figure 5. 3. Three-dimensional coefficient estimation for the plain wing.....	79
Figure 5. 4. Three-dimensional coefficient estimation for the full-slotted wing.	80
Figure 5. 5. CL_{max} for the first peak of all the slotted wings.	82
Figure 5. 6. CL_{max} for the second peak of all the slotted wings.	83
Figure 5. 7. CL_{max} of all slotted wings.	84
Figure 5. 8. Angle of stall for the first peak of all the slotted wings.	85
Figure 5. 9. Angle of stall for the second peak of all slotted wings.....	86
Figure 5. 10. Lift curve slope for the tested models.	87
Figure 5. 11. Lift coefficient at zero angle of attack of all tested models.....	88
Figure 5. 12. Tendency curves for the lift coefficient versus AOA (linear region).....	89
Figure 5. 13. Minimum drag coefficient of all tested models.....	90
Figure 6. 1. Validation of the CL_{max} for the first peak relation.	91
Figure 6. 2. Validation of the CL_{max} for the second peak relation.	92
Figure 6. 3. Validation of the angle of stall for the first peak relation.....	92
Figure 6. 4. Validation of the angle of stall for the second peak relation.	93
Figure 6. 5. Validation of the lift curve slope relation.	93
Figure 6. 6. Validation of the lift at zero AoA relation.....	94
Figure 6. 7. Validation of the minimum drag coefficient relation.	94

Symbols

c	Chord length
b	Wing span
S	Wing reference area
b_S	Slot-span ratio
e	Span efficiency factor for lifting surfaces
AR	Aspect ratio
λ	Taper ratio
Λ_{LE}	Wing sweep at the leading edge
Re	Reynolds number
α	Angle of attack (AoA), deg
α_{ZL}	AoA at zero lift
C_L	Lift coefficient
C_{Lmax}	Maximum lift coefficient
C_{Lo}	Zero angle of attack lift coefficient
C_{La}	Lift curve slope
C_D	Drag coefficient
C_{Dmin}	Minimum drag coefficient

Abstract

Juan F Granizo, MSAE Embry-Riddle Aeronautical University, December 2016. Effect of Slot Span on the Wing Performance.

This report presents new numerically-derived correlations to estimate the aerodynamic properties of a three-dimensional wing that features a partial to full span fixed slot. Fixed slots have been thoroughly studied in the past with regards to their operation and the relation between slot geometry and wing performance. There have also been many studies on the advantages and disadvantages of tip-slotted wings and the comparison between these and full-slotted wings. Up to this point however, a study on the effects of slot span on wing performance has not been performed. Effect of slot span on wing performance is evaluated in an attempt to obtain a relation between the slot span and the wing aerodynamic coefficients. The study is performed by the use of detailed ANSYS – Fluent models which include laminar-to-turbulent transitional flow effects. Convenient mathematical formulations are developed for use in aircraft conceptual design. First, a two-dimensional CFD comparison between different viscous models is performed in order to define the most accurate model at the Reynolds number of interest. Second, a three-dimensional study is performed over a plain and a full slotted wing to validate the model against experimental data. Finally, a three-dimensional CFD study of partially-slotted wings with different slot spans is developed in order to develop direct relations between the slot span with the changes in the lift, drag, and pitching moment coefficient.

I. Introduction

The history of aviation presents many solutions to the problem of allowing airplanes to land and take off at slow speeds, reducing runway requirements, and offering slow speed safety. Gustav Lachmann and Sir Handley Page developed a device that offered all of these solutions, the fixed slot. The slot is an extensible leading edge device that offers a solution against the increased risk of stall encountered at low speeds or high angles of attack by reducing the flow circulation around the surface of the main element. This allows the airflow on the surface of the wing to flow more smoothly, which keeps the wing from stalling up to angles beyond the normal stall.



Figure 1. 1. Zenith STOL series.

Figure 1. 1 shows three light General Aviation aircraft that have effectively implemented slots in the leading edge of their wings, taking advantage of its high lift capability. Because the slot is an extension of the leading edge of the wing, it changes its

geometry. This modification produces not only a change in lift, but also an increase in drag. The extra drag is acceptable at low speeds, where the increase of the stall angle and lift is beneficial. But at high speeds, the use of the slot becomes a disadvantage because its drag contribution reduces the cruising speed and increases the fuel consumption.

A fixed slot can be designed with a partial wing span, in order to reduce the drag penalty. In this case, the slot extends from the wing tip to the inboard section of the wing, and it is called a wing tip slot. The purpose of these slots is to prevent flow separation over the surface of the wing where control surface is located. This allows the wing to maintain its roll control capability to higher angles of attack (or lower flying speeds), providing important safety benefits at stall. At the same time, by reducing the span of the slot, the impact of drag on cruise performance is also reduced.

One of the purposes of this thesis is to develop a method to aid in the conceptual development of aircraft by permitting targeted design of slots. This helps with the design of a slot that allows an aircraft to land and take-off at lower speeds, fly at higher angles of attack in maneuvering flight, and reduce the dependency of flaps for lift augmentation; while maintaining a good lift over drag ratio of the whole configuration.

1.1. Slot Geometry

A summary of all the studies performed on slotted wings [3] shows that the geometric characteristics of the system can be divided in two sections, the slot shape/size, and its position. The geometric parameters that defined the slot shape and size are the following:

- 1) Slot chord
- 2) Cut – off
- 3) Maximum thickness
- 4) Angle of cut

All of these parameters are dimensioned as a percentage of the wing chord. The slot chord defines the length of the slot. The cut-off is the measurement from the leading edge of the original airfoil to the cutting line defined by the angle of cut. The lower surface of the slot (as well as the surface on the fixed wing generated by cutting the slot) has a circular geometry that is defined by a cutting ratio. This ratio is defined by the cut-off, slot chord, and maximum thickness parameters. These parameters are represented in Figure 1. 2.

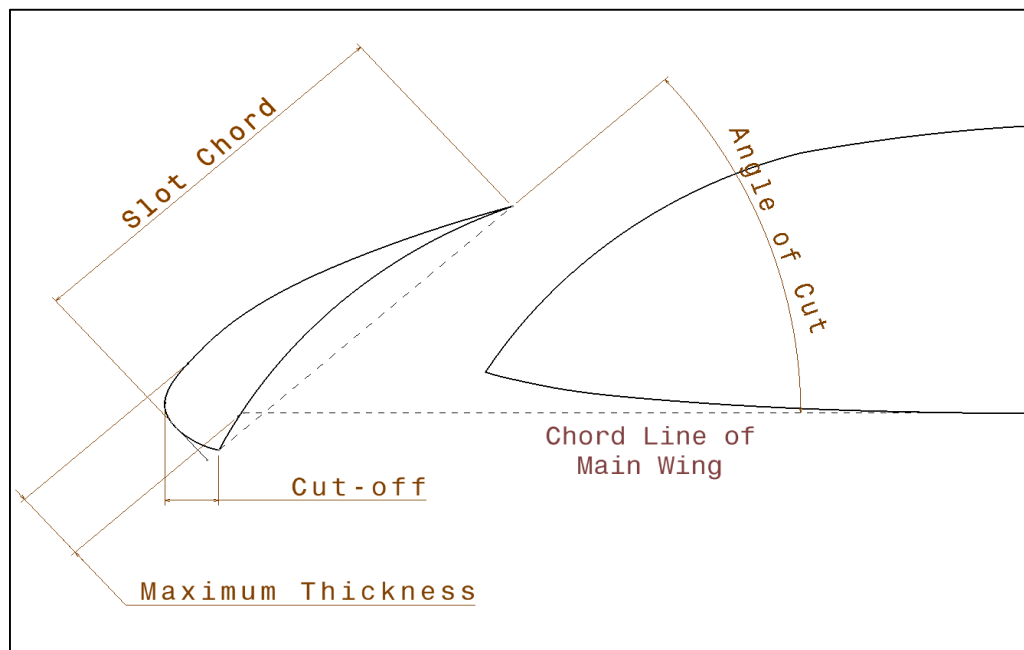


Figure 1. 2. Slot geometric parameters.

Whitman [20] presented a design rule-of-thumb for the geometry of the slot, defining these parameters as follows:

1. Define the angle of stall of the clean airfoil.
2. Identify the flow separation and stagnation points on the plain airfoil for the previously defined angle.
3. The slot cut-off has to be positioned near the stagnation point on the lower surface
4. The slot trailing edge has to be positioned near the separation point on the upper surface
5. The angle of cut has to be parallel to the freestream flow at the defined angle of attack of the first step, see Figure 1. 3.

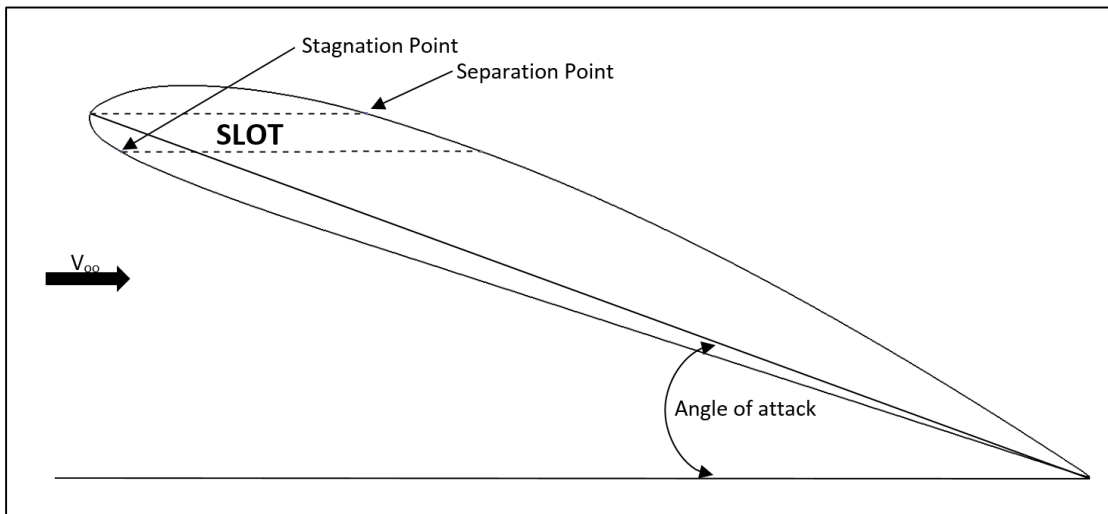


Figure 1. 3. Slot geometry design.

Weick and Shortal [7] studied the effect of multiple slots on a wing. Figure 1. 4 shows the results of the performance of a wing with different slot cut-off's positions. It is seen that the maximum lift coefficient decreases as the cut-off position approaches the trailing edge. Consequently, they concluded that the most efficient cut-off position for a slotted wing is as close to the leading edge as possible.

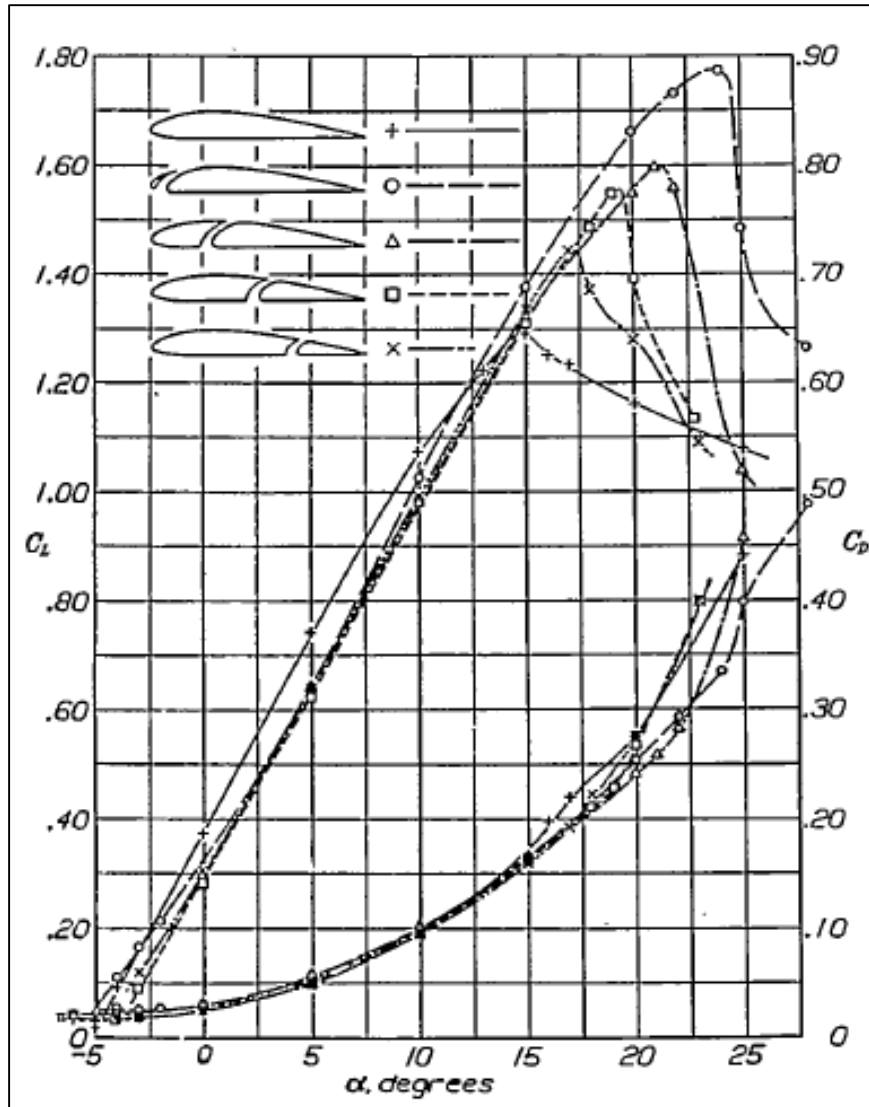


Figure 1. 4. Influence of the slot cut-off in the wing performance.

Adapted from “*The Effect of Multiple Fixed Slots and a Trailing-Edge Flap on the Lift and Drag of a Clark Y Airfoil,*” by Fred E. Weick and Joseph A. Shortal. Report No. 427, N.A.C.A., 1932.

1.2. Slot Position

Wezinger and Shortal [4] studied a wing with a slot located at 100 different locations. They concluded that the shape and size of the slot are not of great consequence in comparison with the location of the slot when it is deployed. The geometric variables that define the slot position are shown in Figure 1. 5 and listed in order of their effectiveness in increasing the lift coefficient:

- 1) Slot gap
- 2) Slot width
- 3) Slot depth

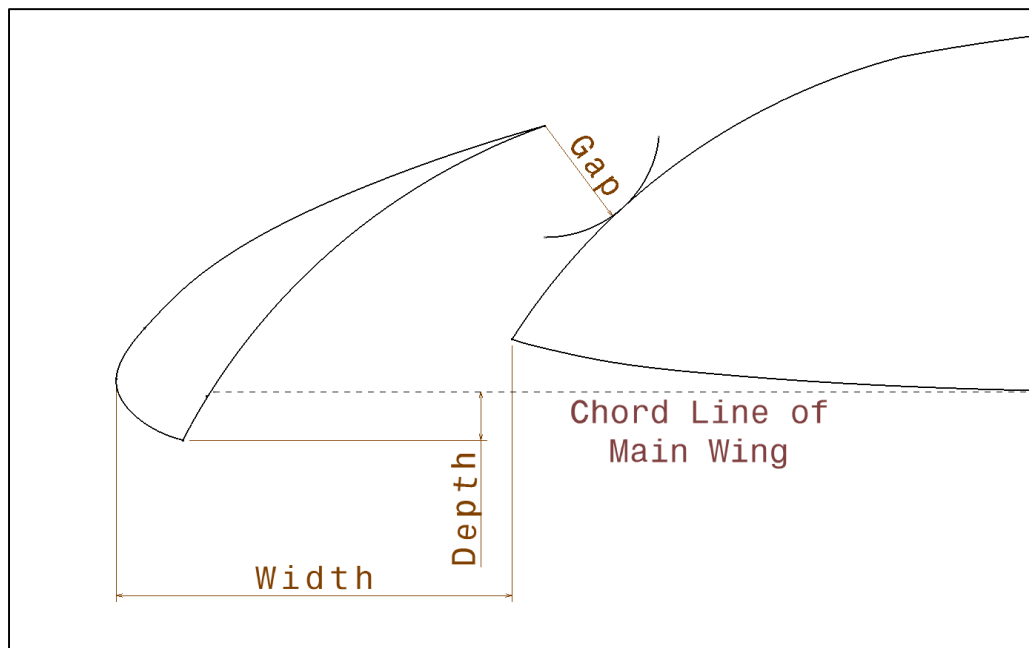


Figure 1. 5. Slot position parameters.

In the same manner as the geometric parameters, the position parameters are given as percentages of the plain chord. The depth of the slot has a positive deflection whenever

it is above the chord line of the plain wing, otherwise it has a negative deflection. In the case of Figure 1. 5, it has a negative depth deflection.

Wenzinger and Shortal [4] studied how the aerodynamic characteristics of the wing depend on each of these parameters. Depending on the airfoil used, the slot has a unique position where it will generate the greatest increase in the maximum lift coefficient. To obtain this increment, the leading edge (*LE*) of the slot has to be below and well forward of the main wing *LE*. Deflecting the slot into a different position will create a smaller increase in the maximum lift coefficient. Also, the slot has a unique position where it will generate the largest increase in the angle of attack range. This position is different than the previously one explained. The *LE* of the slot has to be below but close to the *LE* of the main wing to obtain the largest AoA range. The slot position which generates the minimum increase in the drag coefficient is also unique relative to the aforementioned optimum positions.

Figure 1. 6 to Figure 1. 8 shows how the lift and drag coefficients as a function of the angle of attack reacts on a full-slotted wing model by varying one of the position parameters and keeping the other two fixed. These figures show in common that every slotted wing generates less lift for small angles of attack than the plain wing. Also, a plain wing generates less drag at small angles of attack than a slotted wing. At high angles of attack, a slotted wing generates more lift and less drag than a plain wing.

Wing Lift & Drag Coefficient versus AOA

Clark-Y Wing: AR=6, $\lambda=1$, LE Sweep = 0 [deg]

Slot: 12%Width, 3.5%Gap

Re = 609000, NACA TR 400

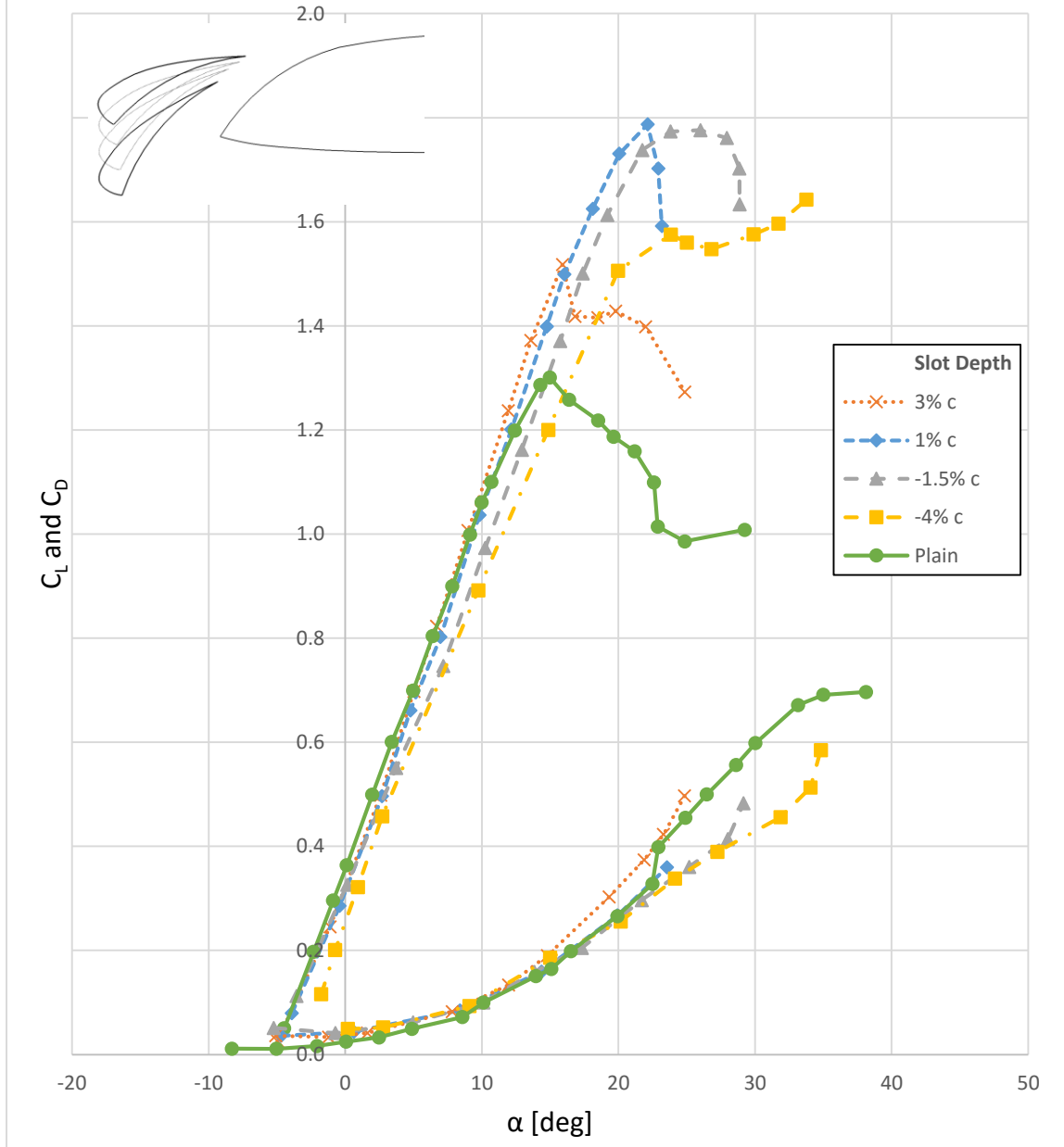


Figure 1. 6. Lift and drag coefficients for a slotted wing – Variable depth.

Wing Lift & Drag Coefficient versus AOA

Clark-Y Wing: AR=6, $\lambda=1$, LE Sweep = 0 [deg]

Slot: 12%Width, -4%Depth

Re = 609000, NACA TR 400

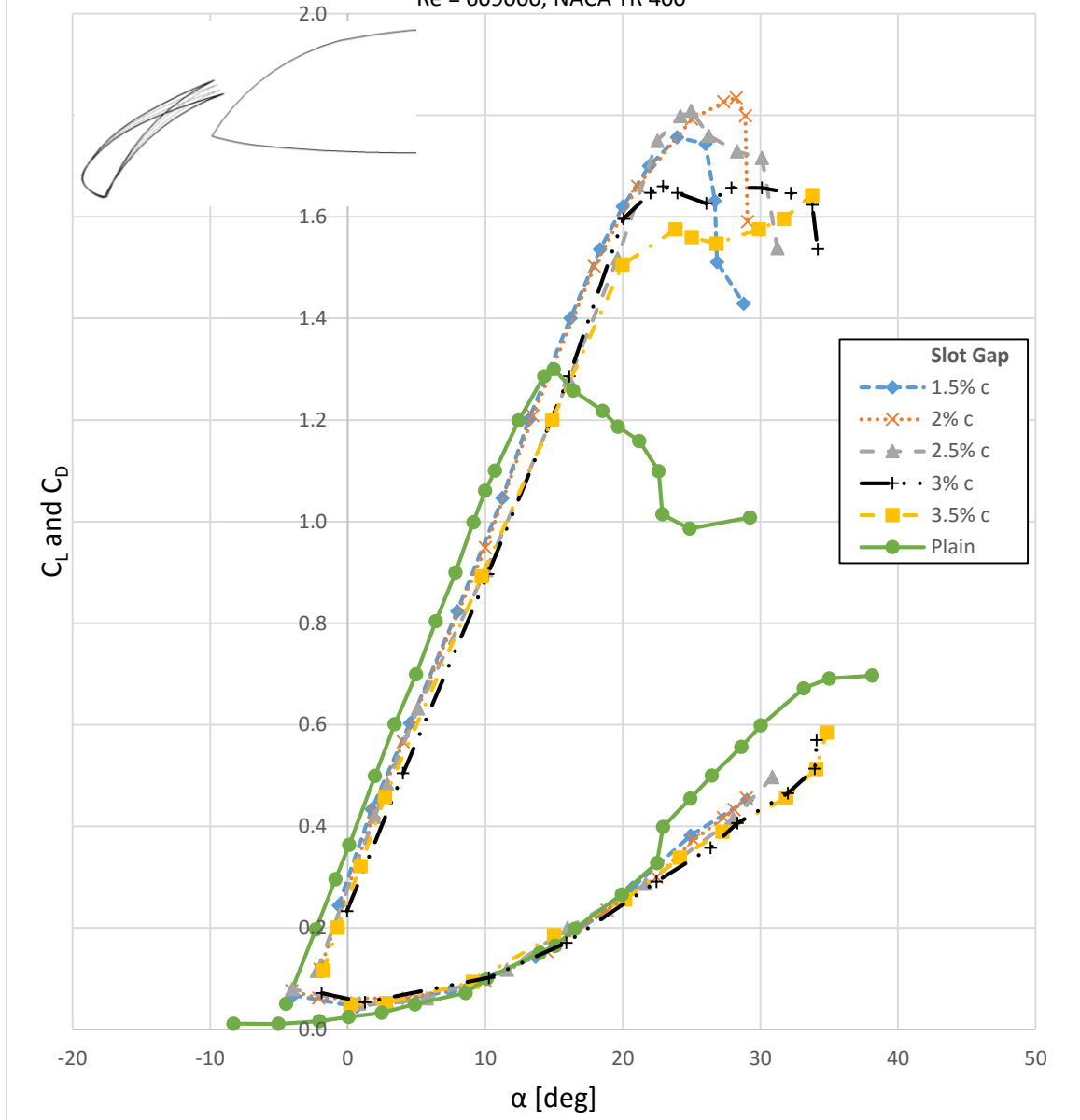


Figure 1. 7. Lift and drag coefficients for a slotted wing – Variable gap.

Wing Lift & Drag Coefficient versus AOA

Clark-Y Wing: AR=6, $\lambda=1$, LE Sweep = 0 [deg]

Slot: 3.5%Gap, -1.5%Depth

Re = 609000, NACA TR 400

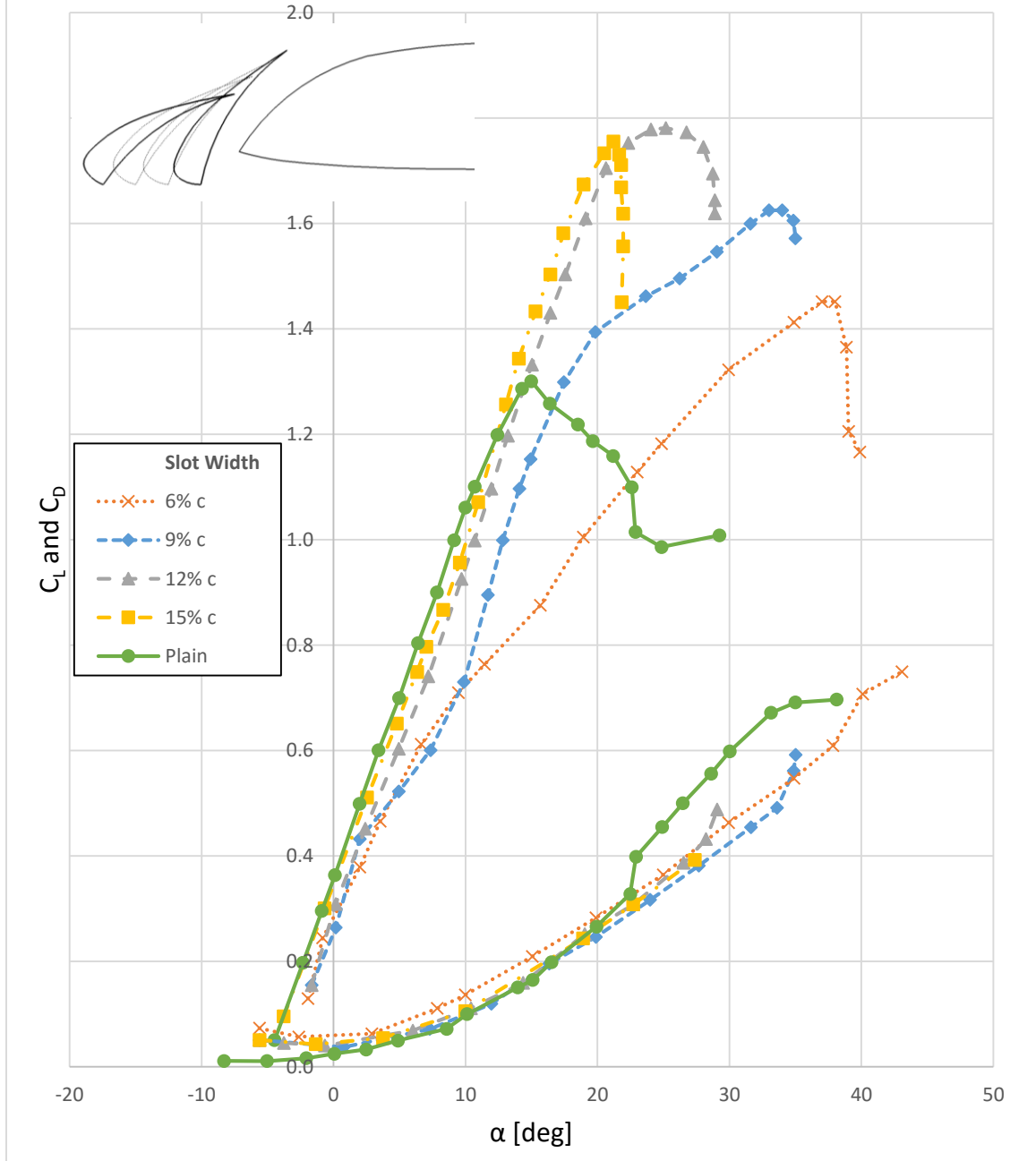


Figure 1. 8. Lift and drag coefficients for a slotted wing – Variable width

1.3. Stability and Control

Slotted wings in use by General Aviation aircraft nowadays offer a great solution to increase the maximum lift coefficient and the corresponding angle of attack. Generally, slotted wings have a limited impact on the longitudinal stability of aircraft due to its slight effects on the lift and pitching moment gradients. Slots have more influence on the lateral stability and control by maintaining the wing controls operational at high angles of attack or low speeds [7].

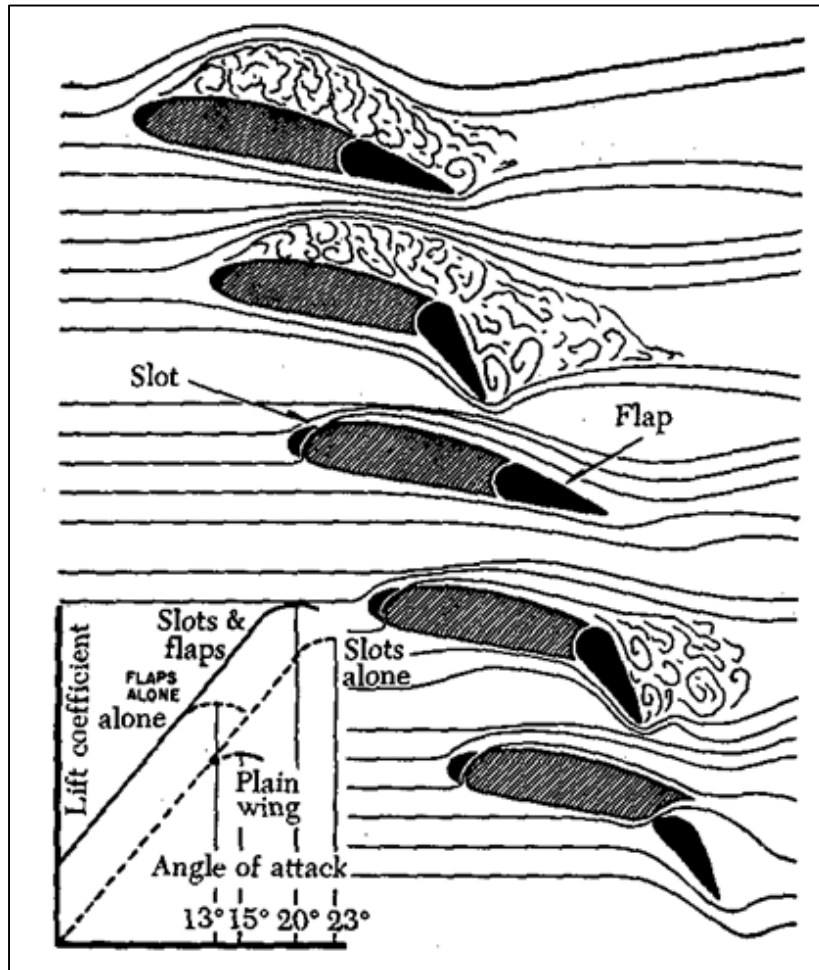


Figure 1. 9. Use of a slot in combination with a flap.
Adapted from “Official Guide to Experimental Aircraft” by Chris Heintz. Retrieved from exp-aircraft.com/library/heintz/airfoils.html

During takeoff and landing, airplanes need to generate more lift in order to compensate the relative low velocity. To generate this high lift, wings need to operate at high angles of attack without stalling. Airplanes use flaps to obtain the necessary increase in lift at a defined angle of attack. But one of the drawbacks in the use of flaps is that it shifts the lift curve in a manner that the airplane will stall at a smaller angle of attack (see Figure 1. 9, flaps alone). Slots can be implemented in conjunction with flaps by obtaining the benefit in the increase of lift, while at the same time it delays the stall by increasing the range of angle of attack (see Figure 1. 9, slot & flaps). Figure 1. 10 shows a commercial aircraft with these two devices activated.



Figure 1. 10. Leading edge slats and flap deflection on an Airbus A310-300.
Photo courtesy of Adrian Pingstone – Public Domain.

The majority of accidents in general aviation at low altitude are not only caused by stalling, but also by spinning [18]. Stalling and spinning count as the major causal factors in aviation accidents, accounting for 61% of the total number of fatalities [30]. These accidents were caused by a combination of a loss in longitudinal or lateral-directional control, spin entry, and ground impact before the airplane could recover from the spinning.

Freid Weick performed various tests on slotted wings in the last century [5-8]. Weick stated that fixed rectangular wings show unstable behavior at high angles of attack by experiencing unstable damping in roll and autorotation [5]. Unstable damping in roll becomes a difficult challenge for a pilot, who has to overcome rapid rolling and yawing motions. Unstable damping in roll also generates high angular rates which could lead to autorotation. This can propel the airplane to higher angles of attack where it could enter into a spinning mode [18]. Weick, by implementing slots at the leading edge of a wing, obtained an improvement in the damping of roll characteristics of the wing at high angles of attack. Slotted wings have an effective aspect ratio smaller than the plain configuration, due to an increase in its effective area. Because of this, slots significantly improve the lateral stability of the wing by delaying the stall on the wing-tips. In addition, the use of slotted wings improves the damping in roll by restricting autorotative moments at high angles of attack, see Figure 1. 11.

The problem of full-slotted wings is that they generate a minimum drag three times larger than the one generated by the plain wing [8]. In order to maintain the maximum speed of the airplane, slotted wings must meet three design guidelines:

1. A defined slot position so that it meets the requirements in lift and drag.
2. Automatic or controlled deployment at high angles of attack.

3. Wing-tip slots instead of full-span slots to reduce the overall drag of the combination.

Partial-span slotted wings need to work in conjunction with aileron and spoilers in order to produce a satisfactory lateral control for the whole angle of attack range. Figure 1.11 shows how a full-slotted wing remains damped at high angles of attack while a plain wing generates autorotative moments.

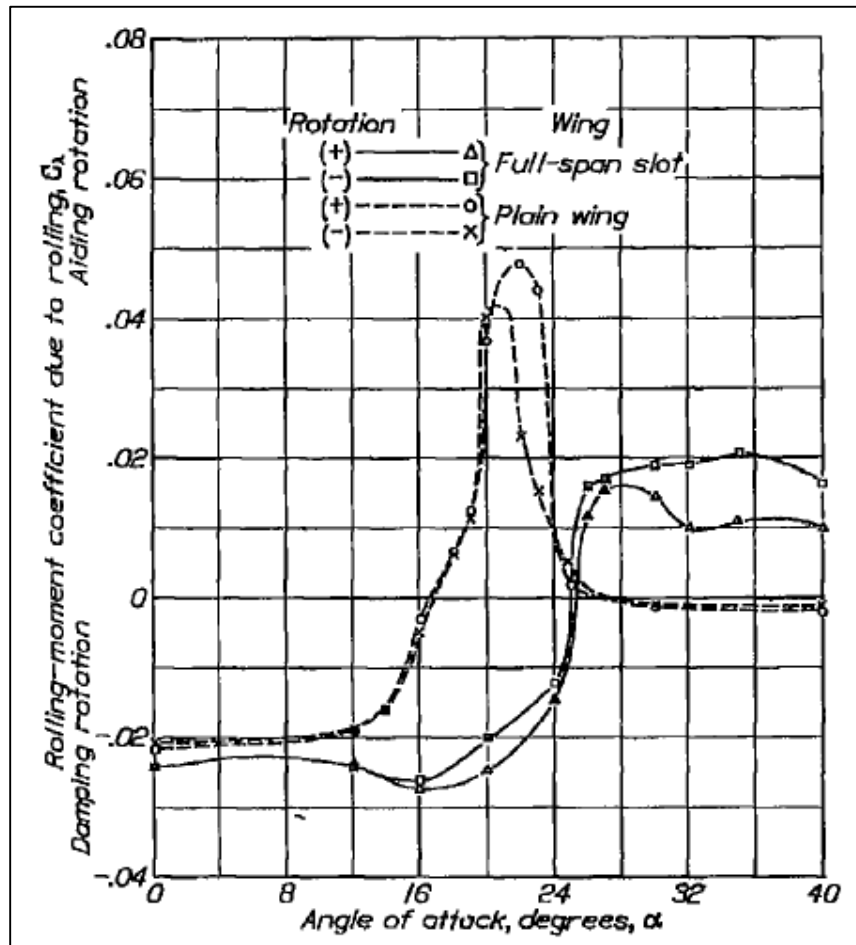


Figure 1.11. Rolling moment coefficients of a Clark-Y slotted wing. Adapted from “*Handley Page Tip and Full-Span Slots with Ailerons and Spoilers*” by Fred E. Weick and Carl J. Wezinger. T.N. No. 443, N.A.C.A., 1933.

1.4. Computational Fluid Dynamics – CFD

Computational fluid dynamics is a division of fluid mechanics that simulates the behavior of fluid flows by implementing numerical analysis and algorithms to solve the Navier-Stokes equations. Because of the amount and complexity of the calculations, computers, or even supercomputers (depending on the level of accuracy that is required and complexity of the model) are needed to solve and analyze the problems that involve the interaction of liquid and gases with surfaces. Figure 1. 12 shows how a CFD software, in this case ANSYS-Fluent, simulates how the flow behaves at a defined angle of attack over a wing. Initial validation of this kind of software is required by wind-tunnel testing, followed by a full-scale testing (flight testing).

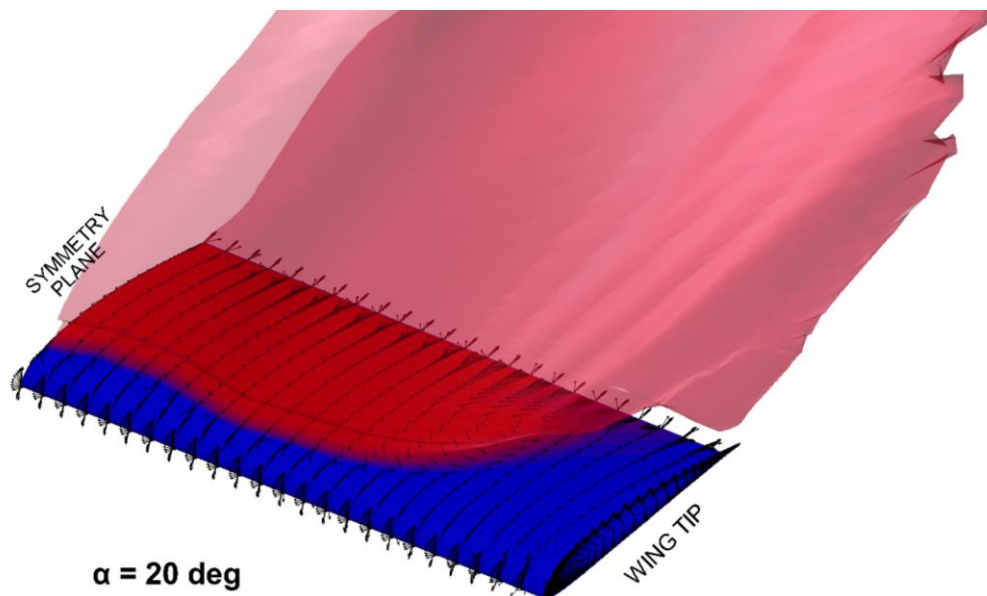


Figure 1. 12. Flow separation over the Clark-Y wing.

The fundamentals of CFD problems are the Navier-Stokes and Euler equations. Because of the advances in the availability and power of commercial softwares that develop schemes and solve the Euler and Navier Stokes equations successfully, computational fluid

dynamics (CFD) works as an important tool to complement, and in some cases even replace experimental methods. An ideal CFD approach takes into consideration the modeling of flow at different ranges of Reynolds number (Re) over simple or complex geometries, while at the same time it is not computationally expensive.

II. Review of the Relevant Literature

2.1. Fixed Wing Aerodynamic Characteristics

Fixed wing aerodynamic characteristics provide an introduction of the basic concepts in the theory of the aerodynamics behind a wing. It concentrates on the forces and reactions that a wing develops while a flow surrounds it. First, a 2-D perspective is represented in order to show a simplified perspective of the fundamental ideas of flow surrounding an airfoil. A 3-D study follows to show the characteristics of flow over a wing, and the effects developed over the wing. For a thorough review, see Anderson [24].

2.1.1. Airfoil Theory

Every object that moves in a fluid creates a pressure field in its surroundings. This pressure field changes the pressure on the surface of the body creating a resultant force, R , that acts on the body. The components of this resultant force are *lift*, L , and *drag*, D . The lift is defined as the component of the resultant force that has the direction normal to the velocity of the fluid. While drag is defined as the component tangent to the velocity of the fluid. See Figure 2. 1 to obtain a graphical representation of these components over an airfoil.

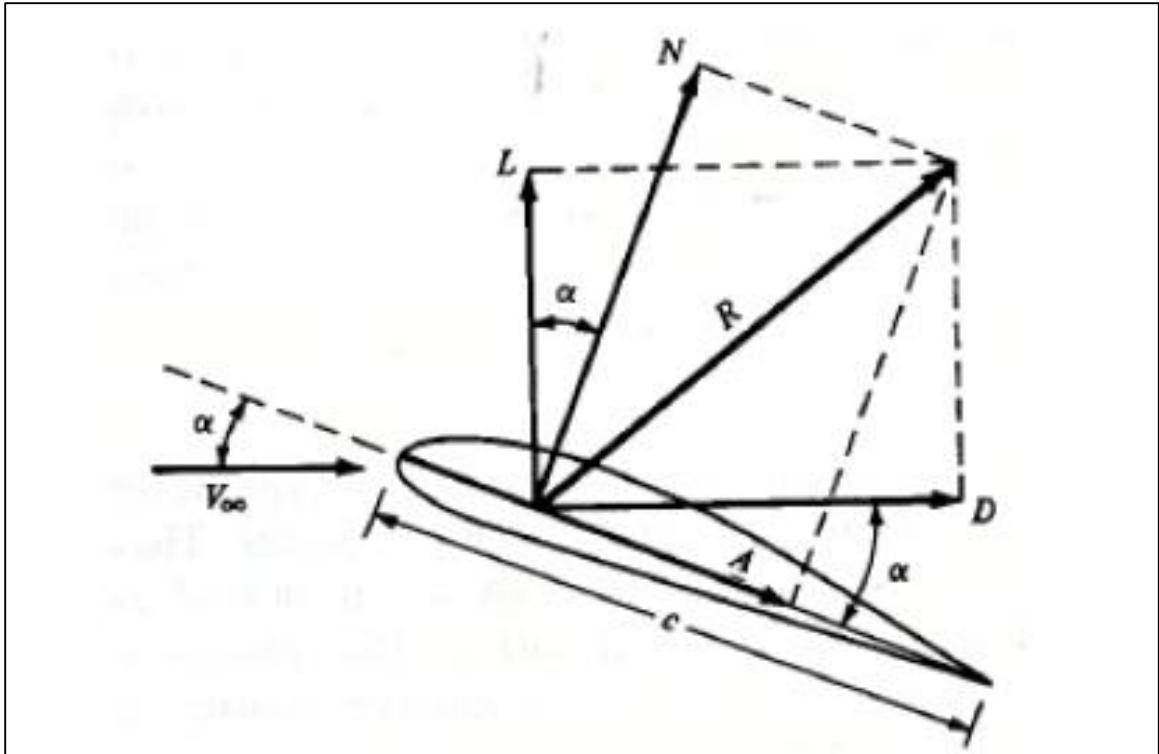


Figure 2. 1. Lift and drag as components of the resultant force R .
Adapted from “Fundamentals of Aerodynamics, 3rd Edition” by Anderson Jr.
Boston, MA: McGraw Hill, 2001.

An airfoil is a geometry that is characterized by generating a resultant force almost perpendicular to the flow direction (see Figure 2. 1.) In other words, this geometry creates a resultant force with a lift component significantly larger than a drag component, far more than other geometric shapes. Because of this, the airfoil shape has a wide range of application possibilities, especially in the aerospace industry with wings, blades of a propeller, rotor, or turbine, and many others.

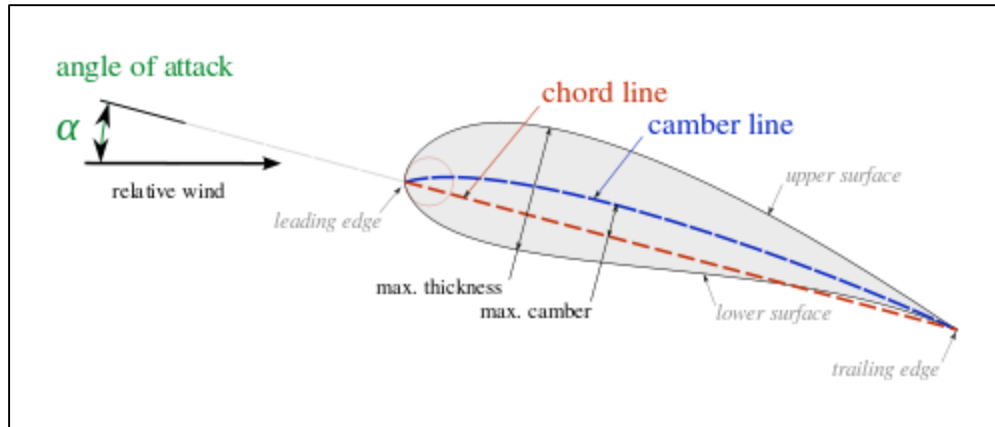


Figure 2. 2. Airfoil terminology representation.

Adapted from “Aerodynamics for Engineering Students, 5th Edition” by Houghton, E.L. Butterworth Heinmann, 2003.

An airfoil’s most forward point is defined as the leading edge, *LE*. This point has the maximum curvature of the shape [8]. The most rearward point on the airfoil is known as the trailing edge, *TE*. The trailing edge is the point of minimum curvature at the rear of the airfoil, or where the upper surface meets the lower surface. The chord line is the straight line that joins the leading edge with the trailing edge. The length of this line is the reference dimension of the airfoil, this is known as the chord, *c*. The camber line is defined by the points located midway between the upper surface and lower surface. The angle of attack, α , is the angle generated between the chord line and the freestream flow direction.

Depending on its geometry, an airfoil will generate a characteristic pressure distribution along its surface. This pressure distribution generates a resultant force that is dependent on the angle of attack. In order to represent the components of the resultant force as non-dimensional parameters, a series of equations were developed by the use of Buckingham’s II theorem [23]. These equations define the aerodynamic coefficients, which are dimensionless quantities that quantify the lift, drag, and the torque generated by

them (pitching moment). Table 2. 1 shows the equations for each one of these coefficients. Whenever a coefficient is identified with a lower case as a subscript, it is referring to a two-dimensional geometry. Three-dimensional geometries are defined with upper case subscripts. An essential quantity in these calculations is the dynamic pressure, q_∞ , which represents the kinetic energy per unit volume of a fluid particle [26]. It is defined in Eq. (2. 1), where ρ_∞ and V_∞ are the freestream density and velocity respectively.

$$q_\infty = \frac{1}{2} \rho_\infty V_\infty^2 \quad (2. 1)$$

Table 2. 1. Aerodynamic coefficients for 2-D and 3-D bodies.

	2-D (per unit Length)	3-D
Lift Coefficient	$C_l = \frac{L'}{q_\infty \cdot c}$	$C_L = \frac{L}{q_\infty \cdot S}$
Drag Coefficient	$C_d = \frac{D'}{q_\infty \cdot c}$	$C_D = \frac{D}{q_\infty \cdot S}$
Pitching Moment Coefficient	$C_m = \frac{M'}{q_\infty \cdot c^2}$	$C_M = \frac{M}{q_\infty \cdot S \cdot c}$

Figure 2. 3 shows a typical curve of the lift coefficient versus the angle of attack for a defined airfoil. For a two-dimensional study, it is called the section lift coefficient. This curve is of great importance because it shows the maximum lift that a defined airfoil produces, and the ranges in the angle of attack where this is effective. It is characterized by two regions, the linear and the non-linear. The linear region is represented by a line equation, where the slope of the line is defined as the lift curve slope, C_{l_α} . The y-intercept of the line represent the zero angle of attack lift coefficient, C_{l_0} . And the x-intercept of the

line represents the angle of attack at zero lift coefficient, α_{ZL} . The equation of the line is defined in Eq. (2. 2), and Eq. (2. 3) shows how to calculate the zero lift angle of attack.

$$C_l = C_{l0} + C_{l\alpha}\alpha \quad (2. 2)$$

$$\alpha_{ZL} = -\frac{C_{l0}}{C_{l\alpha}} \quad (2. 3)$$

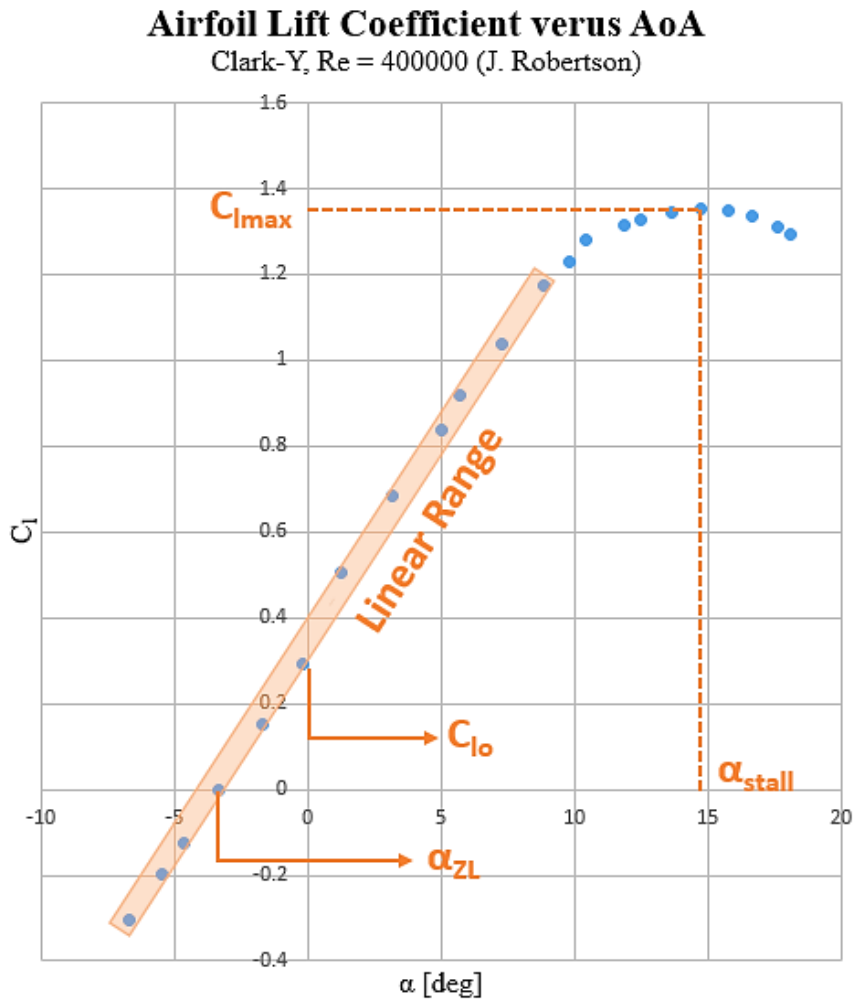


Figure 2. 3. 2-D lift coefficient curve for the Clark-Y with its terminology.

The second region of the curve has a non-linear tendency. This is indicative of flow separation occurring over the body. In this region, the lift coefficient reaches a maximum,

this is known as the maximum lift coefficient, C_{lmax} . This value is of extreme importance because it defines the stalling speed for the airfoil, as well as other characteristics for maneuvering and recovery [23]. The angle of attack where the lift reaches its maximum is known as the stall angle, α_{stall} . After this point the lift coefficient starts to decrease due to flow separation occurring on top of the surface. Figure 2. 4 shows how the flow starts to separate from the upper surface of the airfoil while the angle of attack increases.

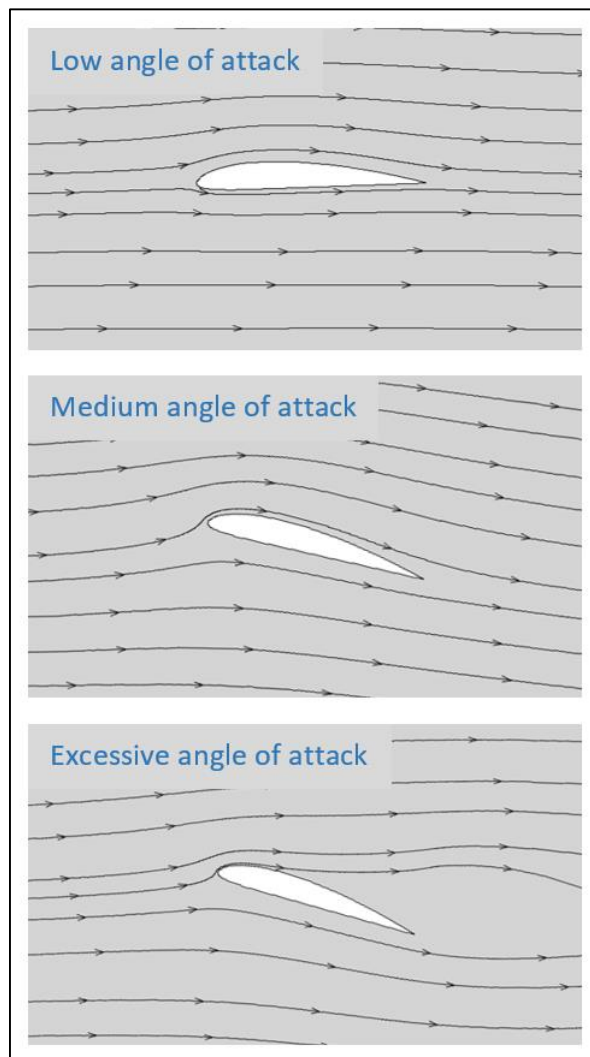


Figure 2. 4. Flow stream-lines around the Clark-Y airfoil at different angles of attack.

Figure 2. 5 shows the drag polar for a defined airfoil. A drag polar shows the drag coefficient for a defined lift coefficient. This helps to understand the drag that an airfoil is going to produce in the range of intended lift coefficient of cruise. The point of lowest drag coefficient is known as minimum drag coefficient, C_{dmin} . This value is vital for the airfoil selection, and should be as low as possible. The lift coefficient corresponding to the C_{dmin} is known as lift coefficient of minimum drag, C_{lmin} ; in the same way, this point impacts the selection of the airfoil.

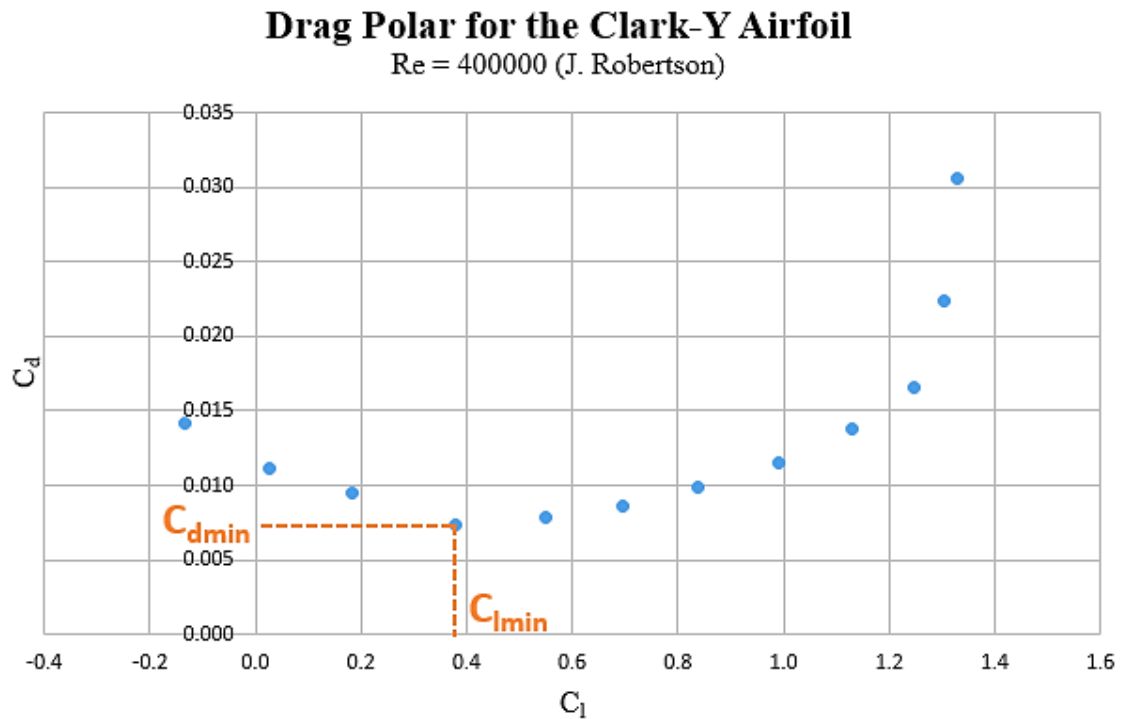


Figure 2. 5. Drag polar for the Clark-Y with its terminology.

2.1.2. Finite Wing Theory

A wing can be defined as an airfoil extrusion whose primary purpose is to generate lift. It needs to be clear that a wing will never produce the same amount of lift or drag as the airfoil in the same conditions because a wing experiences flow in the three dimensions. This is caused by the flow producing a sudden pressure difference at the wing tips. As it

was explained in the Airfoil Theory section, flow around an airfoil produces a difference in pressure between the upper surface and the lower surface. Imagine a wing having the same pressure distribution along its span. At the tip of the wing, the low pressure at the upper surface has to equilibrate with the high pressure at the lower surface. This causes the high pressure on the bottom to wrap around the wing tip to the low pressure of the upper surface, producing a spanwise component of the flow that moves outward on the bottom of the surface and inward in the upper surface [22]. Figure 2. 6 shows the behavior of the airflow around the wing, as well as the representation of a wing-tip vortex. Figure 2. 7 illustrates the wing-tip vortex by showing the velocity components at the plane perpendicular to the freestream velocity.

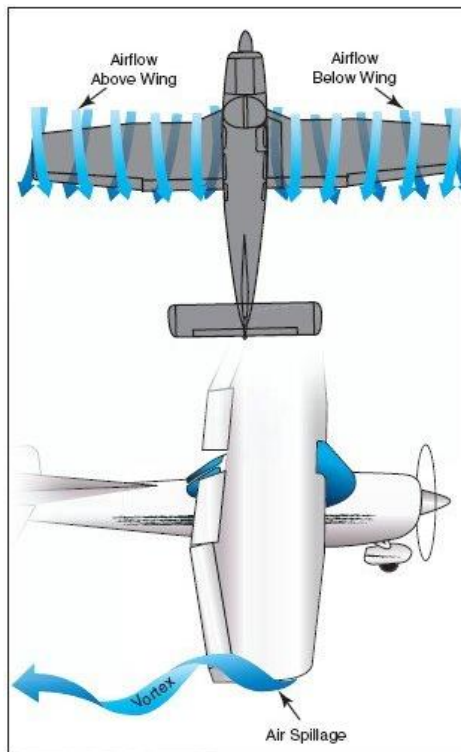


Figure 2. 6. Airflow direction around the wing and wing-tip vortex.
Adapted from “Aerodynamics, Aircraft Assembly, and Rigging” by the Aviation Safety Bureau, Aviation Maintenance Technician.

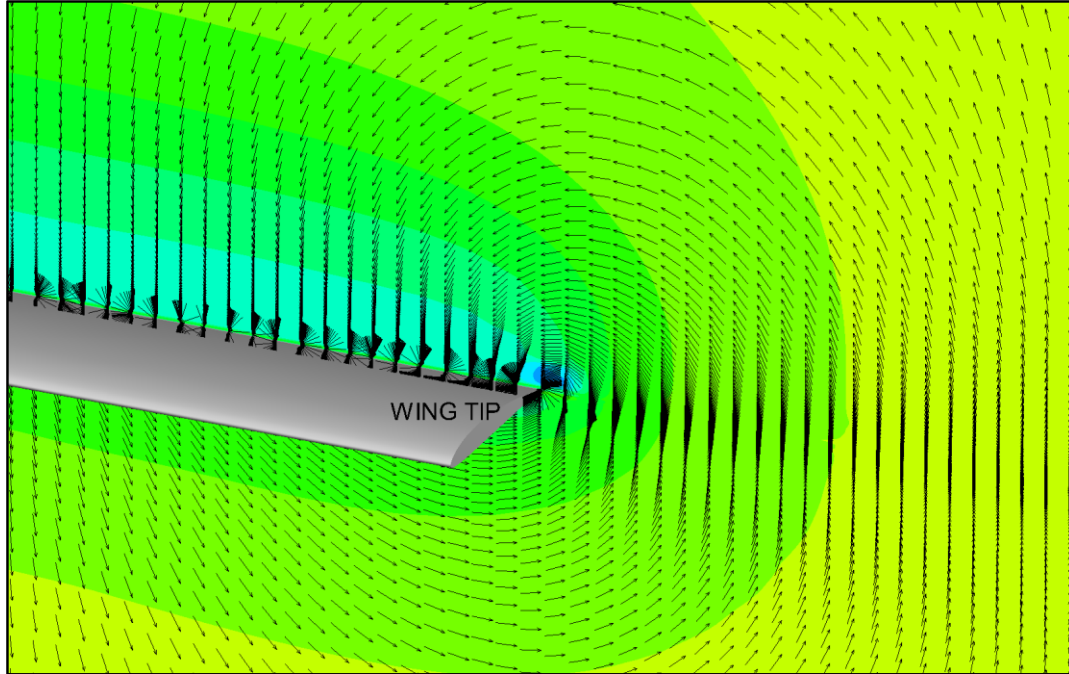


Figure 2. 7. Velocity components of the plane perpendicular to the freestream flow. CFD simulation of a Clark-Y wing with $AR = 6$ at $\alpha=0^\circ$ and $Re = 6 \times 10^5$.

This wing-tip vortex moves downstream as the wing moves forward, creating a vertical induced flow at the wing called downwash, w . This induced flow reduces the geometric angle of attack changing the lift vector direction by an angle called induced angle of attack, α_i . The horizontal component of this change in the lift direction is called induced drag, D_i , and it is a measure of the kinetic energy lost by the generation of the wing tip vortices [24]. The new lift direction is defined from the effective angle of attack, α_{eff} , which is given by Eq. (2. 4). Figure 2. 8 shows the effects of downwash effects on the wing lift's orientation, and the layout of the effective angle of attack.

$$\alpha_{eff} = \alpha - \alpha_i \quad (2. 4)$$

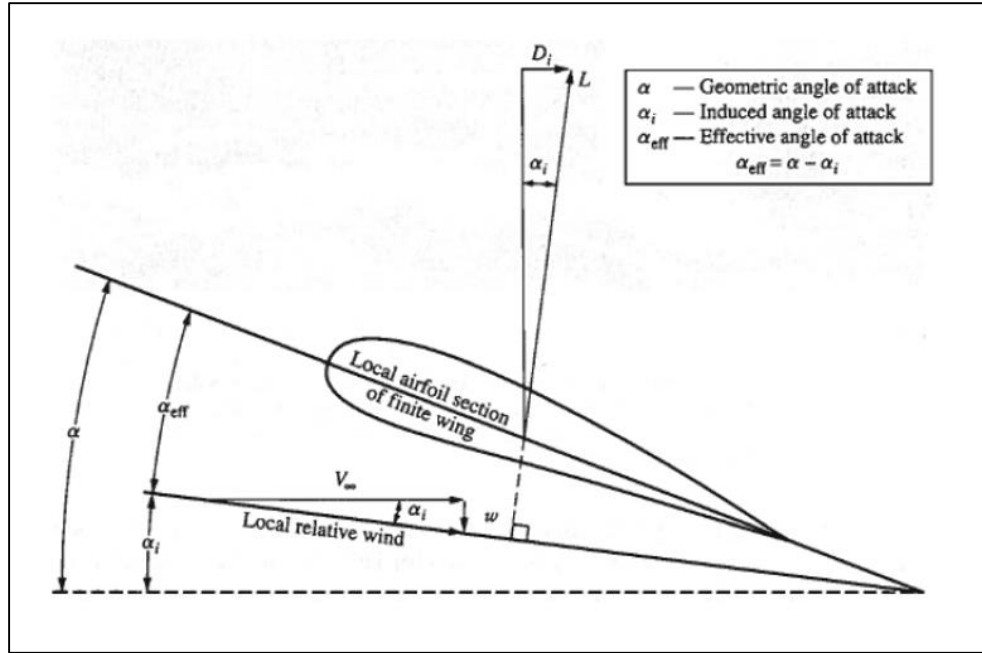


Figure 2. 8. Representation of the lift orientation with downwash effects. Adapted from “Fundamentals of Aerodynamics, 3rd Edition” by Anderson Jr. Boston, MA: McGraw Hill, 2001.

Using the Prandtl’s Lifting Line Method [23], the induced drag can be represented by Eq. (2. 5), where e is the Oswald’s Span Efficiency, and AR is the aspect ratio of the wing. The span efficiency works as a correction factor to represent the change in drag and lift of a three-dimensional wing from a two-dimensional airfoil. The aspect ratio is a parameter that quantifies the slenderness of the wing. Both of these parameters depend on the wing’s geometry. Reference to [23] chapter 9, to find different methods to estimate e and AR .

$$C_{Di} = \frac{C_L^2}{e \cdot \pi \cdot AR} \quad (2. 5)$$

Table 2. 1 shows the equations to convert the lift, drag and pitching moment developed over a three-dimensional wing into dimensionless coefficients. Overall, these

coefficients tend to have similar characteristics as their two-dimensional correspondents, but they are not the same. Figure 2. 9 shows the difference between the two-dimensional with the three-dimensional lift coefficient curves. In general, the lift curve slope, maximum lift coefficient, and the lift coefficient at zero angle of attack of a three-dimensional wing are always less than those produced by the two-dimensional airfoil.

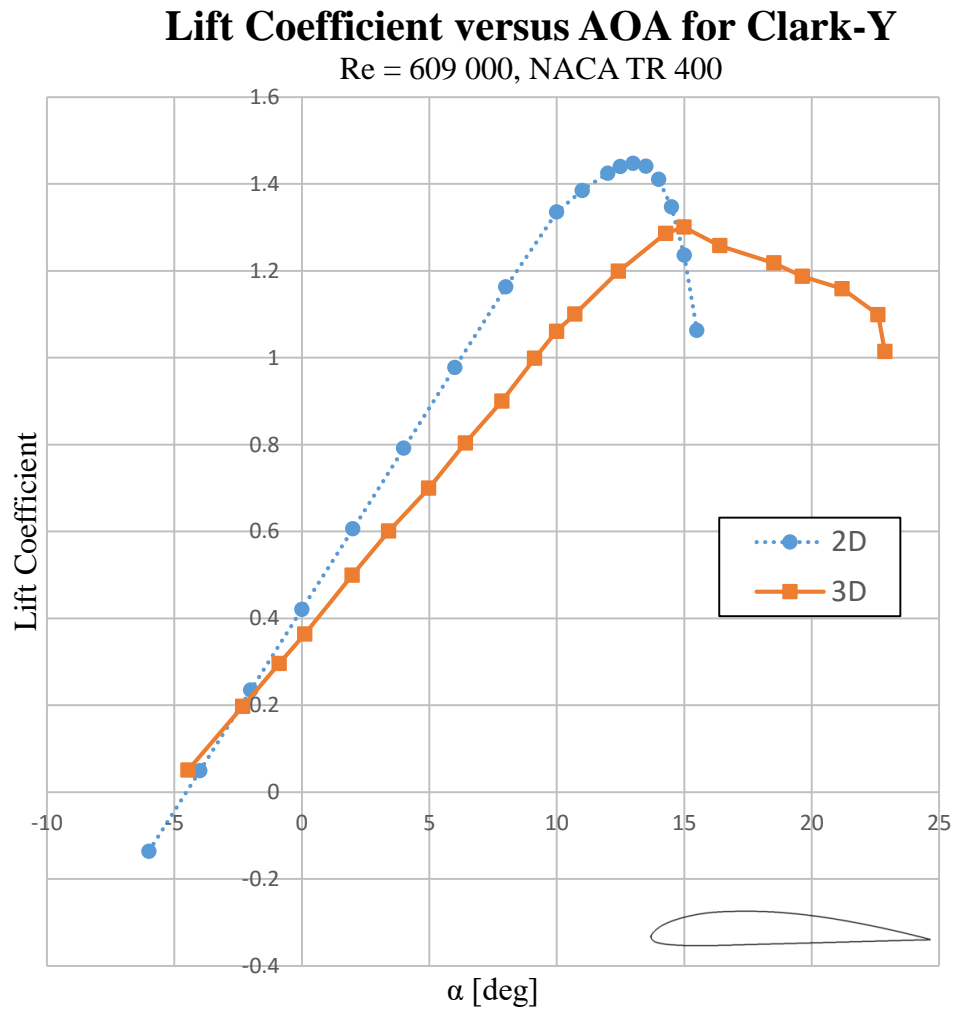


Figure 2. 9. Comparison of 2-D and 3-D lift curve. 3-D case for a Clark-Y wing with AR = 6, $\lambda = 1$, and $\Lambda_{LE} = 0^\circ$

As it was explained previously, because of the induced drag, the lift coefficient at a defined angle of attack is going to be less for a three-dimensional wing than the one

generated by the airfoil. Consequently, the wing needs to operate at a higher angle of attack to compensate the induced angle of attack. Because of this, a series of expressions have been derived in order to estimate the lift coefficient behavior of a wing based on the characteristics of the airfoil that it is made of. Equation (2. 6) shows a transformation expression for the lift curve slope of a general-shape wing taking into account compressibility effects. It is referred as the Polhamus equation [27]. Here, κ represents the ratio of two-dimensional lift curve slope to 2π , and β is the Prandtl-Glauert correction parameter for Mach number. Equations (2. 7) and (2. 8) show how to calculate them.

$$C_{L\alpha} = \frac{2\pi \cdot AR}{2 + \sqrt{\left(\frac{AR \cdot \beta}{\kappa}\right)^2 \left(1 + \frac{\tan^2 \Lambda_{c/2}}{\beta^2}\right) + 4}} \quad (2. 6)$$

$$\kappa = C_{l\alpha} \cdot \frac{180}{2\pi^2} \quad (2. 7)$$

$$\beta = \sqrt{1 - M^2} \quad (2. 8)$$

The only characteristic that the two-dimensional lift coefficient curve has as equal with the three-dimensional curve is the angle of attack at zero-lift. Using this analogy, the 3-D lift coefficient at zero angle of attack can be calculated using Eq. (2. 9).

$$C_{L_0} = |\alpha_{ZL}| \cdot C_{L\alpha} \quad (2. 9)$$

For a straight wing configuration with a single airfoil, Eq. (2. 10) shows how to calculate the maximum lift coefficient of a wing from the maximum lift coefficient of the airfoil that it is made of.

$$C_{L_{max}} = 0.9 \cdot C_{l_{max}} \quad (2. 10)$$

The angle where the wing stalls can be calculated using Eq. (2. 11), where $\Delta\alpha_{stall}$ is a correction factor that is obtained using Figure 2. 10, where Δy represents the Leading Edge Parameter. This is the difference between the airfoil ordinates at 6% and 15% chord [23.]

$$\alpha_{stall} = \frac{C_{Lmax}}{C_{L\alpha}} + \alpha_{ZL} + \Delta\alpha_{stall} \quad (2. 11)$$

Eq. (2. 12) shows the relation to calculate the wing’s pitching moment slope taking into account the lift curve slope and the pitching moment slope from the two dimensional case.

$$C_{M\alpha} = C_{L\alpha} \cdot \left(\frac{C_{m\alpha}}{C_{l\alpha}} \right) \quad (2. 12)$$

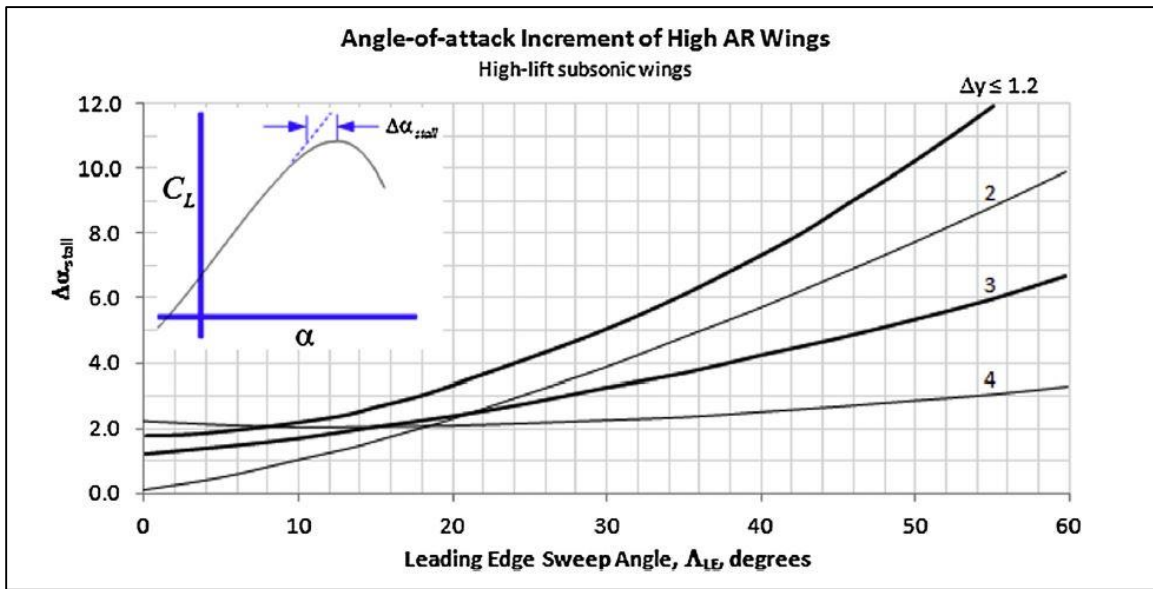


Figure 2. 10. Correction factor for the wing stall angle estimation. Adapted from “General Aviation Aircraft Design” by Gudmundsson S. ELSEVIER, Daytona Beach, 2013

In the same way as the airfoil, once the wing exceeds the stall angle, the flow on the upper surface starts to separate causing the lift to decrease. Figure 2. 11 shows the flow

separation on the upper surface of the wing when it stalls. But this flow separation does not happen over the whole upper surface of the wing at the same time, instead it is a progressive pattern that depends on the geometry of the wing. The first step to understand how the stall progresses on the wing, it is to know how the lift is distributed over the surface of the wing. Wherever this distribution has its maximum, is where the wing will start to stall. Figure 2.12 shows the lift coefficient distribution for a rectangular and an elliptical shaped wings, and how the stall progresses over their surfaces.

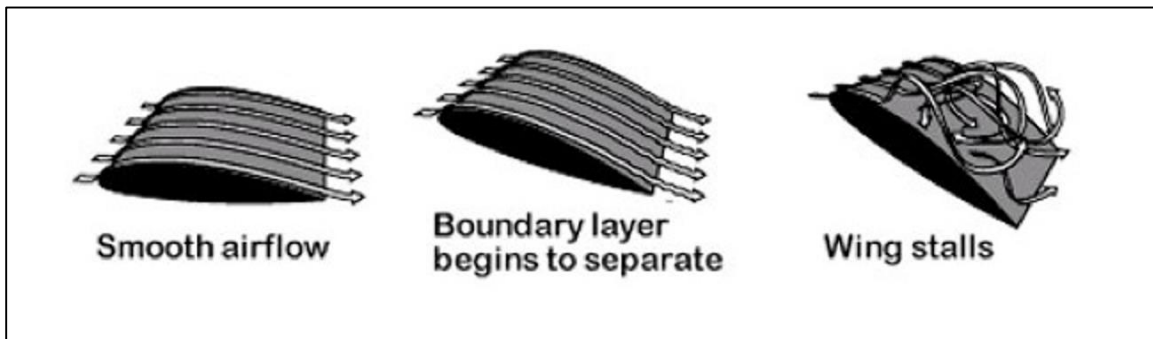


Figure 2. 11. Flow Separation over a wing by increasing the angle of attack. Adapted from “Aerodynamics for Engineering Students, 5th Edition” by Houghton, E.L. Butterworth Heinmann, 2003.

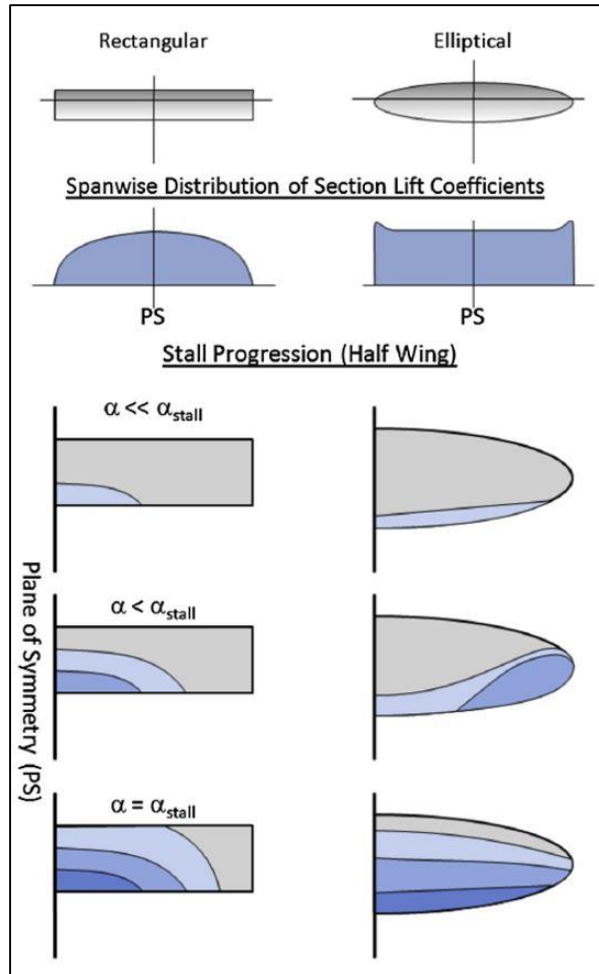


Figure 2. 12. Stall progression comparison between two different wings.
Adapted from “General Aviation Aircraft Design” by Gudmundsson S.
ELSEVIER, Daytona Beach, 2013.

2.2. The Slat Effect

The problem that most high-lift devices encounter is that of developing an increase in lift without causing flow separation. In order to obtain that boundary layer control, a modification in the geometry of the wing is necessary. Smith [31] said that, by the use of properly designed gaps in an airfoil, the increment of lift is possible by controlling the flow circulation on the main element. The leading-edge slot is one of the real-life application of these gaps, by acting as a multielement airfoil system. Smith continues to explain that, a properly designed slot is spaced far enough from the wing so that each component develops

its own boundary layer under the mainstream. Because of this, the slot and the wing generate their own circulation, where the circulation of the slot counters the circulation of the wing. As a result, the velocity on the surface of the main wing is reduced; consequently, the pressure peaks are reduced too, alleviating separation problems. Smith's explanation is defined as the *slat-effect*.

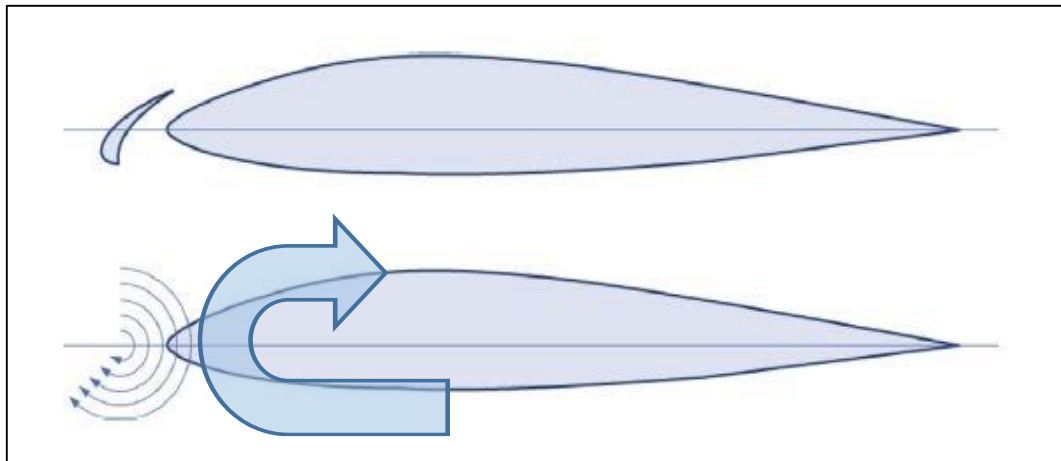


Figure 2. 13. Simplification of a slat by a point-vortex.
Adapted and modified from “General Aviation Aircraft Design” by
Gudmundsson S., ELSEVIER, Daytona Beach, 2013

Liebeck and Smyth [32] explained that the effect of the slat can be approximated by replacing it with a point vortex, see Figure 2. 13. Later investigations showed that a more accurate approximation would account for the thickness of the slot, adding several sinks and sources in order to maintain the Kutta condition. Liebeck and Smyth have shown that the best location of the point vortex was the same location of the slat, where the velocity peak of the airfoil is canceled by the peak generated by the vortex. Figure 2. 14 is one of the tests performed by Liebeck and Smyth, where $C_L \text{ TOTL}$ states the lift coefficient of the total system, $C_L \text{ AIRF}$ is the lift coefficient of the airfoil in the presence of the vortex, and C_L is the lift coefficient of the airfoil with no vortex. This figure shows how the velocity

peak on the nose of the airfoil is canceled by the velocity peak produced by the slat vortex, reducing the velocity in this vicinity. This velocity distribution alleviates separation problems and allows for an increment in the lift.

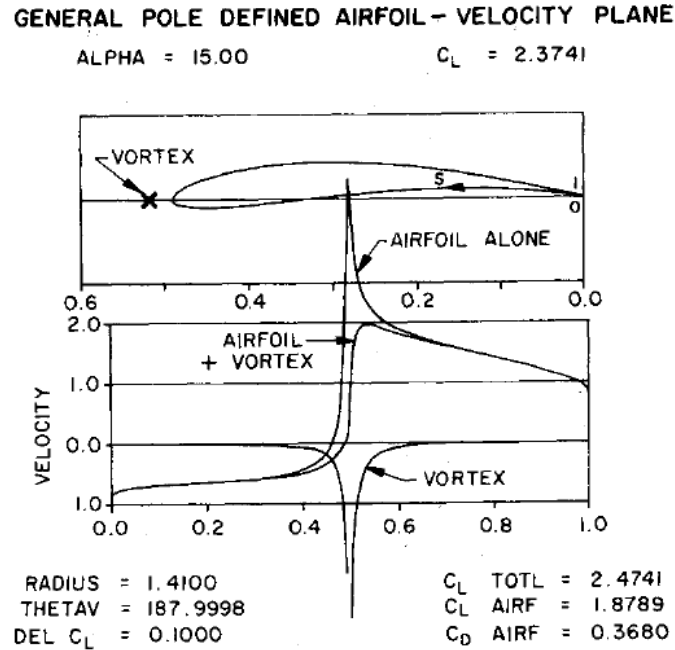


Figure 2.14. Velocity distributions over an airfoil alone and airfoil with vortex. Adapted from “*Study of Slat-Airfoil Combinations Using Computer Graphics*” by Liebeck R. H., and Smyth D. N. *Journal of Aircraft*; Vol. 20, No. 4.

2.3. Low-Drag Fixed Slot

A slotted wing is capable to obtain a higher lift coefficient and fly at higher angles of attack than the one of the plain wing. However, the drag generated by a slotted wing is typically three times larger than the unslotted configuration at low angles of attack [8]. Because of this, the use of the device in fast aircraft requires them to be stowed in cruise and only deployed when needed for low speed operation. This is accomplished using deployable slots, referred to as “slats”. This allows to have the slot closed at low angles of

attack to avoid any unwanted speed loss. The problem with this kind of slotted wings is that they increase the structural difficulty, cost, weight, and maintenance.

Because of these drawbacks, Weick and Wenzinger [8] modified and analyzed different slotted wings in order to obtain a fixed slot that could produce the smallest increment in drag at low angles of attack. The tests were divided in four parts: First, located the best slot position; second, the effect of the slot shape; third, the effect of the fix wing shape; and finally, the effect of moving the slot aft and forward.

2.3.1. The Best Slot Position

Wezinger and Shortal [4] studied a slotted wing and modified the slot position in 100 different locations, covering all possible ranges of slot gap, slot with, and slot depth (see Figure 1. 5). Some of the results obtained in this test can be seen from Figure 1. 6 to Figure 1. 8. The parameters that were taken into consideration to defined which is the best slot position were: the maximum lift coefficient, the angle of attack where this is obtained (α_{STALL}), minimum drag coefficient, and the maximum lift to minimum drag ratio. The first two characteristics determine the landing speed and stalling angle of the airplane. The minimum drag coefficient measures the highest speed attainable by the airplane, and the maximum lift to minimum drag ratio indicates the speed range.

As mentioned previously, the slot position that gives the highest lift coefficient increase is different than the position that gives the highest increase in the range of angle of attack, as well as the slot position that gives the lowest increase in the minimum drag coefficient. Consequently, a compromise had to be achieved in order to define the best slot position. It was found that a $12\%c$ width and a $4\%c$ depth (below the chord) were the most

optimum; and, by looking at Figure 2. 15, a 2%*c* gap gives the best overall increment in the considered parameters.

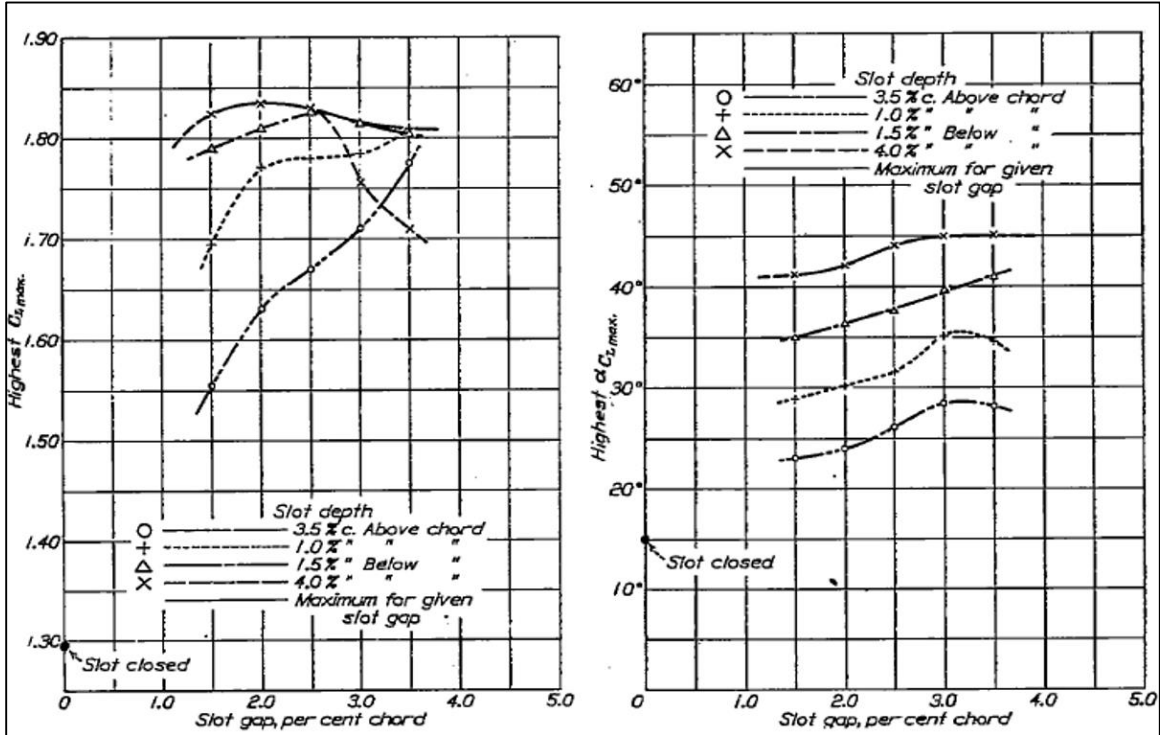


Figure 2. 15. Effect of the slot gap on the maximum lift coefficient and the angle where this is obtained for a given slot depth.

Adapted from “*The Aerodynamic Characteristics of a Slotted Clark-Y Wing as Affected by the Auxiliary Airfoil Position*” by Carl J. Wenzinger, and Joshep Shortal.

Report No. 400, N.A.C.A. 1931

2.3.2. Effect of the Slot Shape

Weick and Wenzinger [8], in an effort to reduce the increment of the drag coefficient generated by slotted wings at low angles of attack, started by modifying the shape of the slot. By looking at the original shape (Figure 2. 16a), Weick and Wenzinger thought that the minimum drag could be reduced by rounding the sharp lower edge (Figure 2. 16b). By doing this, not only the lift coefficient was reduced, but the minimum drag coefficient increased by a small amount. The next approach was changing the whole geometry of the slot with a low drag airfoil (Figure 2. 16c).

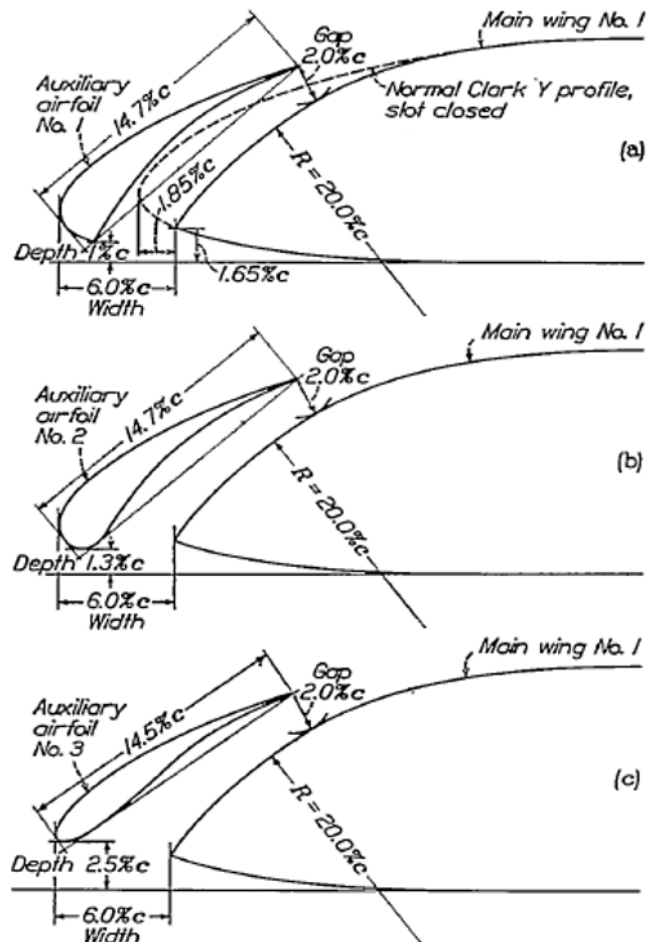


Figure 2. 16. Changes in the slot geometry.

Adapted from “*The Characteristics of a Clark-Y Wing Model Equipped with Several forms of Low-Drag Fixed Slots*” by Fred. E. Weick and Carl J. Wenzinger.

Report No. 407, N.A.C.A. 1931

As a result, the maximum lift coefficient was reduced considerably from the one obtained with the original configuration, and the minimum drag did not change. Consequently, Weick and Wenzinger stated that reducing the minimum drag coefficient of the slot does not necessarily reduce the minimum drag coefficient of the slot-wing combination, and that, it may in fact cause the opposite. Changing the shape of the slot may not only increase the minimum drag, but it could also decrease the maximum lift coefficient of the combination.

2.3.3. Effect of the Fix Wing Shape

Weick expected to reduce the minimum drag coefficient of the combination by rounding the sharp leading edge of the main wing. The leading edge was rounded gradually (in order to find how it affects the overall performance). Rounding the leading edge of the wing decreased the minimum drag, and increased the maximum lift coefficient of the combination to a certain point. If the nose radius was increased past this point, it had an opposite effect. The best-overall combination was obtained with a $2\%c$ nose radius.

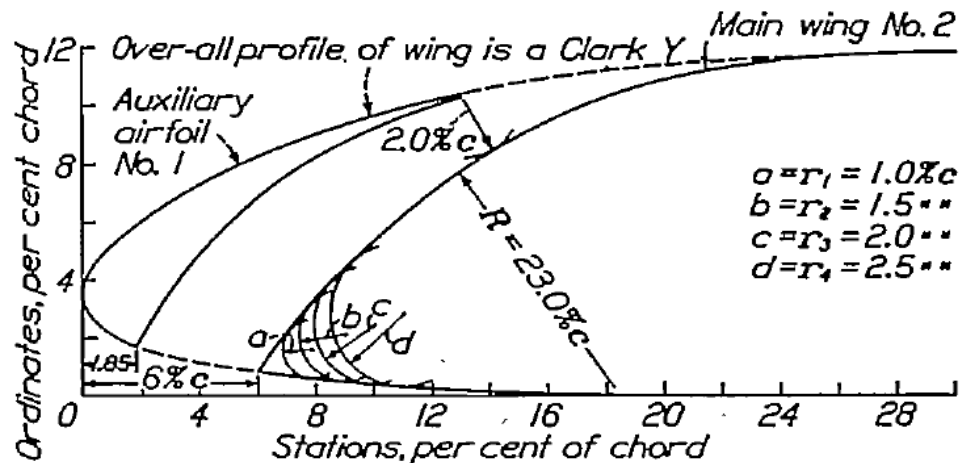


Figure 2. 17. Changes in the shape of the main wing.
 Adapted from "The Characteristics of a Clark-Y Wing Model Equipped with Several forms of Low-Drag Fixed Slots" by Fred. E. Weick and Carl J. Wenzinger.
 Report No. 407, N.A.C.A. 1931

2.3.4. Effect of Moving the Slot Farther Back

Hoping to reduce the minimum drag of the combination even more, Weick and Wenzinger moved the slot farther back from the leading edge of the wing (Figure 2. 18). The tests were performed with the different nose radius at the leading edge of the wing. However, the results showed that moving the slot farther back has no appreciable effect on the aerodynamic characteristics of the combination.

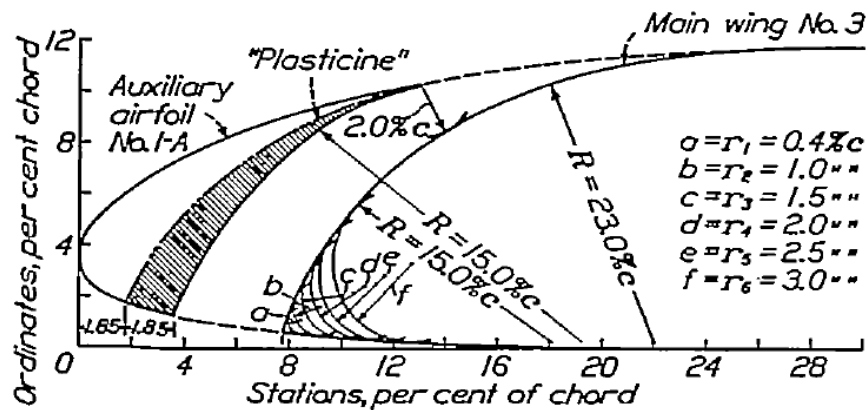


Figure 2. 18. Changes in the shape of the slot.

Adapted from “*The Characteristics of a Clark-Y Wing Model Equipped with Several forms of Low-Drag Fixed Slots*” by Fred. E. Weick and Carl J. Wenzinger. Report No. 407, N.A.C.A. 1931

Weick and Wenzinger concluded from the study that fixed slotted wings could be applied in aircraft with low landing speeds or excessively large wings. Slotted wings allow aircraft to obtain the desired minimum speed without stalling, and reduce the needed wing area (smaller wings). Also, fixed slots could be used only at the wing tips, to improve lateral stability and control at high angles of attack. With this, the maximum speed of the airplane would be less affected by the increased in the drag coefficient of the slot-wing combination.

2.4. Boundary Layer and Flow Separation

The boundary Layer is defined as the flow in the immediate vicinity of a bounding surface where the viscosity effects cannot be neglected. On an airplane's wing, the boundary layer is the section of the flow that gets distorted by the viscous forces. This happens close to the surface of the wing. Figure 2. 19 shows the boundary layer around an airfoil by the representation of the vorticity, which is the measurement of the local spinning motion of a continuum near some point [44] (distortion caused by the viscous forces, in this case). Boundary Layer Theory (BLT) describes the behavior of the flow under the effect of viscosity by the use of conservation laws and the Navier Stokes equations.

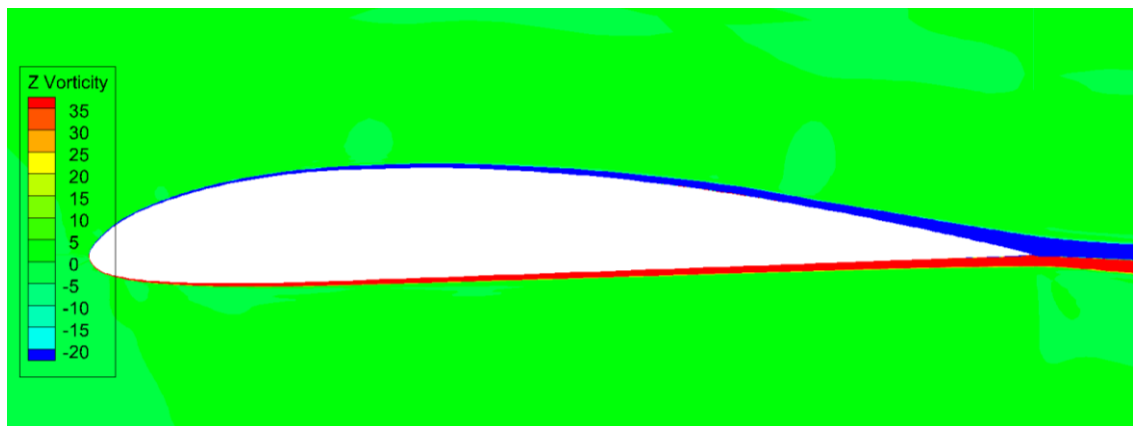


Figure 2. 19. Boundary layer visualization.

2.4.1. Reynolds Number

The *Reynolds Number* (Re) is defined as the dimensionless ratio of the inertial forces to viscous forces in a fluid flow, quantifying their relevance for the prescribed flow condition [40]. The Reynolds Number of an object submerged in a flow can be calculated by Eq. (3. 1), where ρ is the fluid density, U_∞ is the reference speed, L is the reference length (e.g. wing chord), and μ is the fluid viscosity.

$$Re = \frac{\rho \cdot U_{\infty} \cdot L}{\mu} \quad (3.1)$$

The Reynolds number plays an important role at the analysis and testing of objects. For example, a flat plate with 1 [m] in length at an airflow of 1[m/s] exhibits the same flow pattern as a flat plate with 0.1 [m] in length under an airflow of 10[m/s]. This concept is applied in wind tunnel testing, where testing real-sized aircraft is challenging and expensive. Instead, a scaled model can successfully replicate the same aerodynamic characteristics of the airplane of interest. The Reynolds number also helps to characterize the type of flow. At low Re , the flow is considered laminar. This type of flow is characterized by a high diffusion over convection. Large Re is typical of turbulent flows, where inertial forces dominate considerably, resulting in a chaotic flow [40]. Also, a flow goes through a transitioning phase, where it exhibits neither complete laminar nor completely turbulent characteristics. External flows with $Re \leq 10^5$ are considered fully laminar, $Re > 10^5$ are consider fully turbulent; in between those, the flow has transitional behavior.

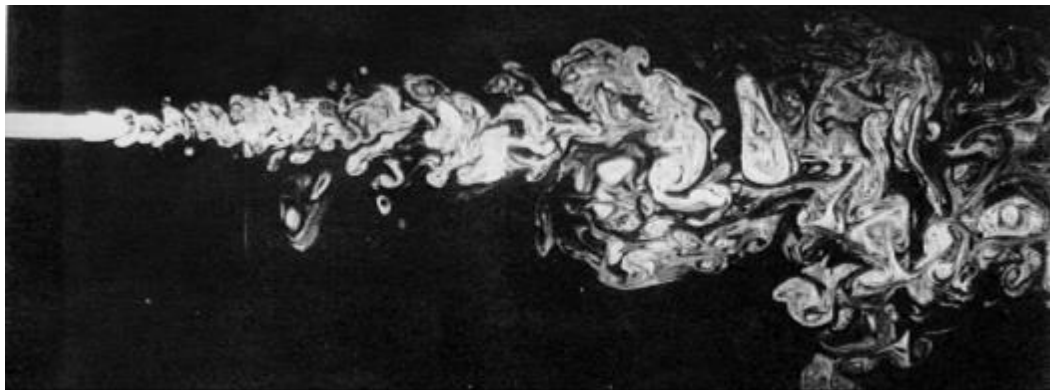


Figure 2. 20. Laminar, transition, and turbulent phases of a free shear flow. Adapted from “How does the Re affect my CFD model” by LEAP CFD Team, 2013.

In CFD analysis, Re is needed to identify the correct model to simulate the flow. At low Re , a model that neglects convective terms would be reasonable to use. While at large Re (turbulent flows), a model that neglect the viscous terms of the momentum equation (inertial forces only) will predict the simulation with more accuracy.

2.4.2. Boundary Layer Transition

Figure 2. 21 is an scaled version of three different sections of Figure 2. 19. Here, it can be appreciated how the flow at the boundary layer behaves at different sections of the airfoil. When flow goes around a body, it will generally present three distinct behaviors; laminar, turbulent, and separated flow. When the streamlines inside the boundary layer flow smoothly, it acts as a laminar boundary layer. Consequently, when the flow acts chaotically, it is under a turbulent boundary layer. As explained in the previous section, the process when the boundary layer goes from laminar behavior into turbulent it is defined as transition. This generally happens when the local Reynolds Number is approximately $5 \cdot 10^5$.

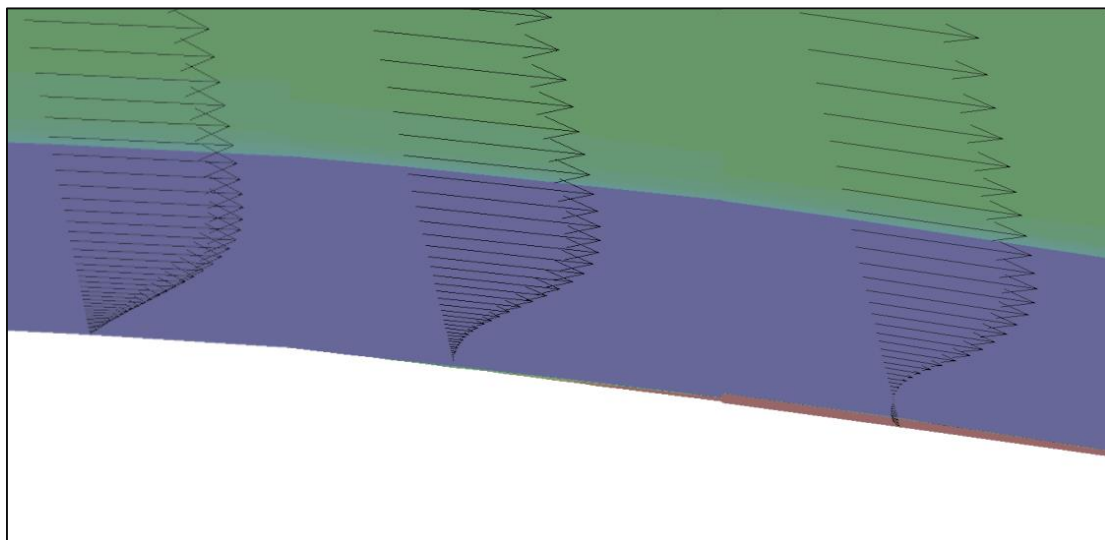


Figure 2. 21.Scaled sections of the boundary layer in an airfoil.

2.4.3. Flow Separation

Figure 2. 22 shows the characteristics of a laminar and turbulent boundary layer. It also shows that when the velocity gradient is zero (in the direction perpendicular to the surface), the flow separates from the surface. Anderson [24], describes that flow separation occurs when the speed of the boundary layer relative to the object becomes almost zero (caused by the adverse pressure gradient). This causes the flow to detach from the surface, creating eddies and vortices. Because the flow may flow upstream, in the opposite direction of the freestream flow, it increases the drag on the body. For this reason, aerodynamic shapes need to be designed in a manner that flow separation is minimized, if not eliminated, at the mission condition. This type of flow behavior usually happened in order, going from laminar to turbulent flow, and ends with the flow separating from the surface.

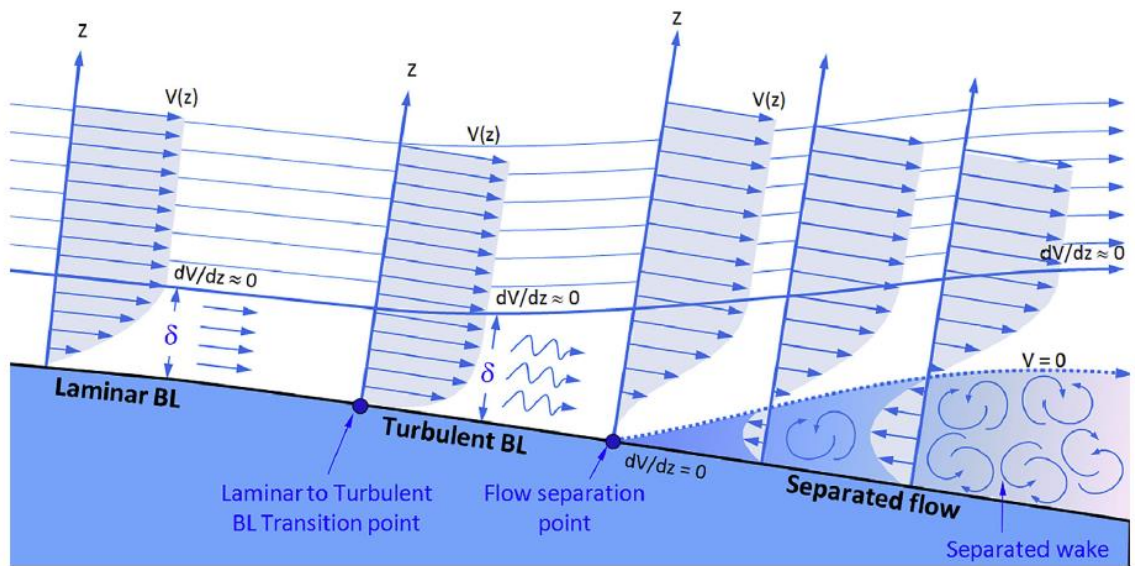


Figure 2. 22. Boundary layer transition from laminar to separated flow. Adapted and modified from “General Aviation Aircraft Design” by Gudmundsson S., ELSEVIER, Daytona Beach, 2013

III. Methodology

This section describes the experimental methods used to analyze the relation of the slot span with the wing performance. First, the two-dimensional geometry is defined, followed by the selection of the viscous model for the CFD analysis in ANSYS-Fluent. Once the model was selected, a deeper study about how the model works at the defined laminar to turbulent transitional Reynolds numbers is performed. With a better understanding about the viscous model, the three-dimensional geometries are defined for the plain and slotted wings. A three-dimensional analysis is performed and compared with experimental data for the plain and full slotted wings. Finally, a deeper study of tip-slotted wings with a variable span is developed with the goal of obtaining a relationship between the slot span and the wing aerodynamic performance.

3.1. The Clark – Y Airfoil

The Clark-Y airfoil was designed by Virginius E. Clark in 1922, and it has been widely used in the history of aviation [23], mostly before World War II. Its geometry is characterized by the flat lower surface, which extends from 30% chord to the trailing edge, see Figure 3. 1. The camber properties allow for a good performance at medium Reynolds number airflows. This has allowed its use in a wide range of model aircraft, from free-flight gliders through multi-engine RC models. The flat lower surface gives the advantage of an accurate and easy assemble on flat mountings at the aircraft fuselage [34]. Table 3. 1 gives the coordinates for the Clark-Y airfoil that were used in this study. The coordinates were imported into CATIA V5, where the airfoil profile was created before being exported into Pointwise V17 for the grid generation.

Table 3. 1. Clark-Y airfoil profile and ordinates [33].

Stations	Upper Surface	Lower surface	Stations	Upper Surface	Lower surface
0	0	0			
0.05	0.23	-0.47	46	0.09	-0.02
0.1	0.37	-0.59	48	0.09	-0.02
0.2	0.58	-0.78	50	0.09	-0.02
0.4	0.89	-1.05	52	0.08	-0.02
0.8	1.37	-1.43	54	0.08	-0.02
1.2	1.79	-1.70	56	0.08	-0.02
2	2.54	-2.03	58	0.08	-0.02
3	3.30	-2.26	60	0.08	-0.02
4	3.91	-2.45	62	0.07	-0.01
5	4.43	-2.60	64	0.07	-0.01
6	4.88	-2.71	66	0.07	-0.01
8	5.64	-2.85	68	0.06	-0.01
10	6.30	-2.94	70	0.06	-0.01
12	6.86	-3.00	72	0.06	-0.01
14	7.34	-3.02	74	0.05	-0.01
16	7.76	-3.03	76	0.05	-0.01
18	8.11	-3.00	78	0.05	-0.01
20	8.39	-2.97	80	0.04	-0.01
22	8.61	-2.91	82	0.04	-0.01
24	8.78	-2.85	84	0.04	-0.01
26	8.91	-2.78	86	0.03	-0.01
28	9.00	-2.71	88	0.03	-0.01
30	9.07	-2.63	90	0.02	0.00
32	9.12	-2.56	92	0.02	0.00
34	9.15	-2.48	94	0.01	0.00
36	9.16	-2.41	96	0.01	0.00
38	9.15	-2.34	97	0.01	0.00
40	9.12	-2.26	98	0.01	0.00
42	9.06	-2.19	99	0.00	0.00
44	8.97	-2.12	100	0.00	0.00

Clark - Y Airfoil Coordinates

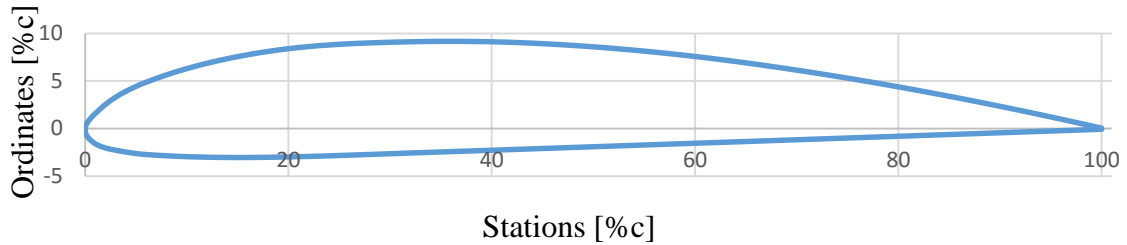


Figure 3. 1. Clark – Y airfoil.

3.2. Viscous Model Selection

For the selection of the most appropriate viscous model in ANSYS-Fluent, a structural C-Grid was created around the airfoil in Pointwise V17 using the guidelines explained at section 3.3.1. Domain Dimension. A two dimensional C-Grid needs only two boundary conditions to be exported into ANSYS-Fluent, *pressure-far-field* for the outer connectors, and *wall* for the connectors that represent the airfoil, see Figure 3. 2. The grid was exported into ANSYS-Fluent to be analyzed at 4×10^5 Re using different viscous models in order to determine which is the most accurate at the defined Reynolds number.

The analyzed models were:

- Spalart - Allmaras
- $\kappa - \epsilon$
- $\kappa - \omega$
- Transition SST

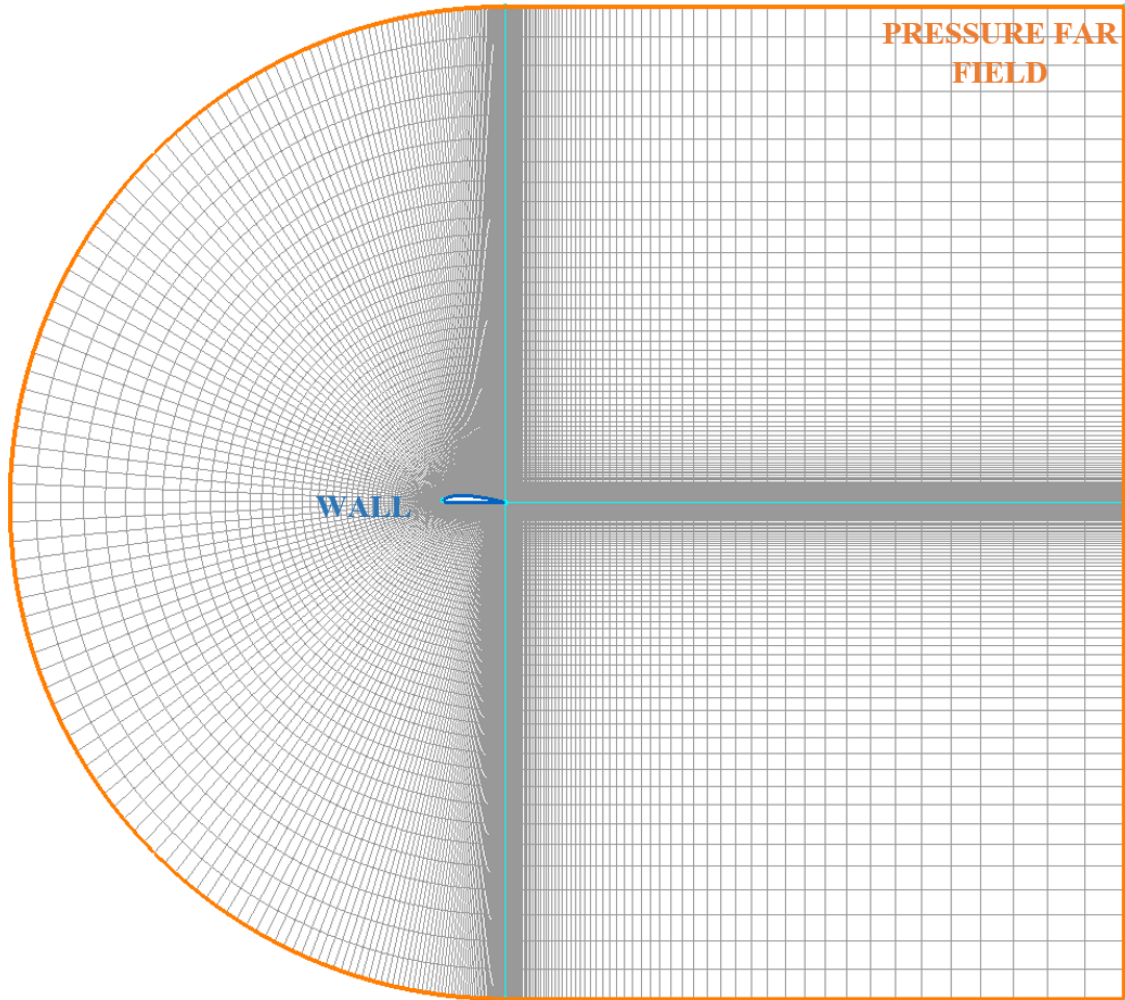


Figure 3. 2. Two-dimensional C-Grid boundary conditions.

Each model analyzed a range in angle of attack, from -8° to 18° in order to compared the linear and non-linear region in the lift coefficient, the drag coefficient, and the pitching moment coefficient. The results where later compared with the experimental data obtained by Lyon [1], as well as with the predicted results generated by XFOIL [2]. The results of this comparison are shown from Figure 4. 1 to Figure 4. 3.

3.3. SST Transition

Once the SST Transitional model was determined as the most accurate under the given conditions, a deeper study about how this model works was developed. It began by analyzing the required domain dimension, followed by a mesh resolution analysis, the determination of the criteria for convergence, and a grid independence study.

3.3.1. Domain Dimension

Before performing the three-dimensional CFD analysis, a study to understand the limitations of the viscous model was developed. First, the grid domain dimensions were analyzed in order to ensure that the airfoil/wing has no influence at the boundary conditions in the free-stream. The grid used is a C-grid that has two constrains, the radius of the C that covers the upcoming flow as well as the flow in the upper and lower portion of the airfoil, and the length of the grid that covers the downstream flow, see Figure 3. 3. If these constrains are not dimensioned correctly, the solution gets reflected on the boundaries, obtaining a wrong solution, see Figure 3. 4(left). After a series of tests, taking into account all the range in the angles of attack, the most efficient domain dimension was determined to be 16 chords as a radius and 20 chords in the downstream length. Figure 3. 4 (right) shows the results of a properly dimensioned C-Grid with a uniform solution on the freestream.

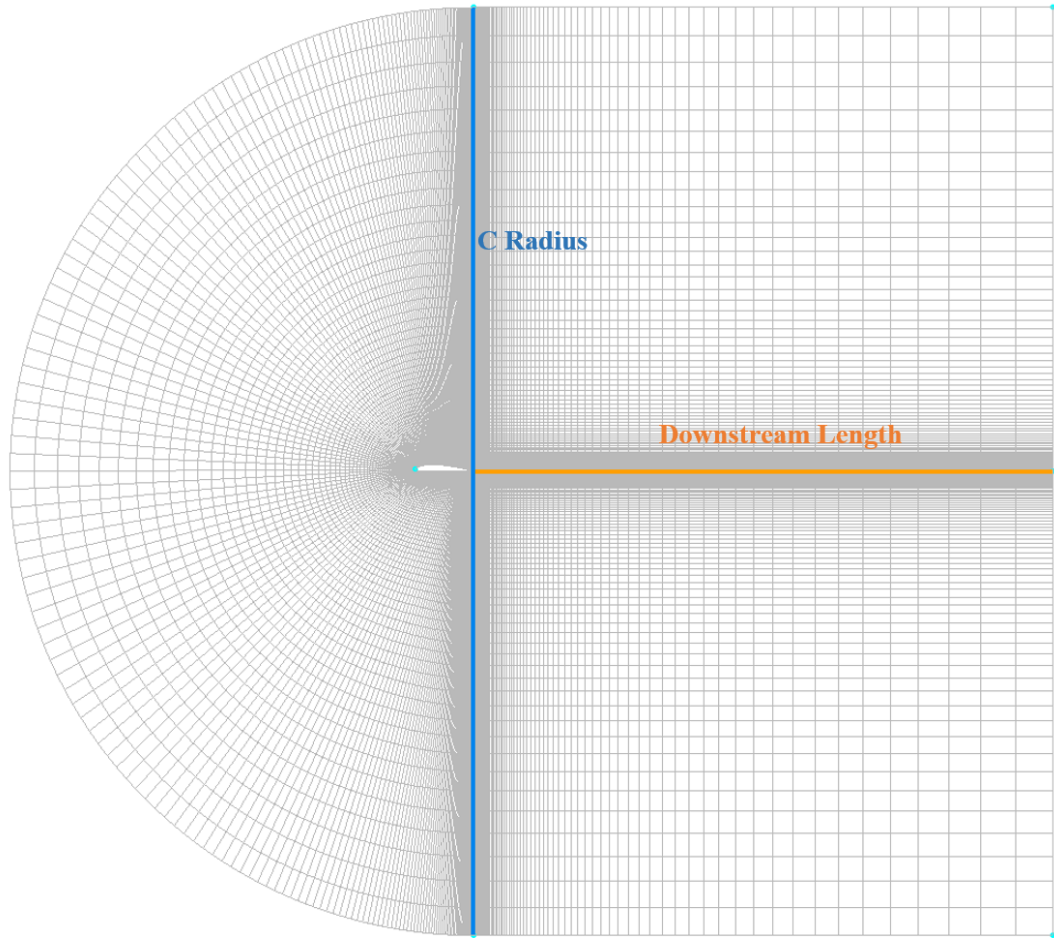


Figure 3. 3. C-Grid geometrical constrains.

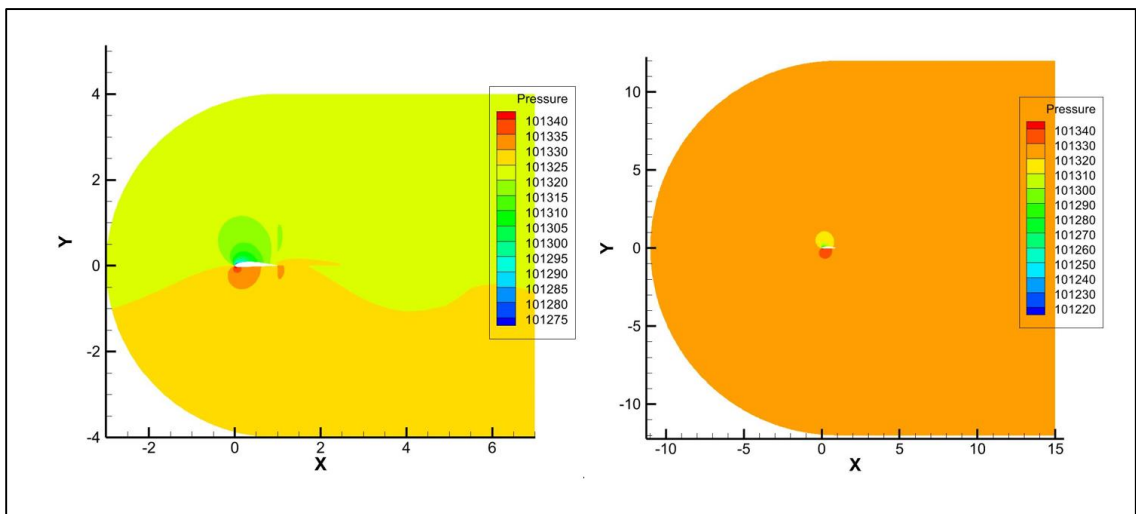


Figure 3. 4. Comparison of results between an incorrectly dimensioned grid (left) and a correctly dimensioned one (right).

3.3.2. Mesh Resolution

Because the Shear Stress Transport (SST) model aims to resolve the problems domineering at the boundary layer of transitional Reynolds numbers, it is important to have an appropriate mesh resolution in the proximity of the wall. For this, the placement of the first node near the wall (y^+) is of high importance [35]. The y^+ value is a non-dimensional distance, based on the flow direction and magnitude, from the wall to the first mesh node. To ensure a correct solution from the model, the y^+ value cannot be so large so that the first node is not contained into the boundary layer region. If this is the case, the wall functions from the model may predict incorrectly the flow properties in this area, producing a wrong solution. Because the analysis will run for angles of attack up to flow separation, it is highly important to resolve the boundary layer area with a finer mesh. Figure 3. 5 shows how, by the use of two connectors, it was easier to obtain a finer mesh along the boundary layer. In order to obtain good results with the SST Transitional model, the y^+ value did not exceed 3 for any configuration along the whole surface of the wall. Figure 3. 6 shows how the y^+ value depends on the angle of attack, and how this was ensured not to be greater than 3.

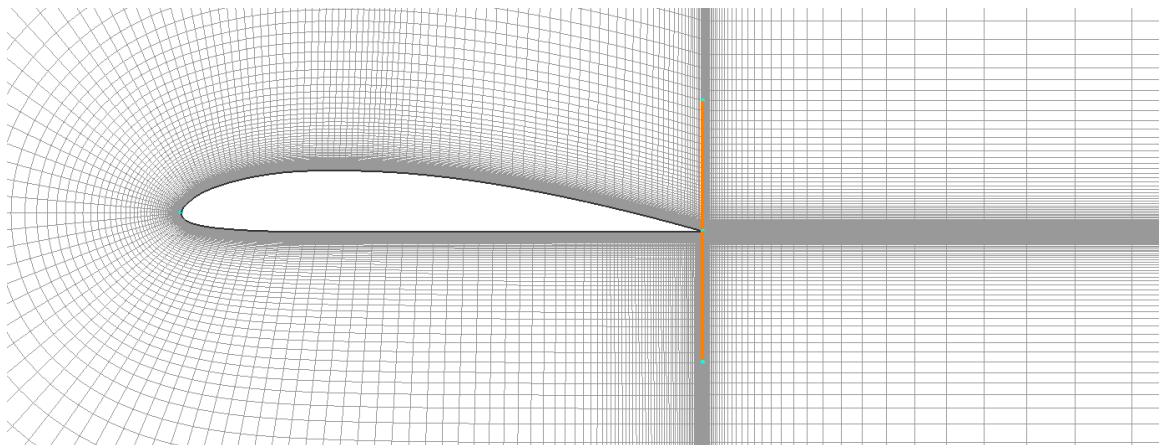


Figure 3. 5. Mesh density along the surface of the airfoil.

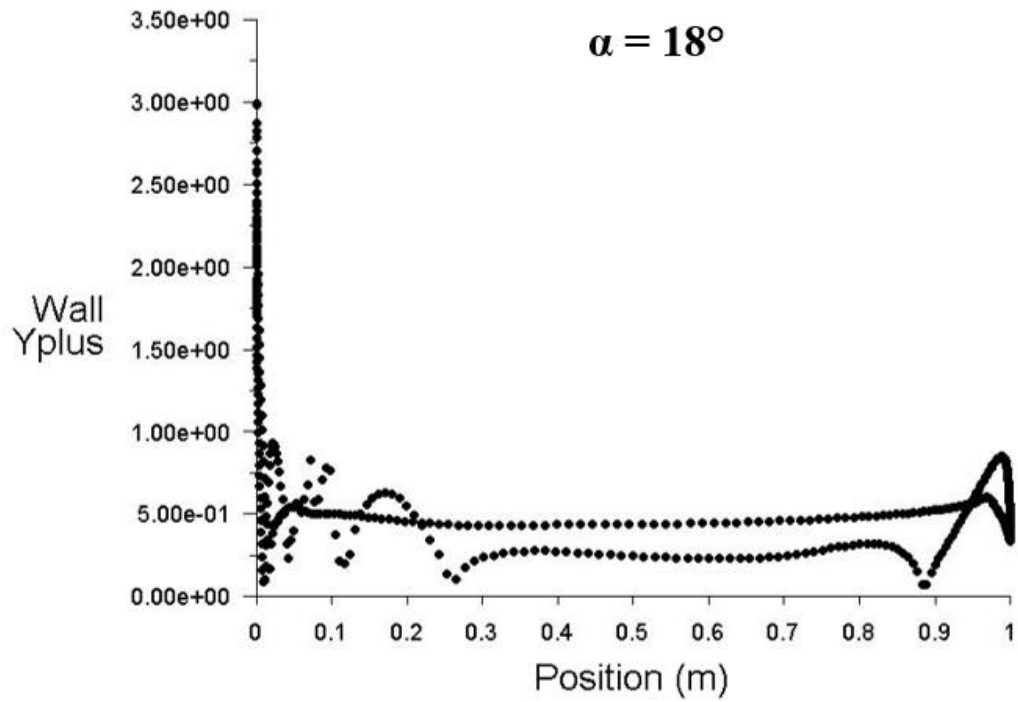
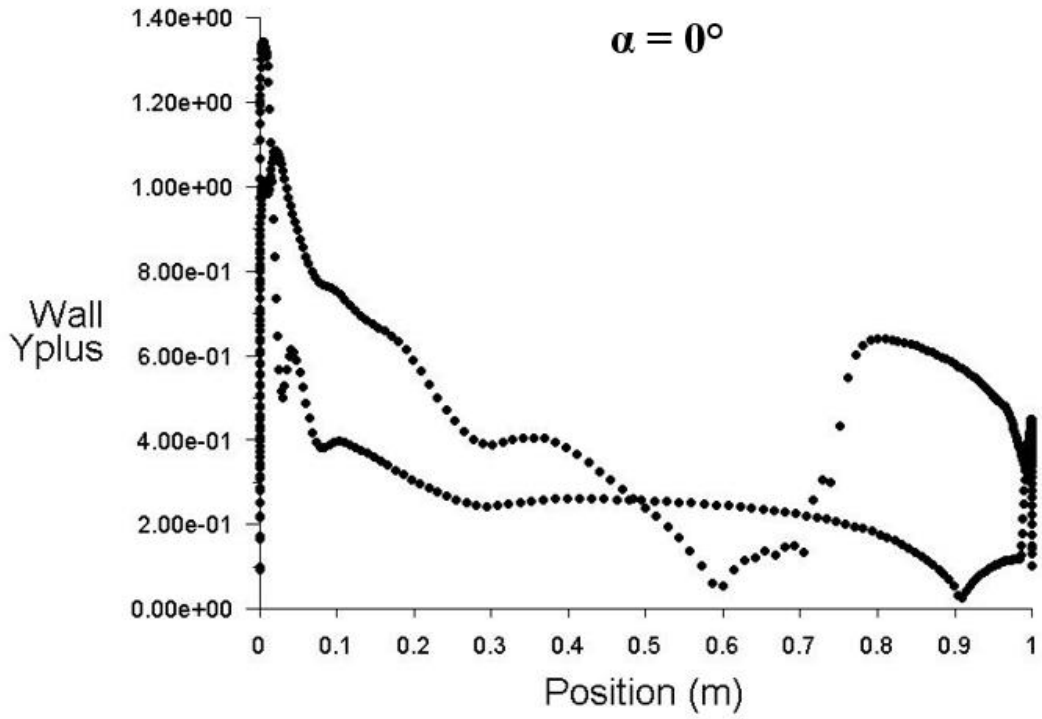


Figure 3. 6. Y+ distribution along the Clark-Y airfoil surface.

3.3.3. Solution Convergence

A converged solution was determined visually by inspecting the history in the force coefficient monitors. For the analysis performed at low angles of attack, where the lift coefficient is in the linear region, an steady state convergence was obtained, see Figure 3. 7 (top). For large angles of attack, where the lift curve is non-linear, pseudo-steady-state convergence was obtained, see Figure 3. 7 (bottom). The cause of these oscillations was studied by Petrilli [43], which stated that these are the result of a periodic vortex shedding from the upper surface of the airfoil. To handle a solution for this case, an average from peak to peak was calculated. The model converged at 20000 iterations for small angles of attack, while it took up to 50000 iterations to converge for large angles of attack.

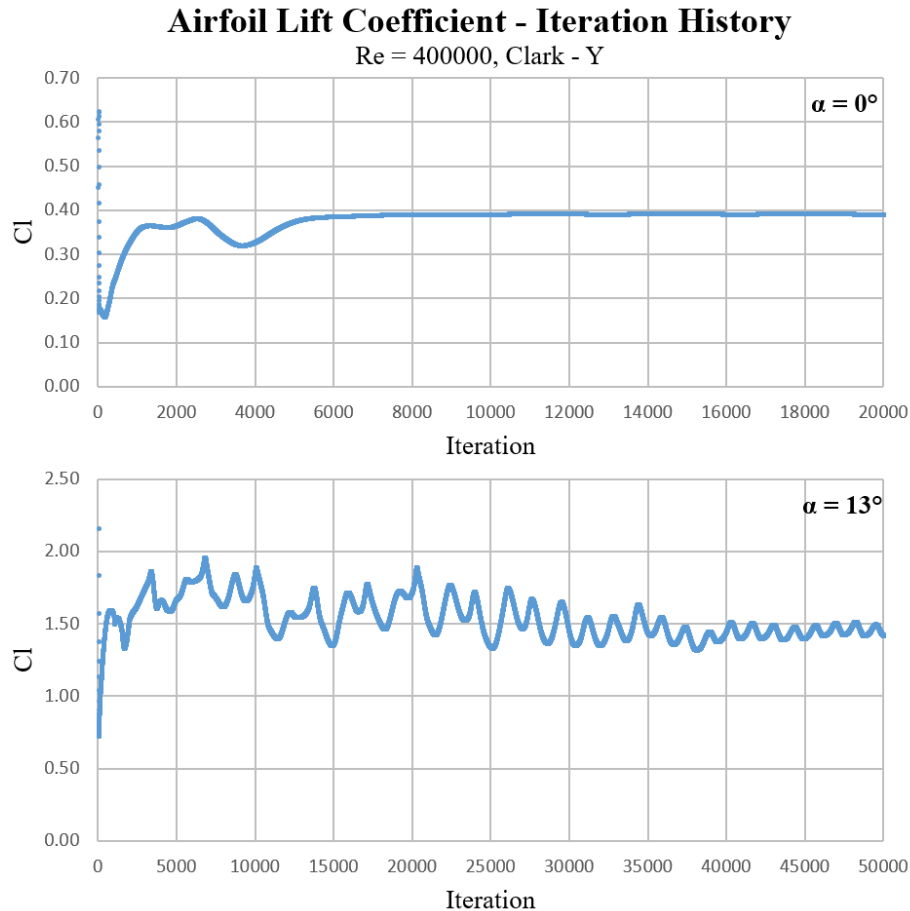


Figure 3. 7. Convergence history of the lift coefficient for the Clark-Y airfoil.

3.3.4. Grid Independence

In order to ensure that a CFD model results in a valid solution, a convergence criteria is only the first step. For a Steady State simulation, a valid simulation needs to satisfy three conditions [42]:

- Residuals RMS Error of less than 10^{-5}
- Monitors values reached a steady solution
- The domain has imbalances of less than 1%

Not checking that a model is independent of the mesh resolution is a common cause of erroneous results in CFD. Doing a mesh resolution independence study is a process that improves the quality of the results of models that are tested multiple times at different conditions, by applying the mesh resolution that gives the best results. The grid independence study was performed by, first, getting a converged solution for all the angles of attack of interest with an initial grid, this was defined as the *coarse grid* (Table 3. 2). The same procedure was repeated with a grid twice the amount of cells than the previous one, this grid was defined as the *medium grid*. Because the differences between the results were less than 1%, the method was repeated with a third grid which has twice the size of the last one explained. This grid was defined as the *fine grid*. Each grid was developed using the criteria explained in sections 3.3.1 and 3.3.2, and Table 3. 2 shows the number of cells for each grid density. The results of this study are represented in Figure 4. 4 to Figure 4. 6. The grid distribution that showed better accuracy with experimental data was used for the rest of the models.

Table 3. 2. Number of cells for each mesh density

Mesh Density	# of Cells
Coarse	15000
Medium	33000
Fine	64000

3.4. Plain Wing

The Clark-Y rectangular wing had an aspect ratio of 6. The three-dimensional grid was created from an extrusion of the two-dimensional grid. Following the instructions on the model tested by Wenzinger [4], the wing was defined with a sharp wing tip. In order to maintain a structural grid in the free stream portion of the wing-tip, a new distribution of the connectors at the airfoil was needed. The upper and lower surface connectors were divided into three sections, and 5 connectors were added in the interior section of the airfoil, see Figure 3. 8. The connectors that were split, as well as the added connectors had a specific distribution of points. The connectors defined as A in Figure 3. 8 (top) had to had the same number of points between them. The same between the 3 remaining connectors (defined as B). The grid was extruded in the span wise direction, half span for the flow around the wing, and half span to analyze the flow from the wing-tip to the freestream, see Figure 3. 9. The grid had more resolution at the wing tip in order to capture the vortex generated in this area. The three-dimensional C-Grid needed three boundary conditions to be exported into ANSYS-Fluent, *pressure-far-field*, *symmetry*, and *wall*, see Figure 3. 10. The grid was exported into ANSYS-Fluent to be analyzed at 6.1×10^5 Re using the SST Transitional model. Figure 4. 7 and Figure 4. 8 show the results and the comparison with experimental data for the three-dimensional plain wing.

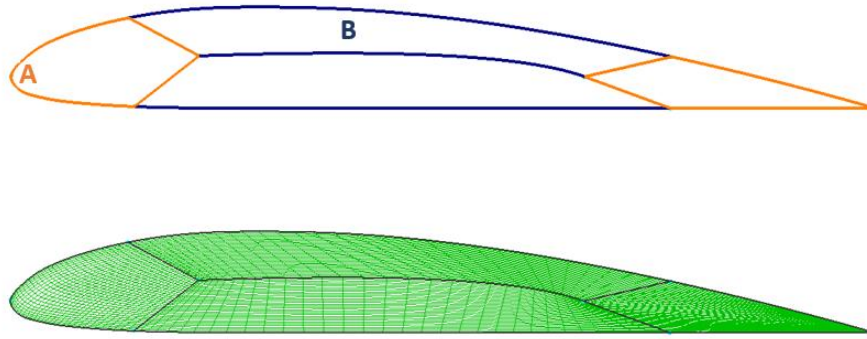


Figure 3. 8. Grid distribution at the wing-tip.

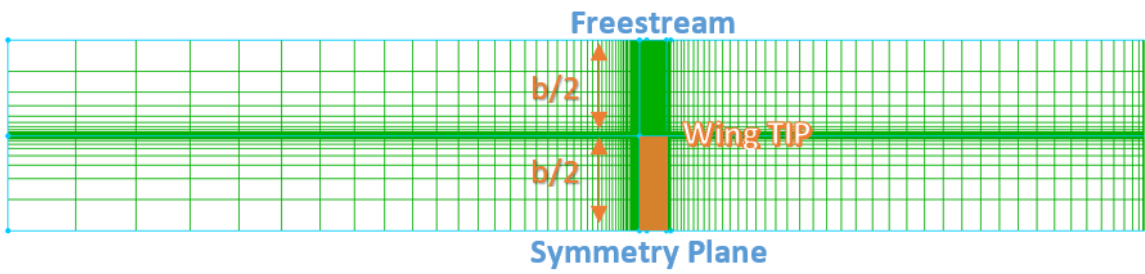


Figure 3. 9. Three dimensional grid. Top view dimensioning.

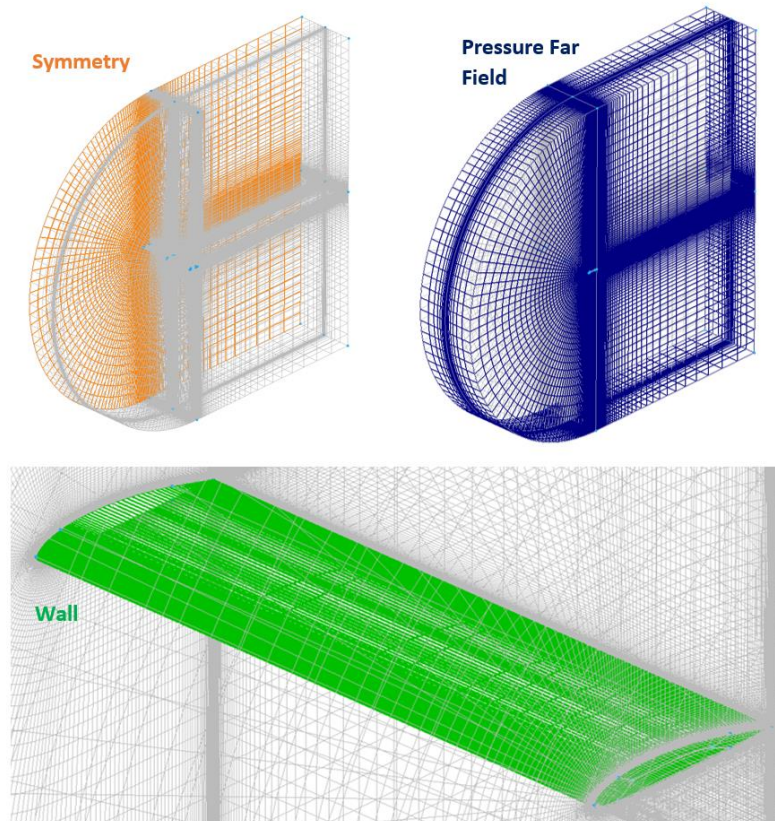


Figure 3. 10. Three-dimensional grid boundary conditions.

3.5. Full – Slotted Wing

The slot was defined as a cut on the leading edge of the airfoil, so that when the slot is closed, the profile will be of the normal Clark-Y airfoil. The slot geometry was defined using the slot used by Wezinger [4] in his study. The chord of the slot was defined as $14.7\%c$, the “cut-off” was $1.85\%c$. The lower surface of the slot and the upper surface of the cut-airfoil was defined with a radius of $20\%c$. Figure 3. 11(left) shows the geometry of the slot taking the original Clark-Y airfoil as a reference. As was explained in section 1.2, the position of the slot is determined by the three parameters. For the analyzed slotted wings, the position of the slot was the position that Wezinger [4] defined as the best position for the slot, which is also explained in section 2.3.1 and it is represented in Figure 3. 11 (right).

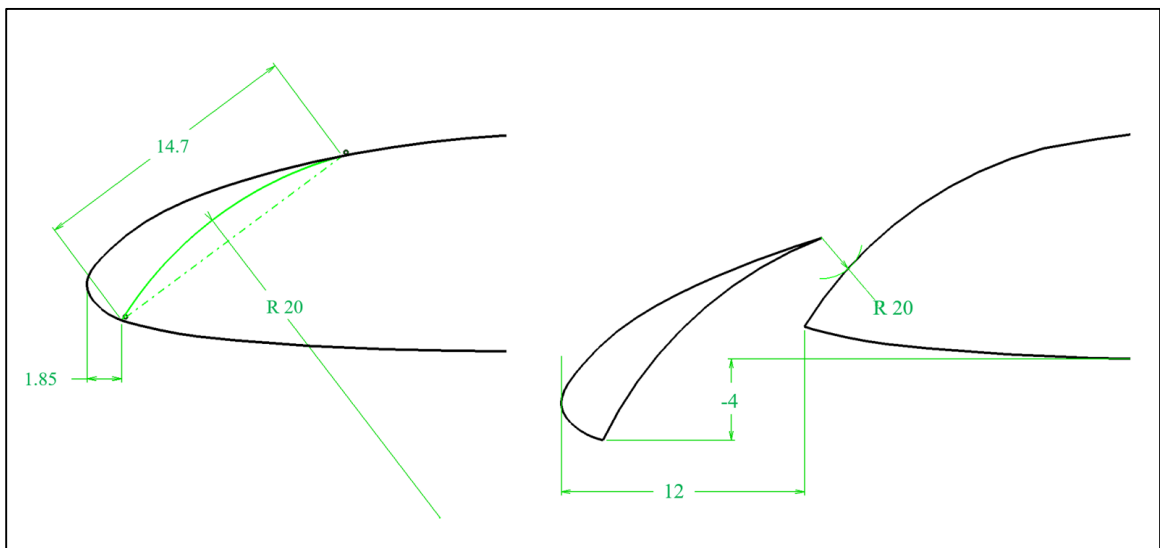


Figure 3. 11. Slot geometry (left) and position (right) in reference with the plain Clark-Y airfoil

The grid distribution followed the same principle used for the plain wing at the tip, but for the slotted wing the grid generation took into account the section of the slot, the fixed wing, and the flow that goes in-between these two. The three-dimensional grid followed the same procedure used for the plain wing. Figure 3. 13 shows the grid over the full-slotted wing, where the color orange was used to differentiate the mesh of the slot with the one of the fixed wing. The grid was exported into ANSYS-Fluent to be analyzed at 6.1×10^5 Re using the SST Transitional model. Figure 4. 9 and Figure 4. 10 show the results and the comparison with experimental data for the three-dimensional full-slotted wing.

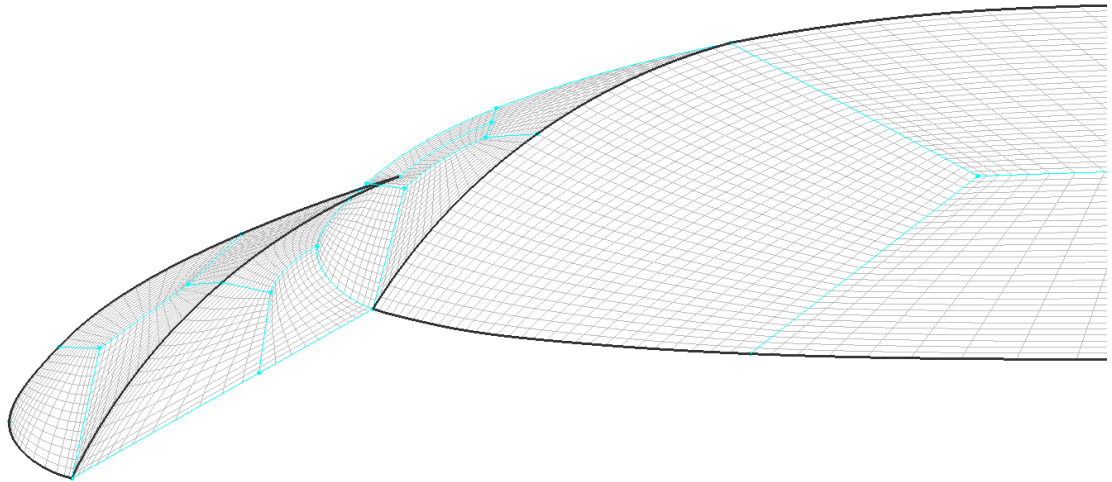


Figure 3. 12. Grid distribution at the tip of the slotted Clark-Y wing.

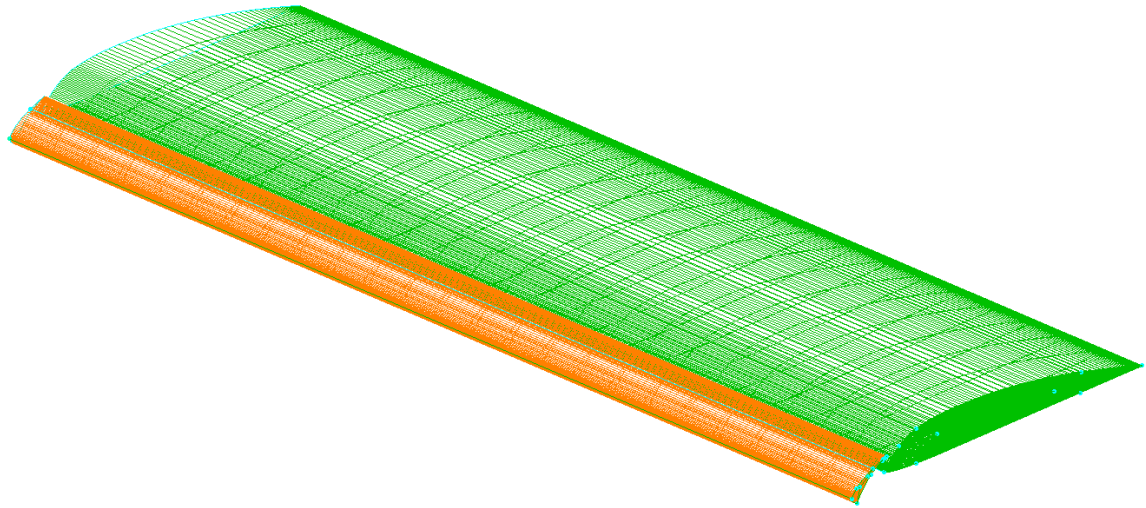


Figure 3. 13. Grid over the full-slotted Clark-Y wing.

3.6. Partially – Slotted Wings

The partial-span slot is defined by the slot-span ratio, b_s , which is defined as the length of the slot divided by the wing semi-span, see Figure 3. 14. The grid distribution for partially-slotted wings followed the same principle base used for the last model at the tip, but the extrusion in the span direction had to be done twice, one for the plain section of the wing, and one for the slotted portion. Figure 3. 15 shows the grid over on the partially-slotted wing ($b_s = .4$), where the color orange was used to differentiate the mesh of the slot with the one of the fix wing. The mesh had more resolution on the root and tip of the slot to capture the effect produced by the tips with more accuracy. Five different models were created with the slot-span ratios of 0.25 , 0.4 , 0.5 , 0.6 , and 0.8 to find the relation of this length with the aerodynamic performance of the wing. The model were exported into ANSYS-Fluent to be analyzed at 6.1×10^5 Re using the SST Transitional model. Figure

4. 9 and Figure 4. 10 show the results and the comparison with experimental data for the three-dimensional plain wing.

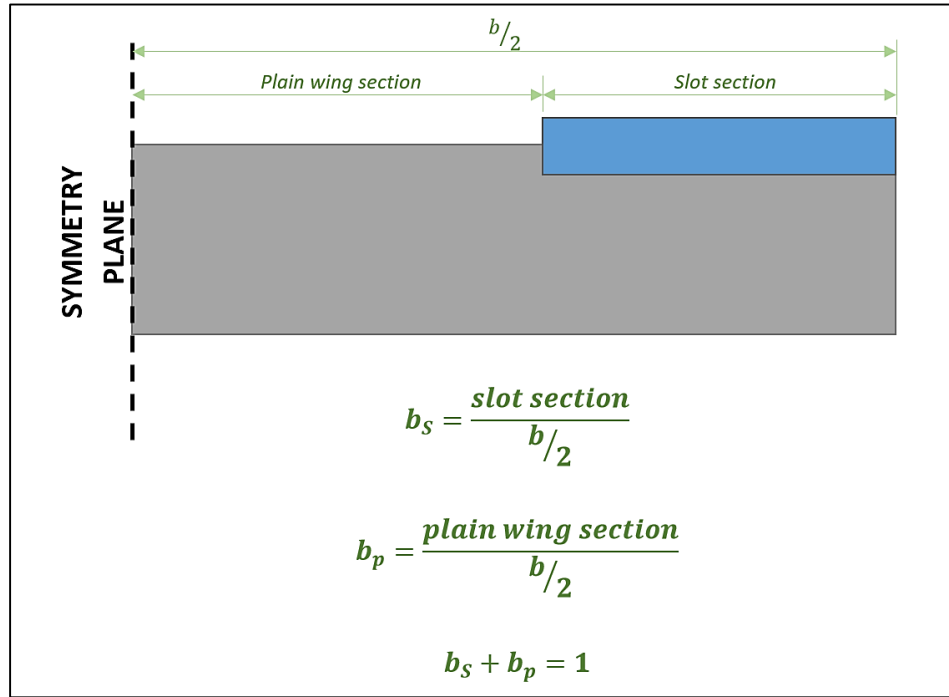


Figure 3. 14. Slot-span ratio definition.

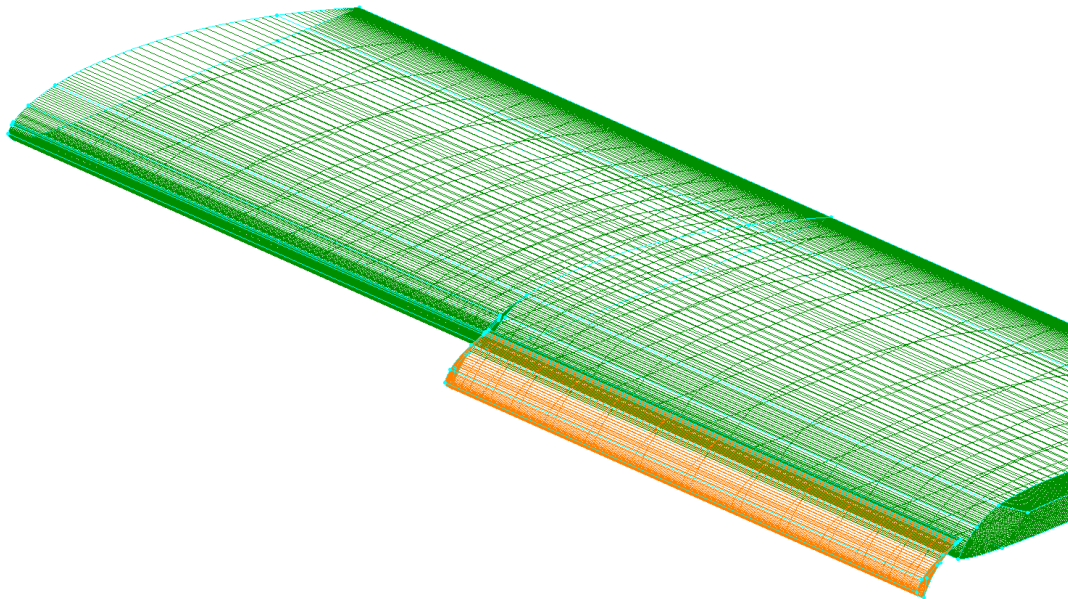


Figure 3. 15. Grid over the 50% tip-slotted Clark-Y wing.

IV. Results

4.1. 2-D Plain Airfoil Analysis

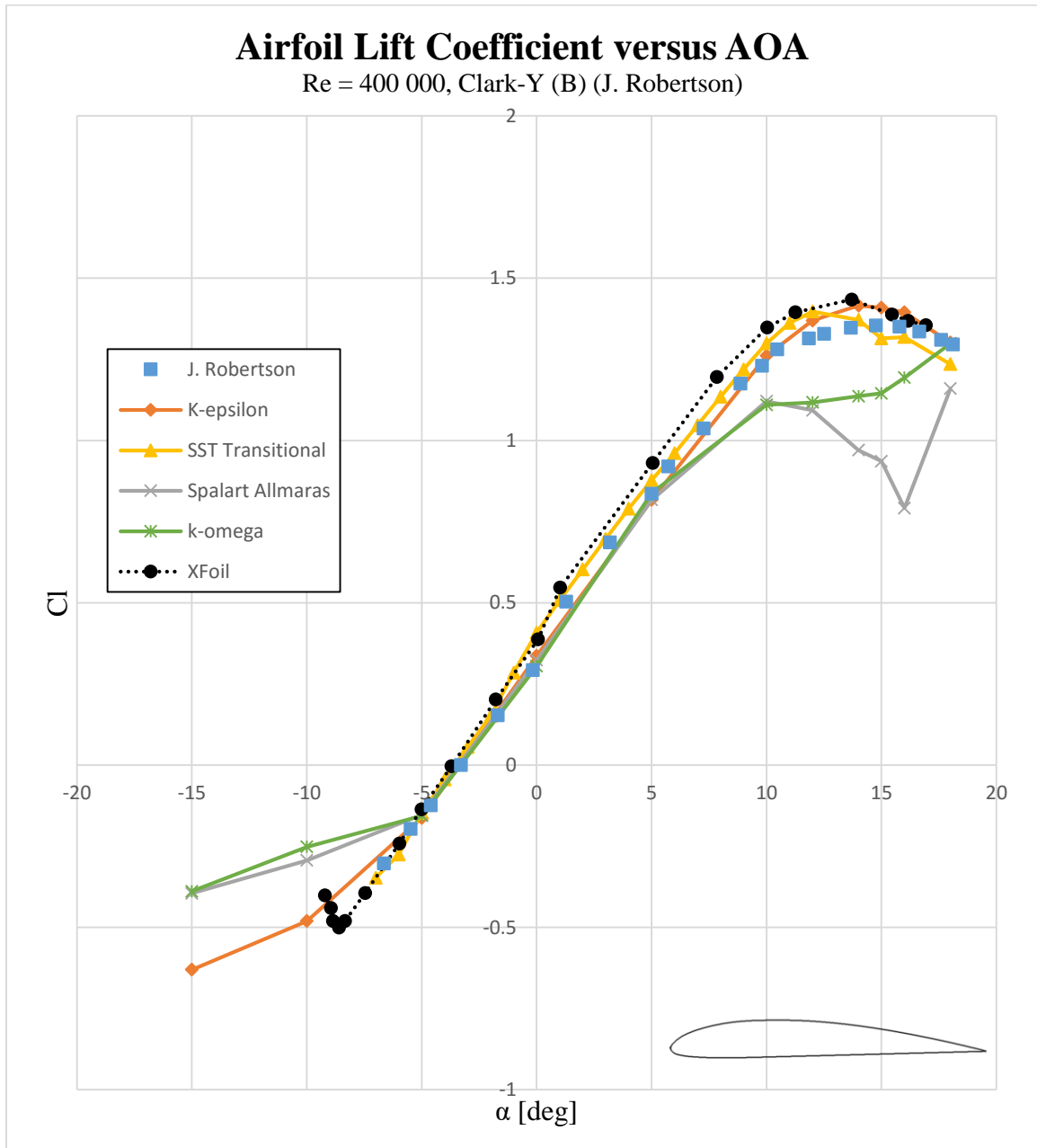


Figure 4. 1. 2-D lift coefficient versus angle of attack of the Clark-Y airfoil

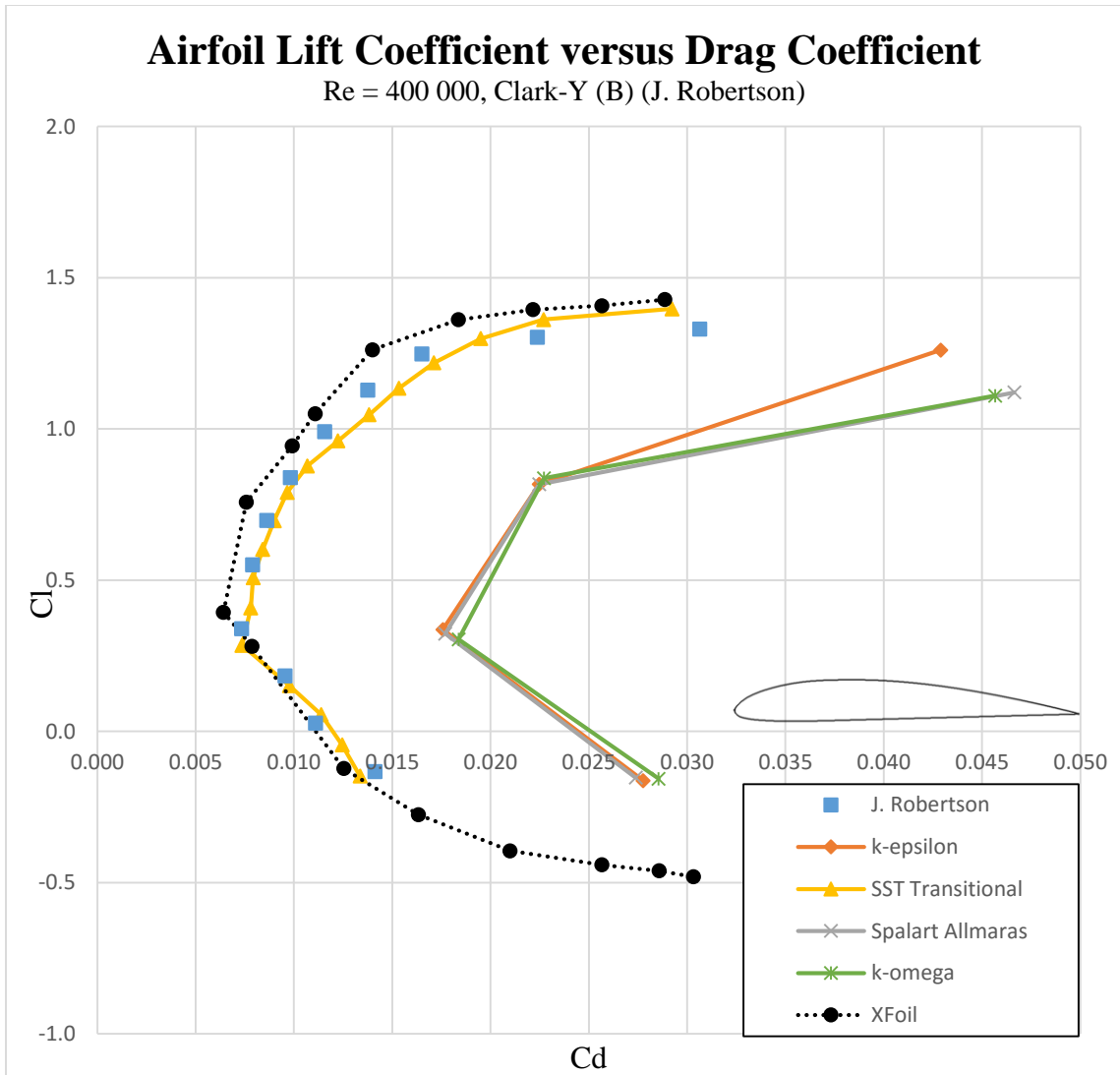


Figure 4. 2. 2-D drag coefficient versus lift coefficient of the Clark-Y airfoil

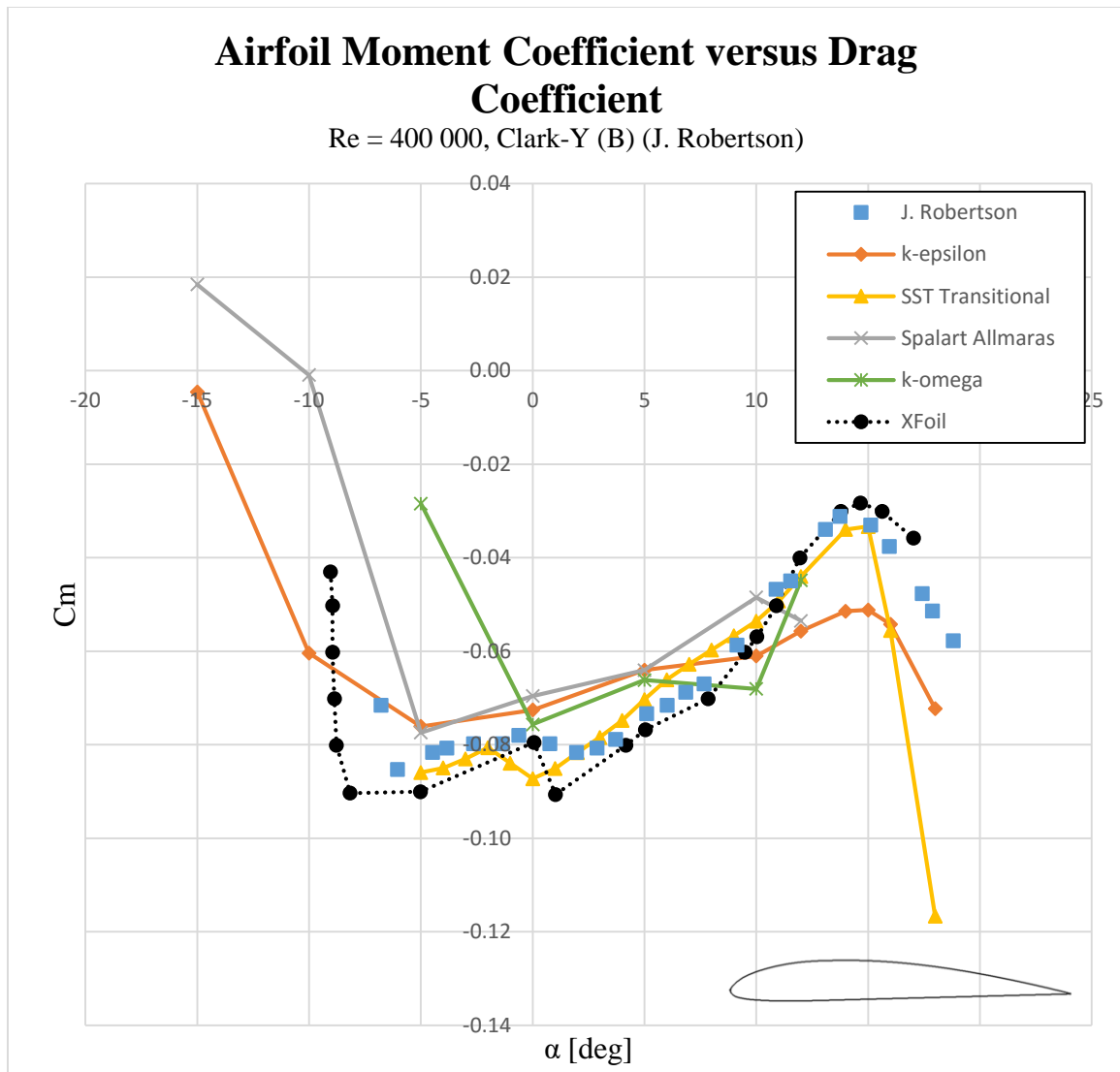


Figure 4. 3. 2-D pitching moment coefficient versus angle of attack of the Clark-Y airfoil.

4.2. Grid Independence Analysis

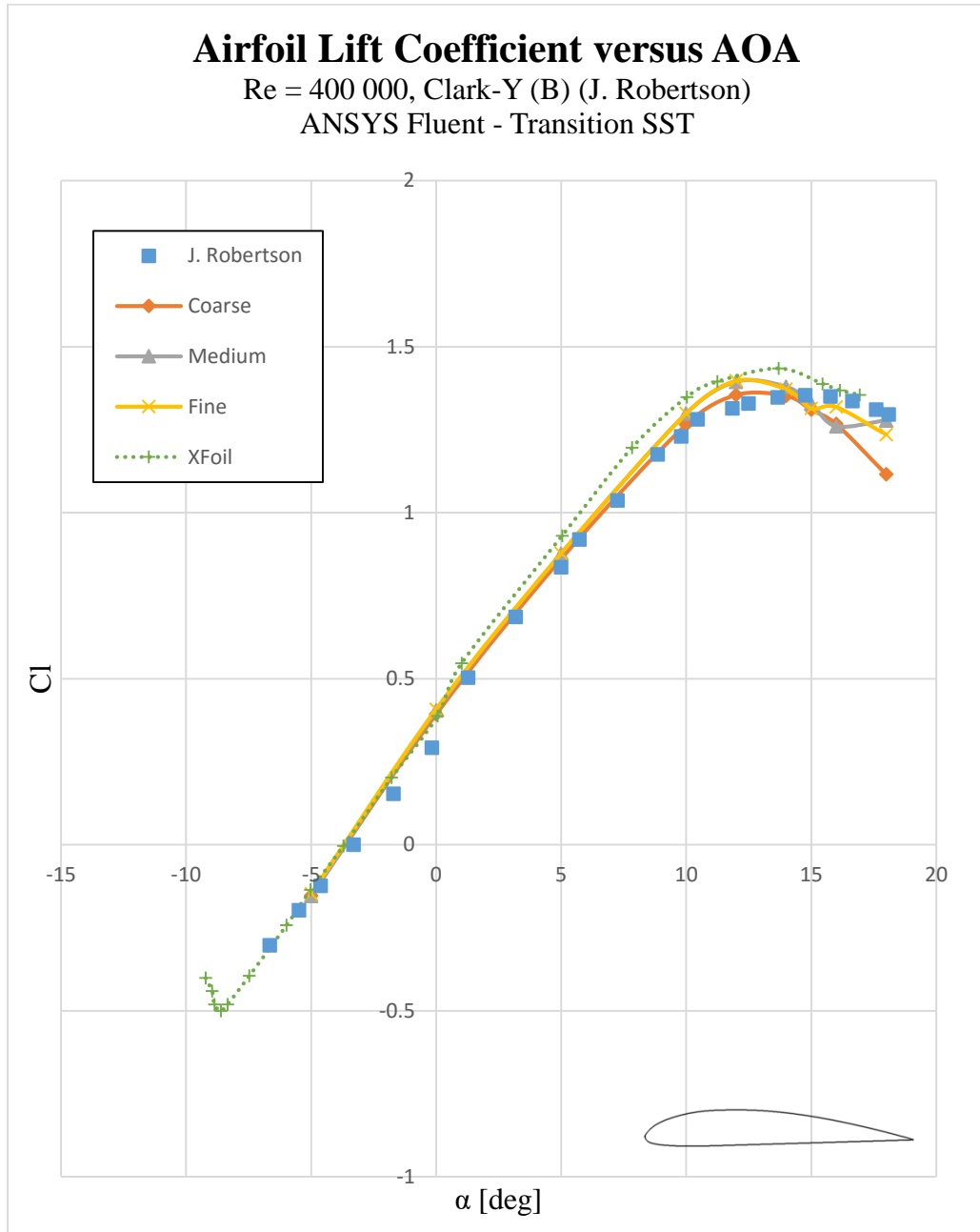


Figure 4. 4. 2-D lift coefficient versus AoA. Grid comparison for the Clark-Y airfoil.

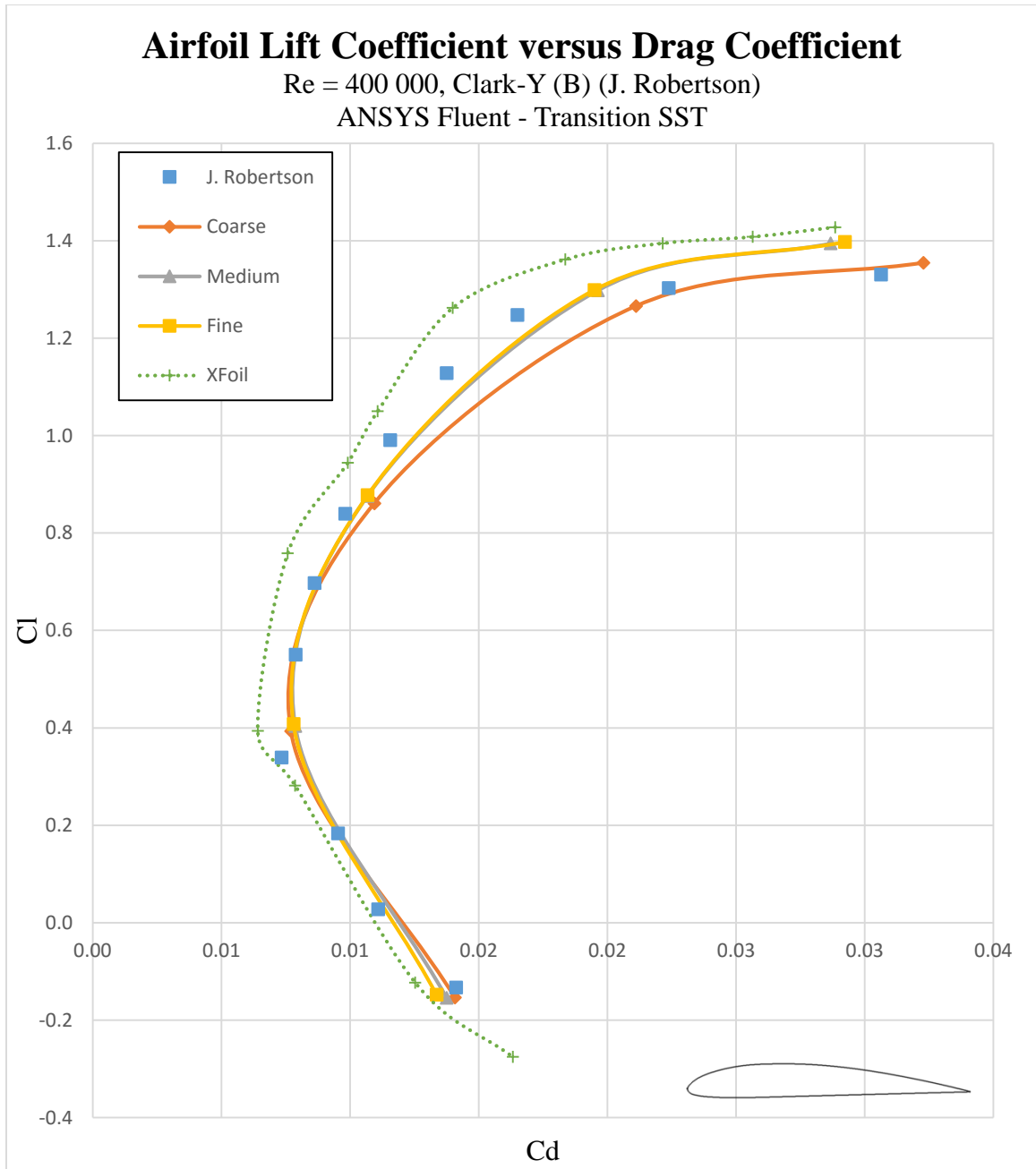


Figure 4. 5. 2-D drag coefficient versus lift coefficient grid comparison for the Clark-Y airfoil.

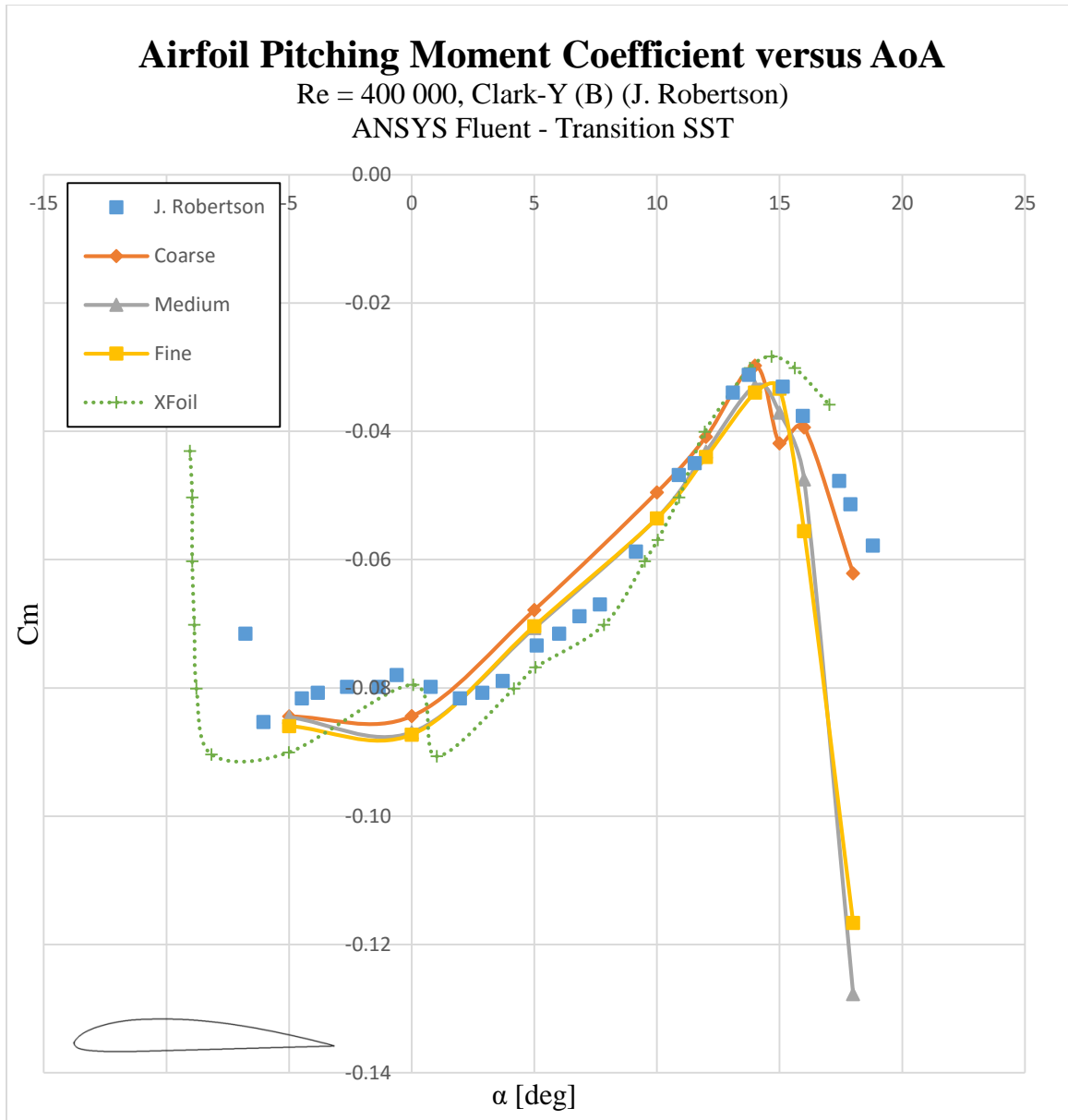


Figure 4. 6. 2-D pitching moment coefficient versus AoA. Grid comparison for the Clark-Y airfoil.

4.3. Plain Wing Analysis

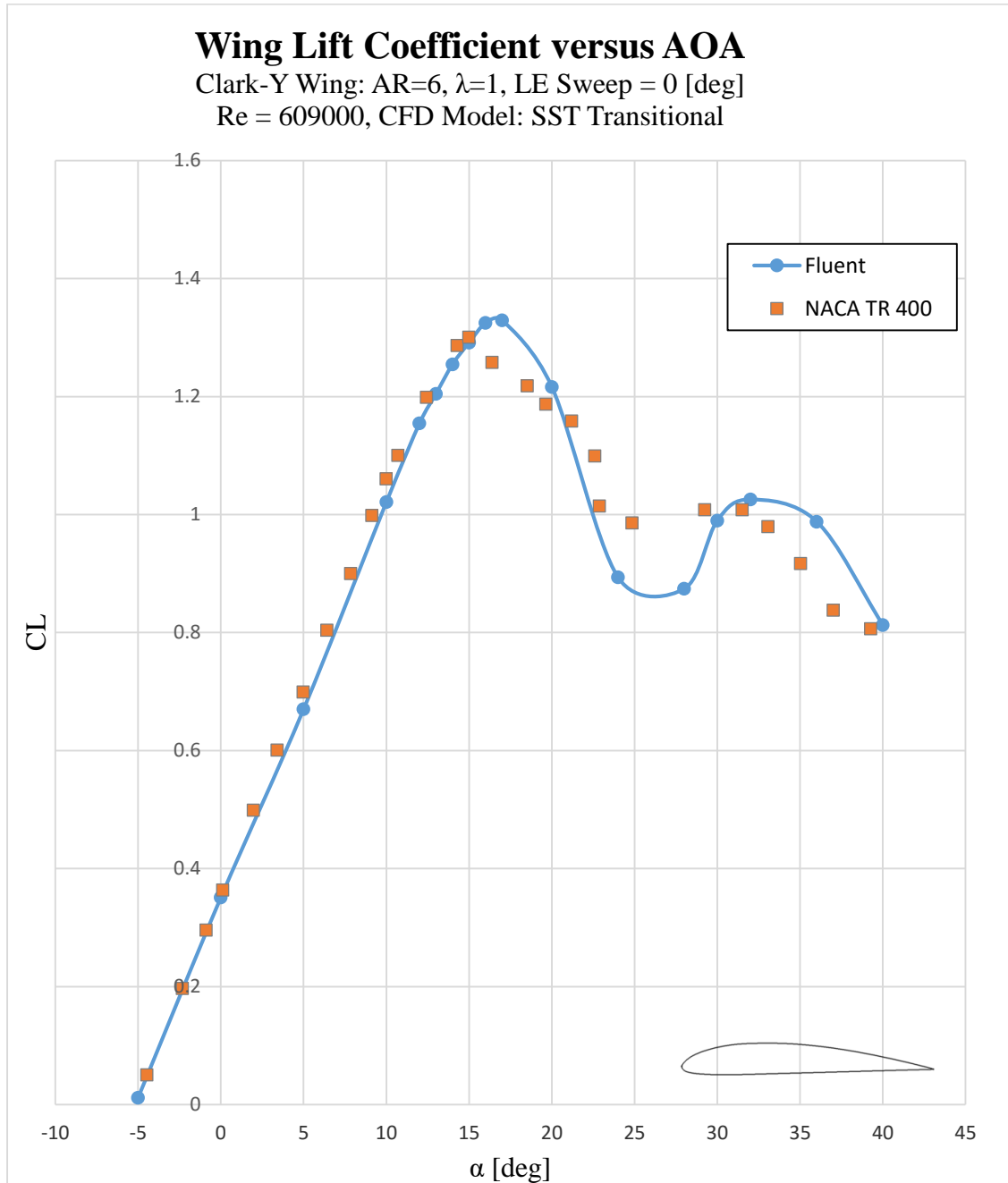


Figure 4. 7. Clark-Y wing lift coefficient versus angle of attack.

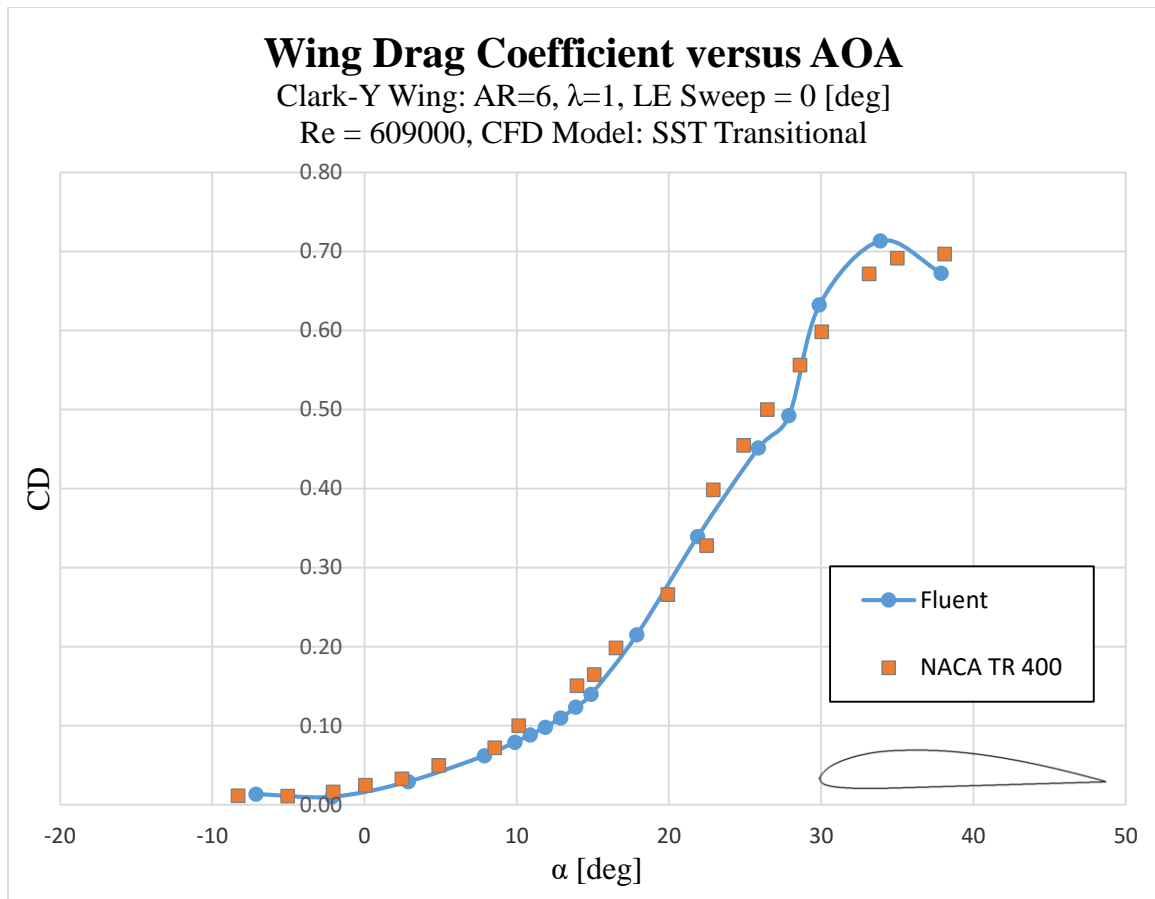


Figure 4. 8. Clark-Y wing drag coefficient versus angle of attack

4.4. Full – Slotted Wing Analysis

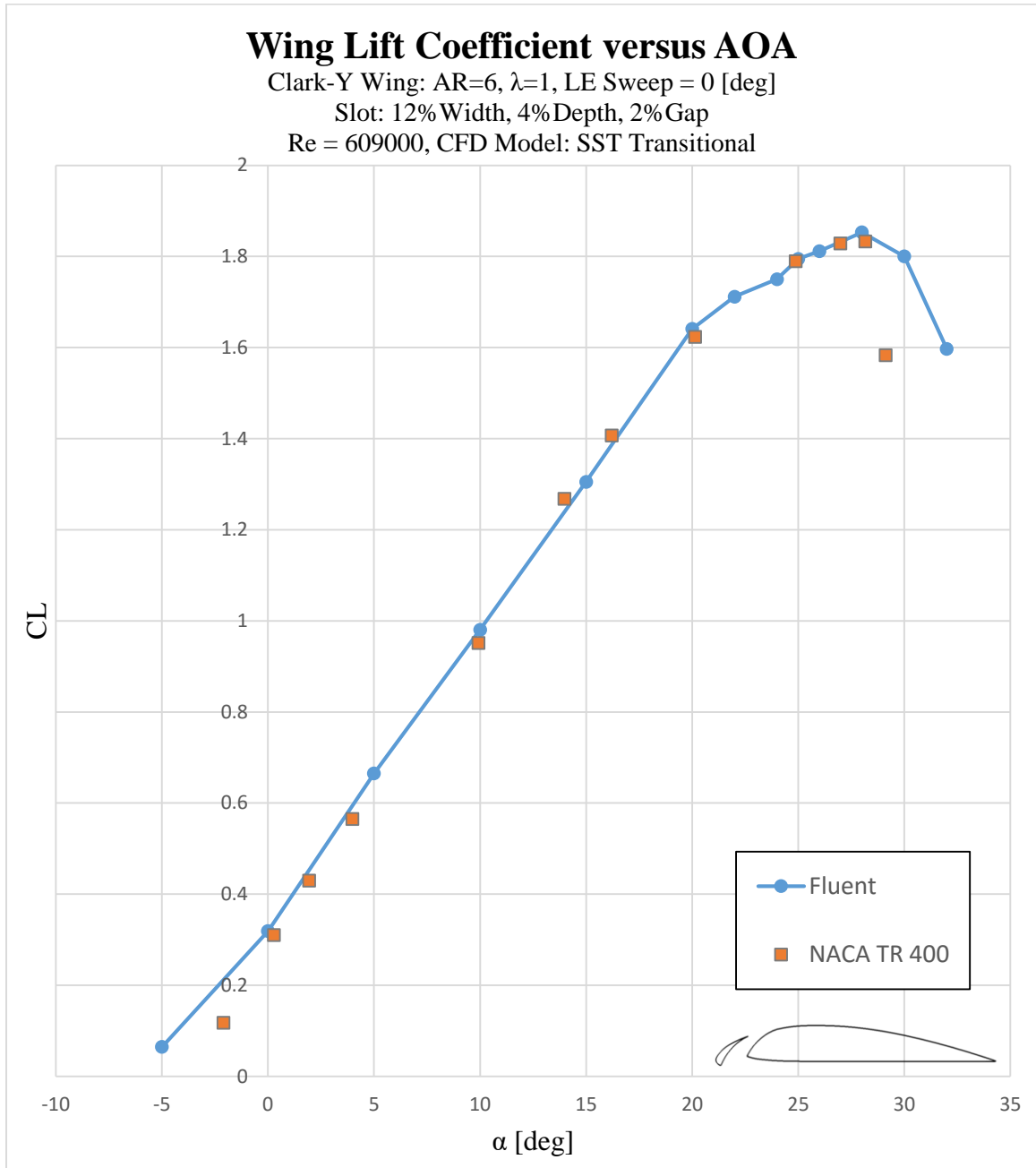


Figure 4. 9. Full-span slotted wing. Lift coefficient versus angle of attack.

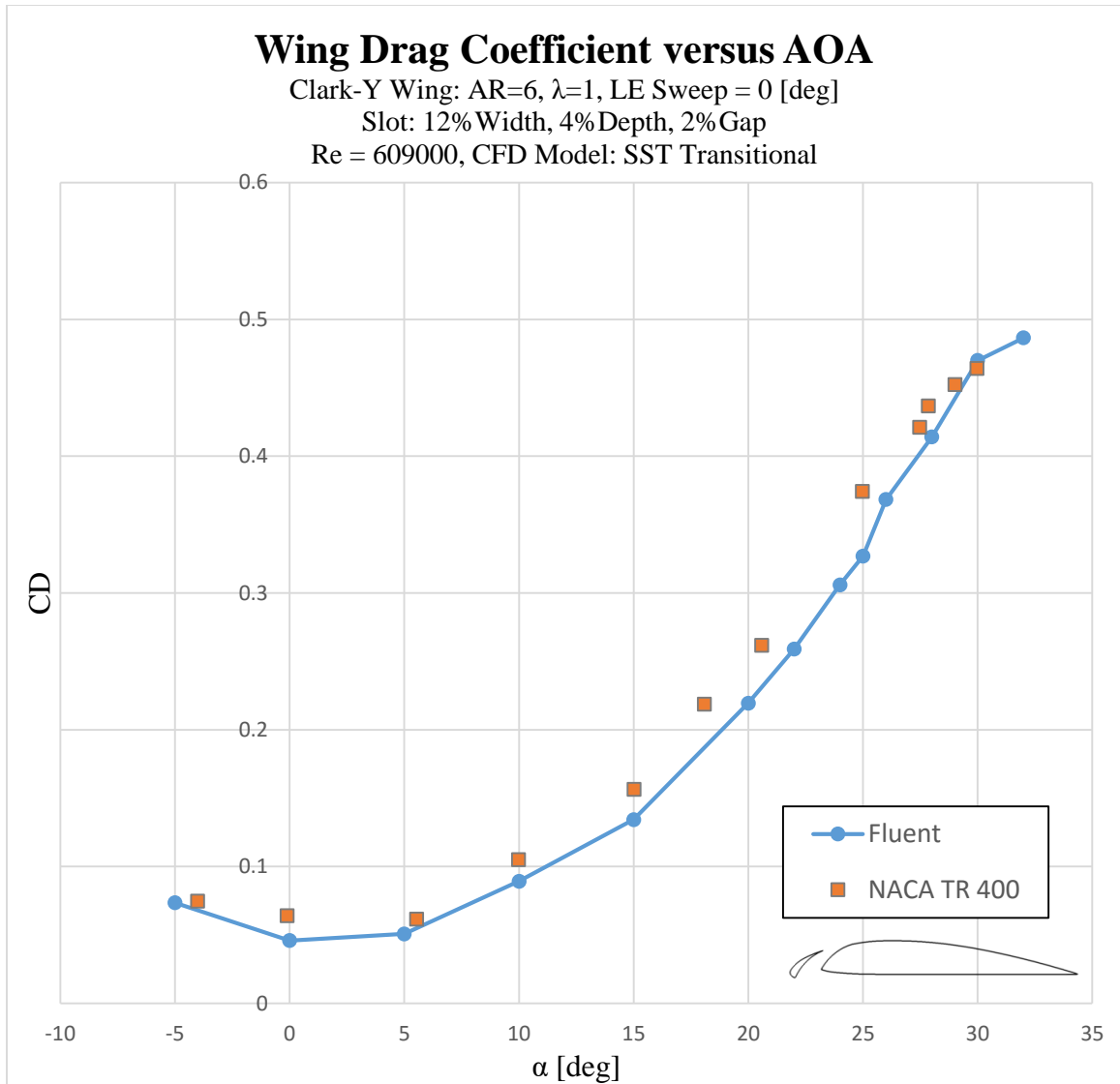


Figure 4. 10. Full-span slotted wing. Drag coefficient versus angle of attack.

4.5. Partially – Slotted Wings Analysis

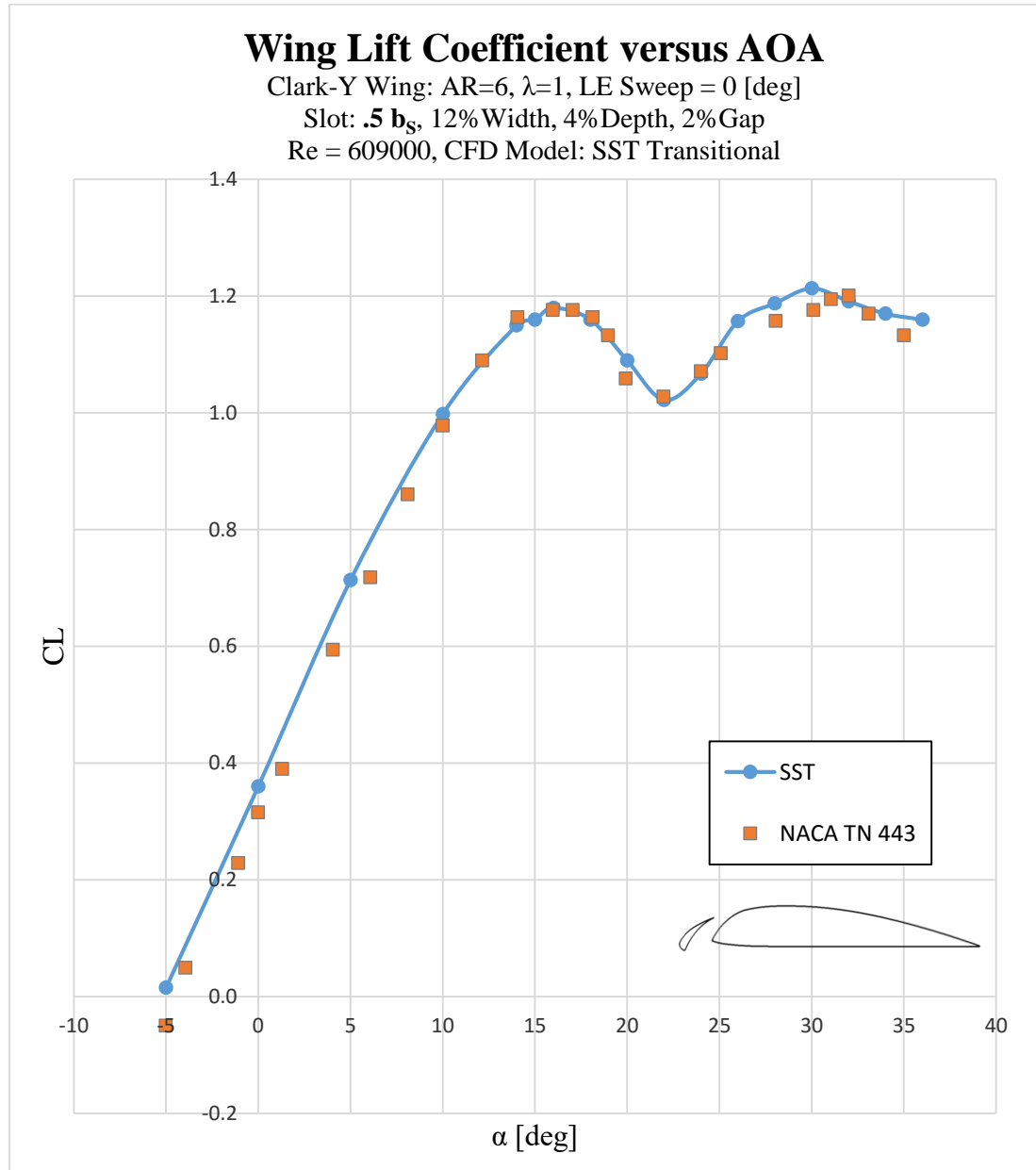


Figure 4. 11. Tip-slotted wing, $0.5b_s$. Lift coefficient versus angle of attack.

Wing Drag Coefficient versus AOA

Clark-Y Wing: AR=6, $\lambda=1$, LE Sweep = 0 [deg]

Slot: $.5 b_s$, 12% Width, 4% Depth, 2% Gap

Re = 609000, CFD Model: SST Transitional

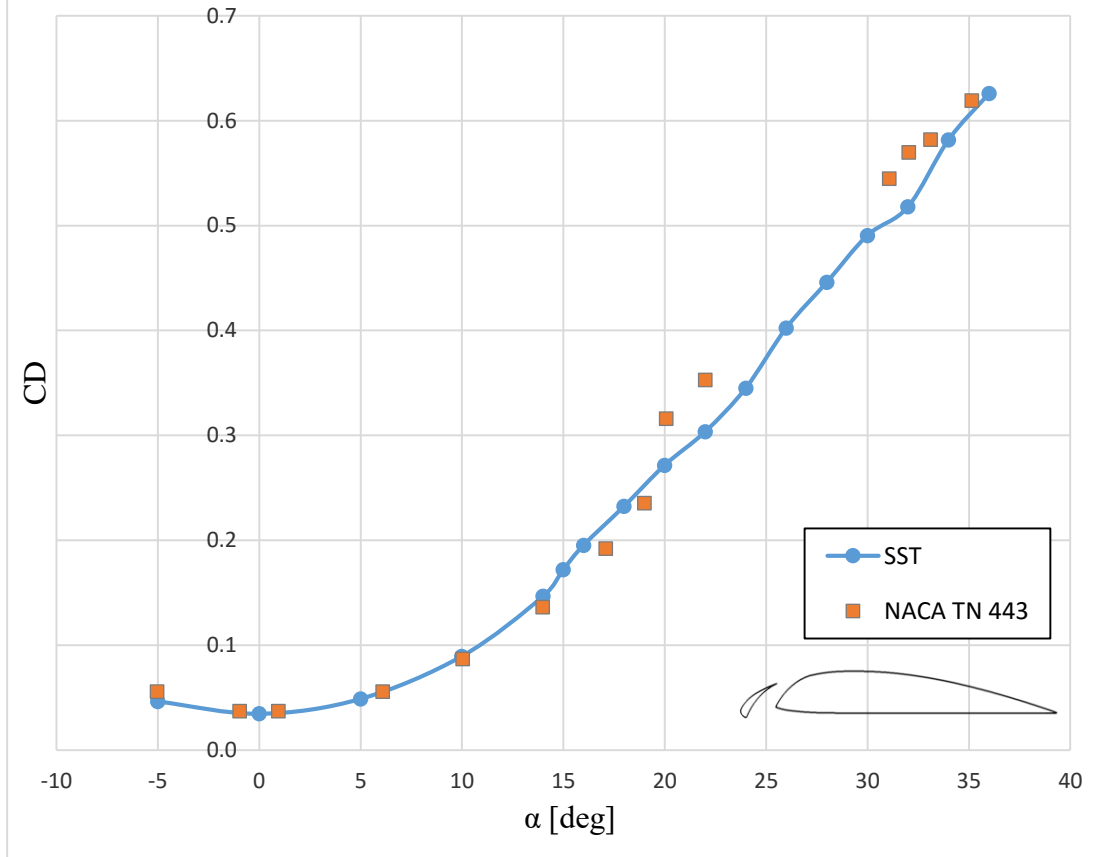


Figure 4. 12. Tip-slotted wing, $0.5b_s$. Drag coefficient versus angle of attack.

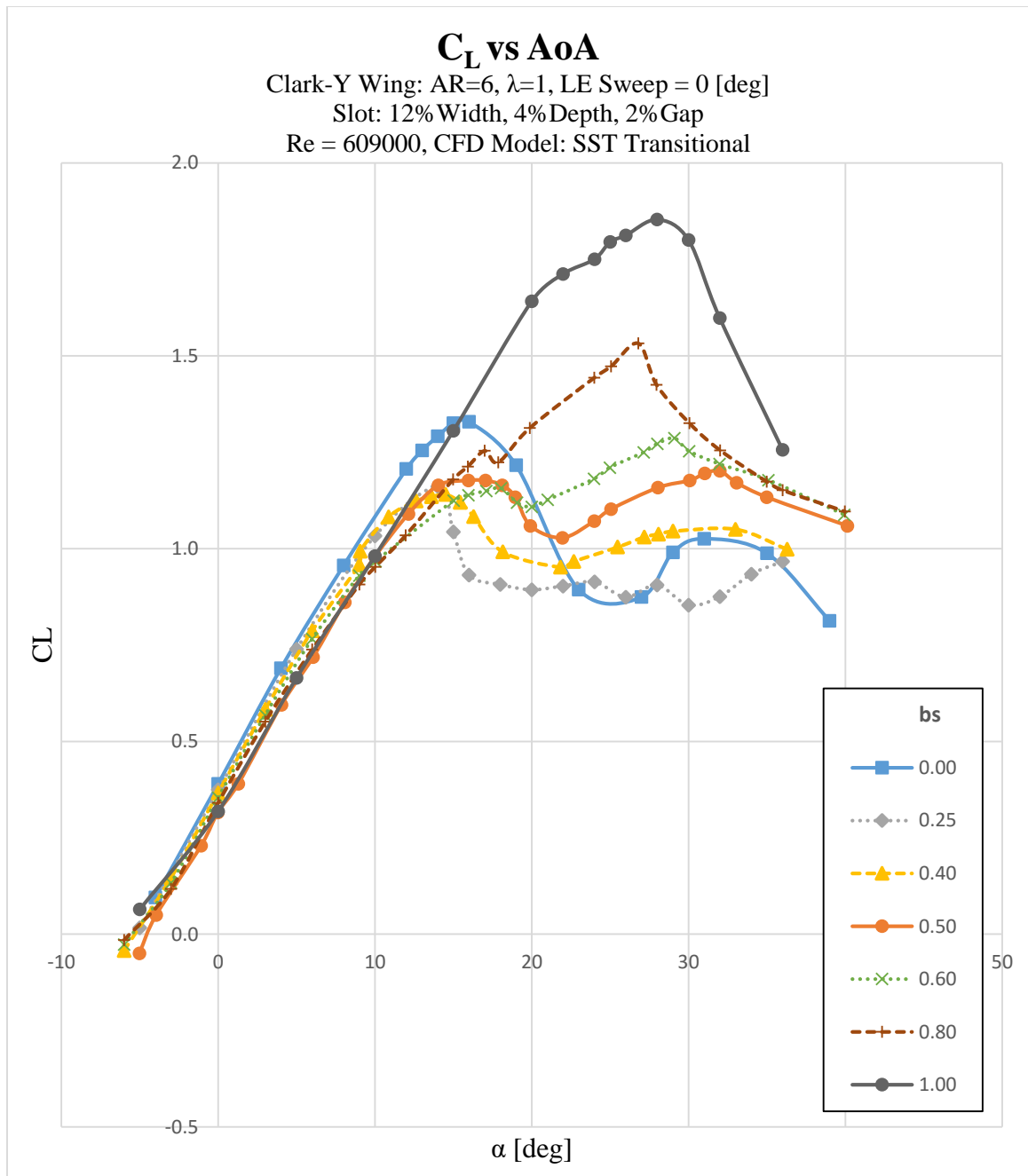


Figure 4. 13. Lift curves for all slotted wings

V. Analysis

5.1. CFD Prediction

Figure 4. 1 to Figure 4. 3 show the results obtained with the four different viscous models: K-Epsilon, SST Transitional, Spalart-Allmaras, and K-Omega. These figures also compare these results with experimental [1] and theoretical data [2]. By analyzing the lift coefficient curve (Figure 4. 1), all the models predicted results close to the experimental and theoretical data for small angles of attack (less than 10 degrees). Once the lift curve became non-linear, only the K-Epsilon and SST Transitional models produced similar data to the experimental and theoretical data. Predicting the flow characteristics is more difficult once flow starts to separate from the surface of the airfoil, hence the prediction of wrong results of the other two models. Observing the results at the drag polar curve (Figure 4. 2) and the pitching moment coefficient curve (Figure 4. 3), only the SST Transitional model yield results close to the experimental and theoretical data.

The Spalart-Allmaras is a viscous model that uses one-equation that solves the kinematic eddy viscosity, which is specifically for turbulent models [45]. K-Epsilon is a common model used for turbulent flows, solving two equations that simulate the turbulent properties of the flow (convection and diffusion) [46]. K-Omega is another model used for turbulent flows, solving two equations that account the scale and energy of the turbulence. Because the experimental data was obtained a transitional Reynolds number, all these previous models predicted wrong results by taking into account only turbulent flow into its equations. The SST Transitional model, on the other side, is a combination of the SST $\kappa - \omega$ transport equations with two additional equations that account the intermittency and transition criteria, in terms of momentum-thickness Reynolds number. This is why the SST

Transition model simulated the flow properties with more accuracy at the transitional Reynolds number.

Once the SST Transitional model was determined as the most accurate under the given conditions, a series of tests were performed to obtain a better understanding of this viscous model. The domain size needs to have a minimum dimension so that the solution does not reflect at its boundaries. For a C-grid type, the minimum dimensions are 16 chords as a radius and 20 chords in the downstream length. The model also showed to have a high dependency on the mesh resolution around the airfoil due to its wall-functions. In order for these functions to resolve the problems domineering at the boundary layer correctly, a y^+ of 3 was required for all the models. Finally, the grid independence study showed how the model, with a properly dimensioned grid, converged to the same solution independent on the grid density.

The two-dimensional and three-dimensional solutions that the SST Transitional model converged were compared with experimental data. Figure 4. 7 to Figure 4. 12 show the comparisons for the three-dimensional wings. The obtained results, for all these cases, showed the same values as the experimental data for small angles of attack, where a steady state convergence was obtained. For large angles of attack, the solutions were not the same as the experimental data, but they had the same trend. This difference is due to the pseudo-steady-state convergence obtained for large angles of attack, where the solution was an average of the oscillations in the force coefficient monitors.

5.2. Wing Properties Estimation

The purpose of this section is to predict the three-dimensional capabilities of a wing from the two-dimensional properties of its airfoil. Section 2.1.2. shows the methodology

to perform this estimation. This is applied to the data obtain for the plain and slotted airfoil, and compared to the obtained data of the plain and full-slotted wing in order to find the accuracy of the method.

5.2.1. Data Trend

To define the characteristic points in the lift curve, a trending analysis was performed on the obtained data for both, the linear and the non-linear regions. This helped identifying important parameters easily, such as, the lift curve slope, maximum lift coefficient, and the angle of attack for stall. Figure 5. 1 shows the trending lines for the linear region of the two-dimensional lift curve for the plain and slotted airfoil. The same procedure was used for all the obtained data, including the use of polynomials of higher grade for non-linear regions. All the trendlines have a R-squared of 0.98. Figure 5. 2 shows the trendlines for the lift curves of the plain and slotted airfoils for all ranges in the angle of attack. The equation of these trendlines facilitate the determination of the properties of these curves, which are shown in Table 5. 1.

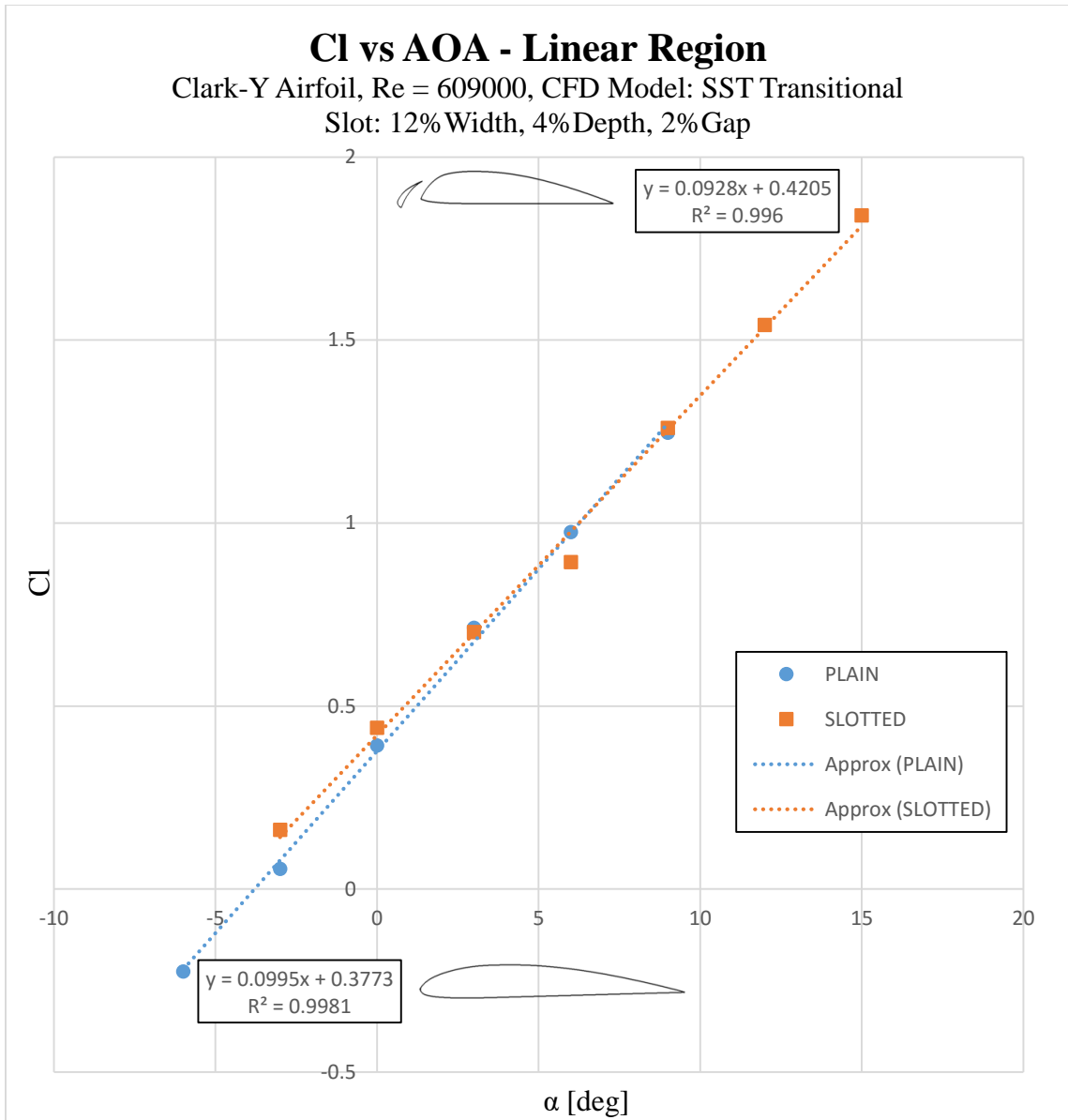


Figure 5. 1. Trendline for the linear region of the lift coefficient for the two-dimensional airfoils.

Airfoil Lift Coefficient versus AOA

Clark-Y Airfoil, Re = 609000, CFD Model: SST Transitional
Slot: 12% Width, 4% Depth, 2% Gap

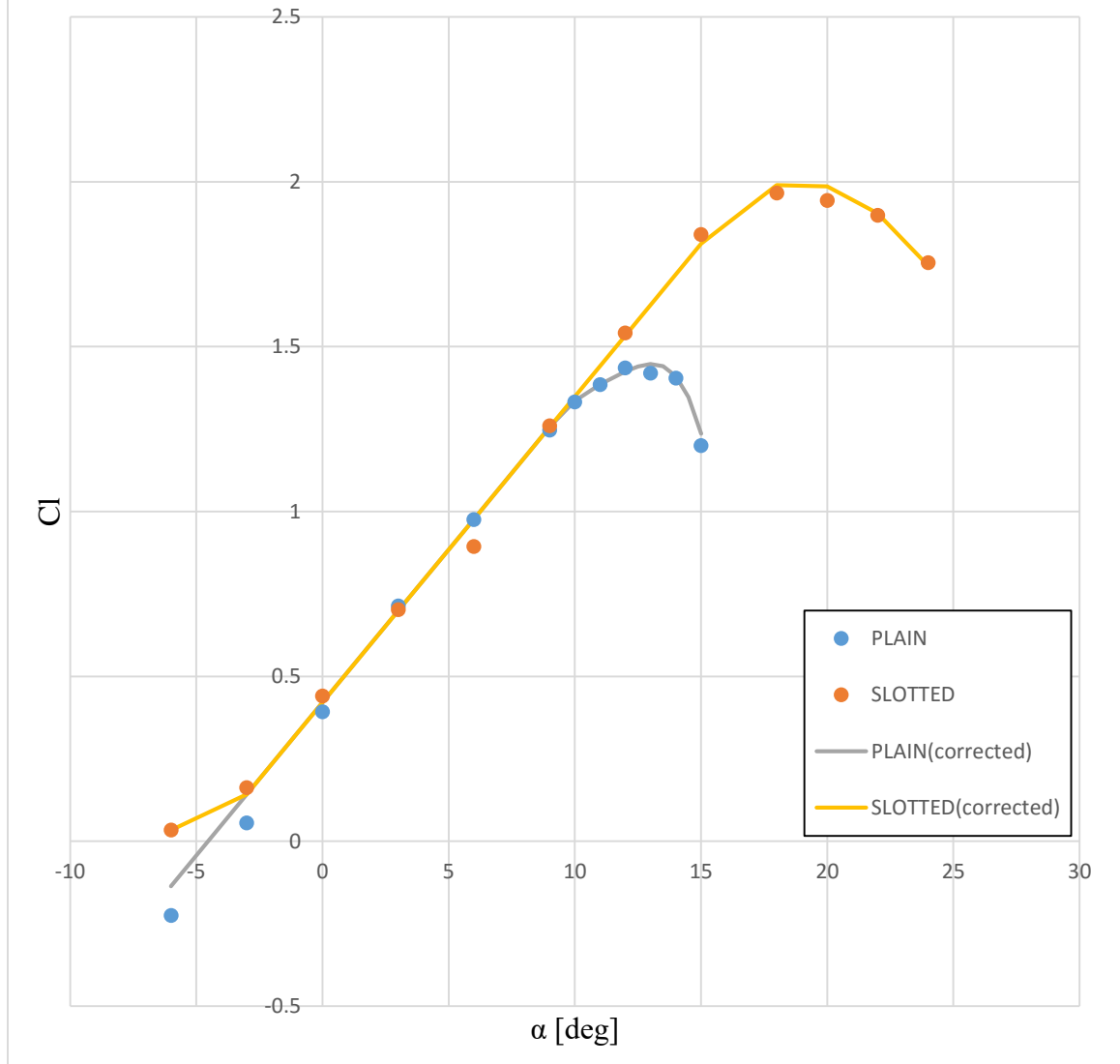


Figure 5. 2. Lift curve trending curve for all angles of attack.

Table 5. 1. Properties form the lift curves of the plain and slotted airfoil, and the plain and full-slotted wing.

	2-D		3-D	
	Plain	Slotted	Plain	Slotted
$C_{L\alpha}$ [deg]	0.0995	0.0928	0.0745	0.0680
C_{Lo}	0.38	0.42	0.26	0.35
C_{Lmax}	1.45	2.00	1.32	1.81
α_{stall} [deg]	13.06	18.90	16.91	23.77
α_{zL} [deg]	-3.79	-4.53	-3.53	-5.14

5.2.2. Transformation from 2D to 3D

The three-dimensional properties where estimated using the coefficients in Table 5. 1 for the two-dimensional cases and the equations (2. 6) to (2. 11) from section 2.1.2. The results and comparison with the CFD results are shown at Table 5. 2 and Table 5. 3. Also, Figure 5. 3 and Figure 5. 4 shows how the method predicts the three-dimensional properties for the plain and full-slotted wing, and how these compared to the CFD results.

Table 5. 2. Three-dimensional coefficient estimations for the plain wing.

	PLAIN WING		
	3D - Theoretical	3D - CFD	% Difference
$C_{L\alpha}$ [deg]	0.0739	0.0745	0.84
C_{Lo}	0.28	0.26	6.42
C_{Lmax}	1.30	1.32	1.22
α_{stall} [deg]	15.84	16.91	6.50
α_{zL} [deg]	-3.79	-3.53	7.26

Table 5. 3. Three-dimensional coefficient estimation for the full-slotted wing

	FULL-SLOTTED WING		
	3D - Theoretical	3D - CFD	% Difference
$C_{L\alpha}$ [deg]	0.070	0.068	3.27
C_{Lo}	0.32	0.35	9.26
C_{Lmax}	1.80	1.81	0.39
α_{stall} [deg]	23.06	23.77	3.03
α_{zL} [deg]	-4.53	-5.14	12.53

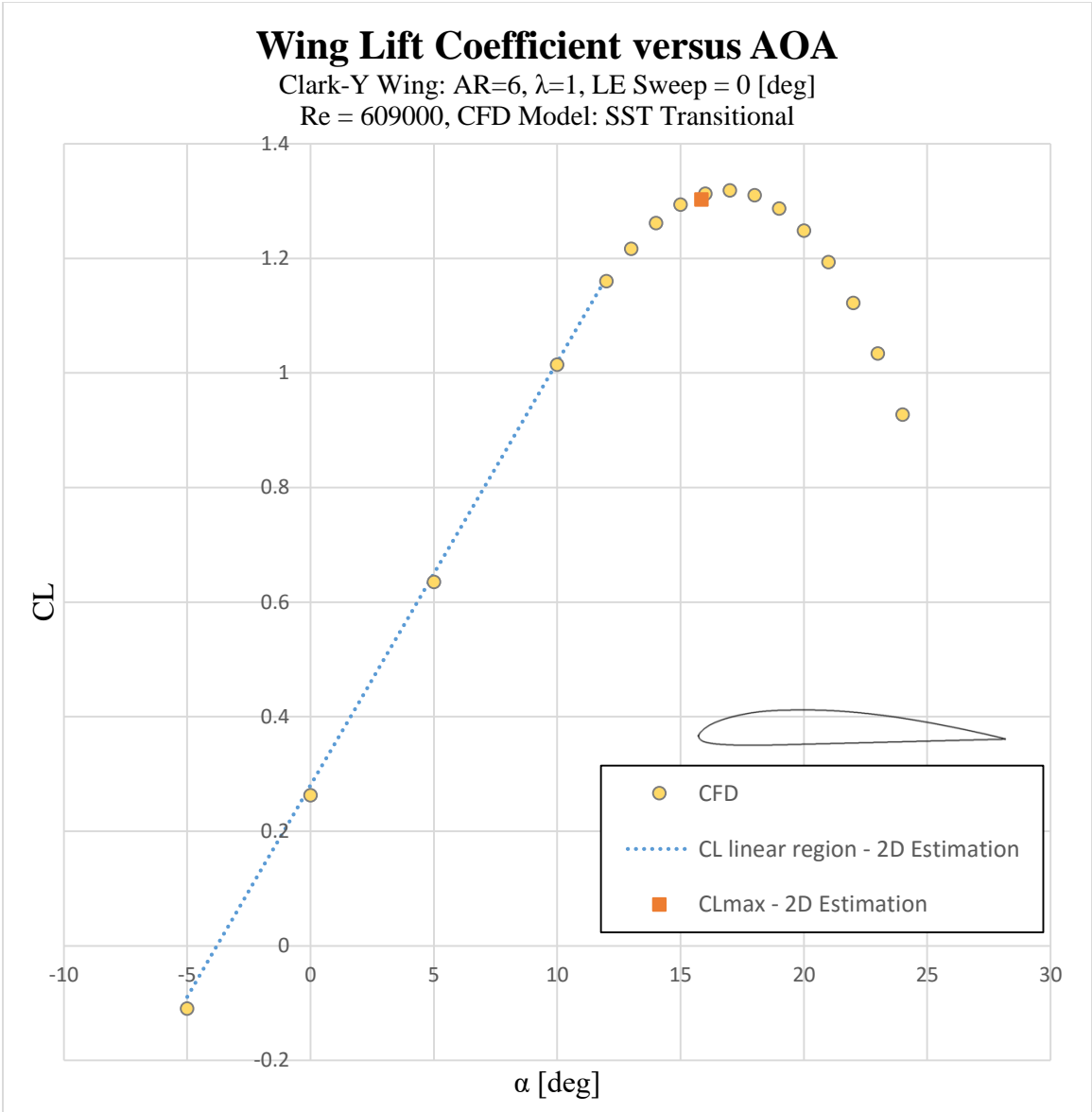


Figure 5. 3. Three-dimensional coefficient estimation for the plain wing.



Figure 5. 4. Three-dimensional coefficient estimation for the full-slotted wing.

It can be seen that the method to predict a three-dimensional wing behavior from two-dimensional data is accurate, especially for the linear region of the lift curve. The method works for the plain wing (taking the plain airfoil as a reference), and for the full-slotted wing (taking the slotted airfoil as a reference). This is highly important because it saves time during the design phase of a wing (plain or full-slotted). There is the need to do

only a two-dimensional CFD analysis of the airfoil of interest to predict its properties as a three-dimensional wing. A three-dimensional analysis is needed only if the post-stall properties are required.

5.3. Lift Comparison

After all the CFD simulations were performed in the different slotted wing models, all the data was compiled by sections to be analyzed independently from each other. In this section the lift coefficient curve of all the models is analyzed by its characteristic parts, such as, maximum lift coefficient, stall angle, and lift curve slope.

5.3.1. Maximum Lift Coefficient

Figure 4. 13 shows the lift curves for all the slotted wings. It can be seen that the curves have two peaks. The first peak corresponds mostly to the lift generated by the unslotted portion of the wing, while the second peak corresponds to the slotted portion. For shorter slots, the unslotted wing generates most of the lift, making the first peak the maximum between the two. This is why the second peak for small slotted-wings (slots smaller than 40% span) is neglected. Both of these peaks have the same value with a 50% span slot (the unslotted and slotted section generates the same amount of lift).

Figure 5. 5 shows the compilation of the first peak in the lift curve for all the analyzed models. It also shows a comparison between the different polynomials used to create an approximation that matches the tendency of this property. Equation (5. 1) shows the 4th order polynomial that fits the data to accurately predict the behavior of the first peak for all cases.

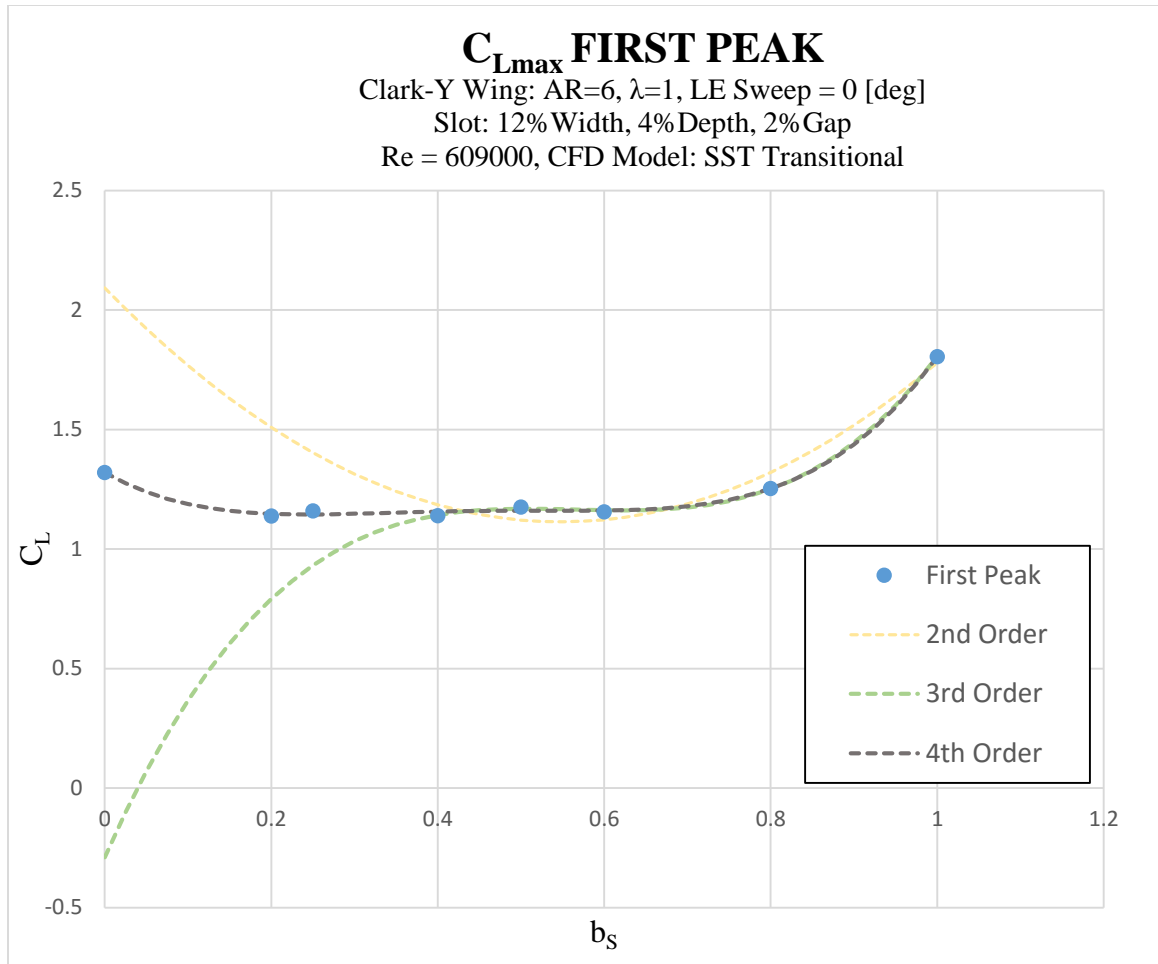


Figure 5. 5. C_{Lmax} for the first peak of all the slotted wings.

$$C_{L_{max1}} = (5.66 \cdot b_s^4 - 9.82 \cdot b_s^3 + 6.05 \cdot b_s^2 - 1.52 \cdot b_s + 1) \cdot C_{L_{mo}} \quad (5.1)$$

Where b_s stands for the slot span ratio (see Figure 3. 14), and $C_{L_{mo}}$ is the maximum lift coefficient for the plain wing.

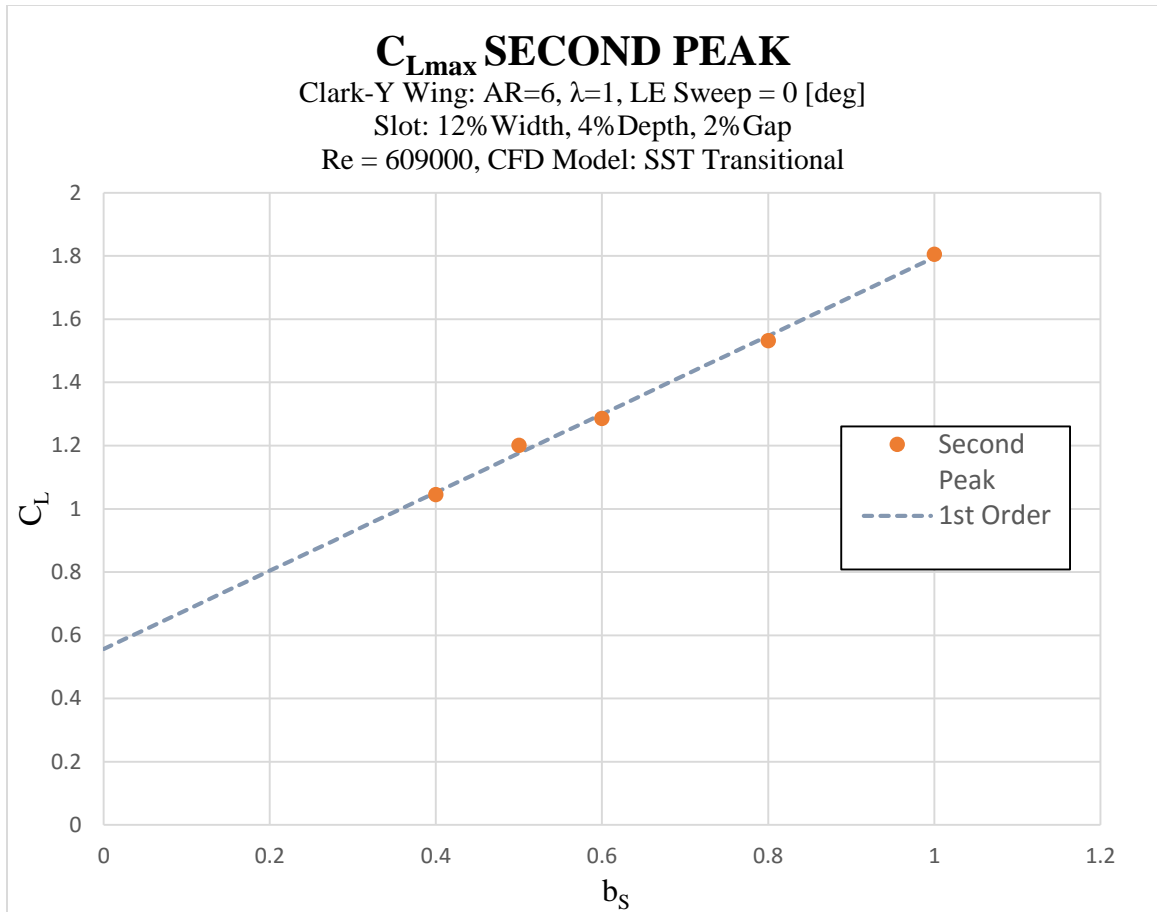


Figure 5. 6. C_{Lmax} for the second peak of all the slotted wings.

As was stated previously, not all the slotted wings showed a second peak in the lift curve. The second peak becomes significant for wings with slots bigger than 40% of the wing span. Figure 5. 6 shows the compilation of the second peak of the lift curve for all the models where it was significant. It also shows how the change in the slots size affects proportional to the magnitude of the second peak of the lift coefficient. This linear relation can be expressed using equation (5. 2).

$$C_{Lmax2} = 1.24 \cdot b_s + 0.557 \quad (5. 2)$$

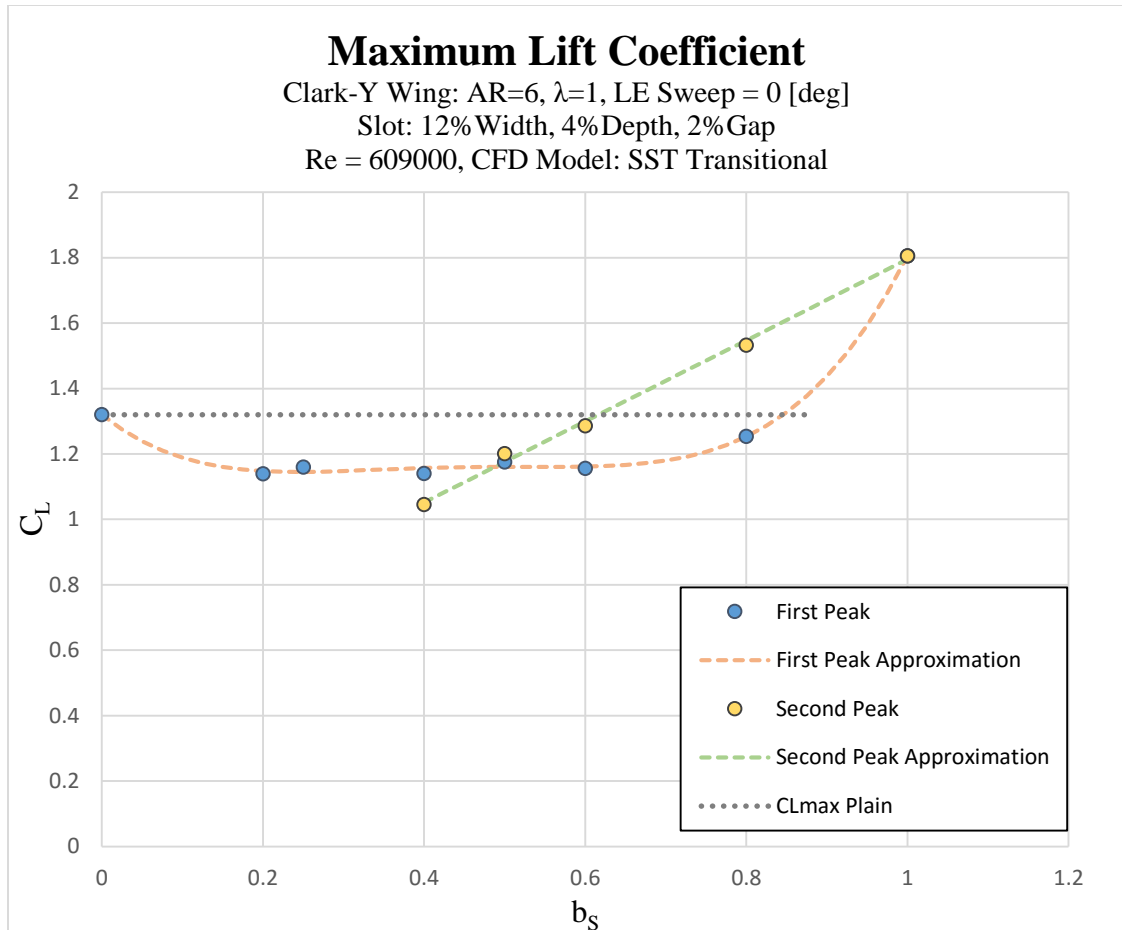


Figure 5. 7. C_{Lmax} of all slotted wings.

Figure 5. 7 shows the compilation of the maximum lift coefficients of all the models. It can be seen that both peaks become equal with a 50% span slot. It also shows how the maximum lift coefficient from the slotted wings compares to the one produced by the plain wing. A wing needs a slot span larger than 60% of the wing's span in order to generate, at the second peak, a maximum lift coefficient larger than the one produced by the plain wing. Wings with slots spans greater than 85% of the wing span generate, at the first peak, a maximum lift coefficient greater than the one generated by the plain wing.

5.3.2. Stall Angle

Because the lift curve for every analyzed wing has two peaks, both of the angles of attack where this peaks occurs are of interest. The first peak is of high importance for slotted-wings with slots smaller than 40% span, where the lift curve has a predominant post-stall decrease. Figure 5. 8 shows the angles where the first peak of the lift curve occurs for all analyzed wings. These angles are not related directly with the slot size, but they can be approximated to a single value (shown as 1st order in Figure 5. 8). Equation (5. 3) shows the approximation to find the angle of stall for the first peak (α_{stall1}) in the lift curve for all the different slot sizes.

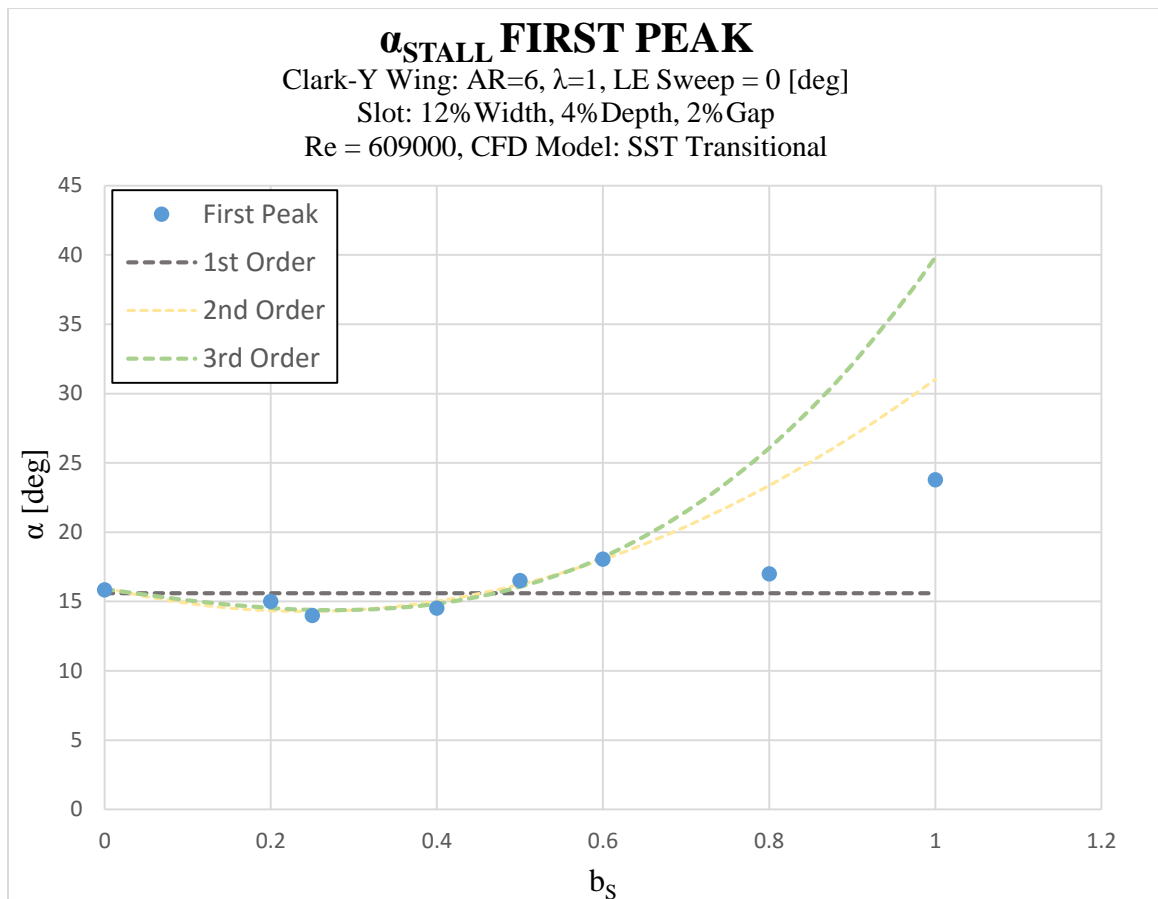


Figure 5. 8. Angle of stall for the first peak of all the slotted wings.

$$\alpha_{stall1} = 0.985 \cdot \alpha_{So} \quad (5.3)$$

The second peak the lift curve predominates for wings with slots larger than 40% of the wing span. Figure 5. 9 shows the compilation of the angle of stall for the second peak of the lift curve for wings with slots larger than 40% of the wing span. It can be seen that the angle of attack for the second peak (α_{stall2}) decreases proportionally with respect the slot span ratio (b_S). Equation (5. 4) shows the relation between these two.

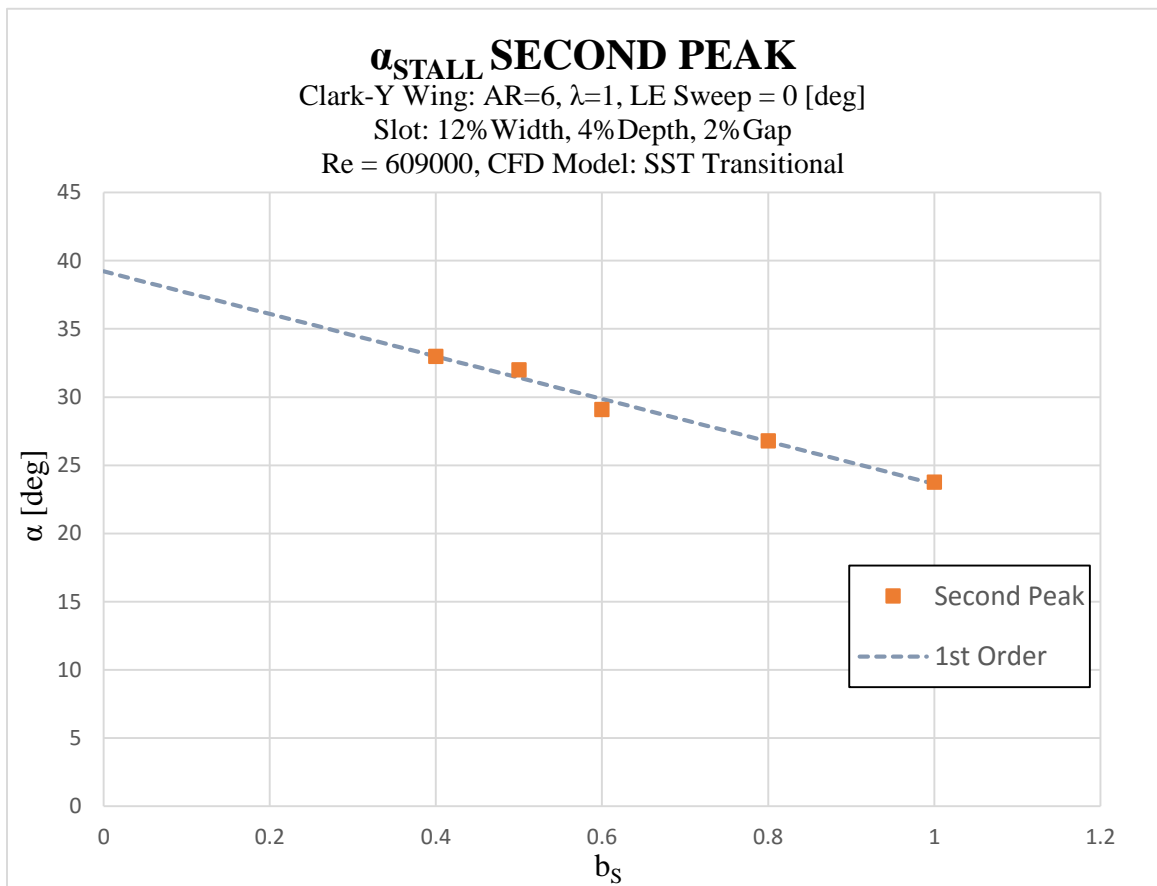


Figure 5. 9. Angle of stall for the second peak of all slotted wings.

$$\alpha_{stall2} = -15.426 \cdot b_S + 39.2 \quad (5.4)$$

5.3.3. Lift Curve Slope

Figure 5. 10 shows the relation between the lift curve slopes and the slot span ratio of all tested models. Equation (5. 5) expresses how the lift curve slope reduces gradually in function of the slot span ratio, where $C_{L\alpha_0}$ stands for the lift curve slope of the plain wing. This reduction in the lift curve slope shows that partially slotted wing has a larger induced drag than a plain wing. The larger the span of the slot, the larger the induced drag that the wing is going to produce. This is expected because a slotted wing has a lower aspect ratio than a plain wing (the reference area increases maintaining the same wing span), which creates a larger induce drag, decreasing the lift curve slope.

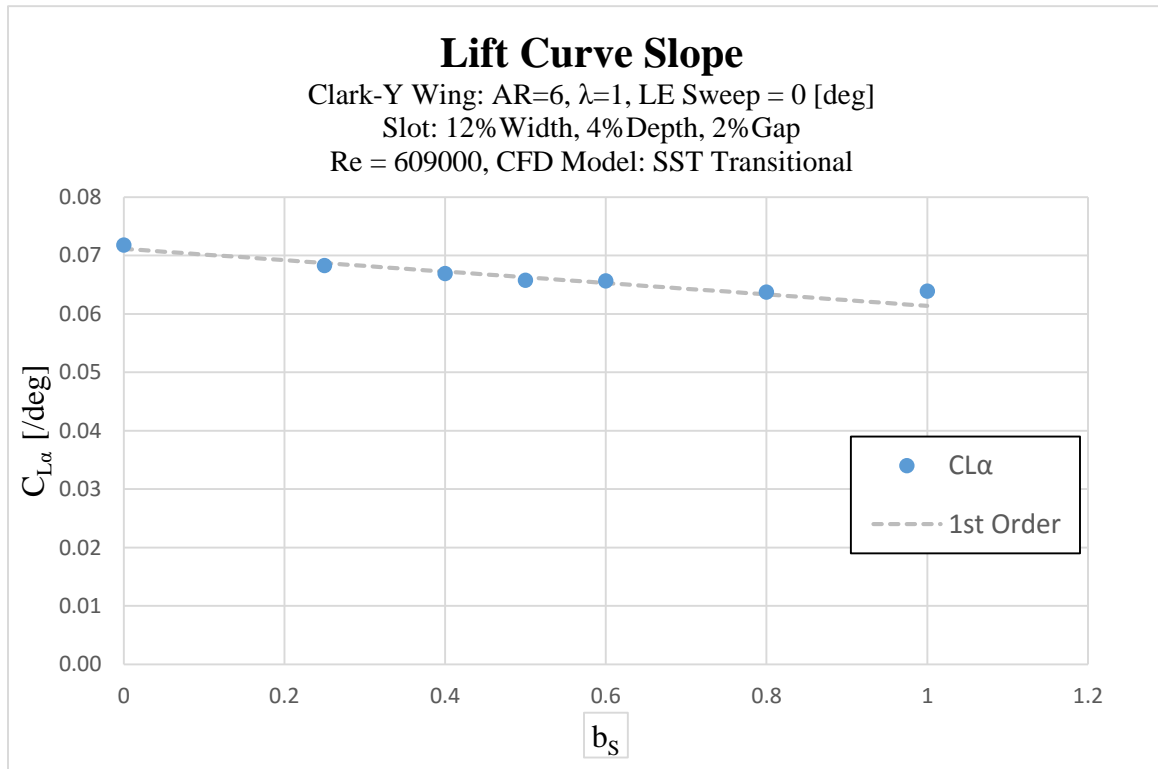


Figure 5. 10. Lift curve slope for the tested models.

$$C_{L\alpha} = -0.0096b_s + C_{L\alpha_0} \quad (5. 5)$$

5.3.4. Lift Coefficient at Zero AOA

Figure 5. 11 shows the lift coefficient at a zero angle of attack for the tested models. As the span of the slot increase its size, the wing starts to produce less lift at low angles of attack (see Figure 5. 12). For this reason, slots are only efficient for high angles of attack. Equation (5. 6) states the relation between the slot span ratio and the lift coefficient at zero angle of attack, where C'_{Lo} stands for the lift coefficient at zero AoA of the plain wing.

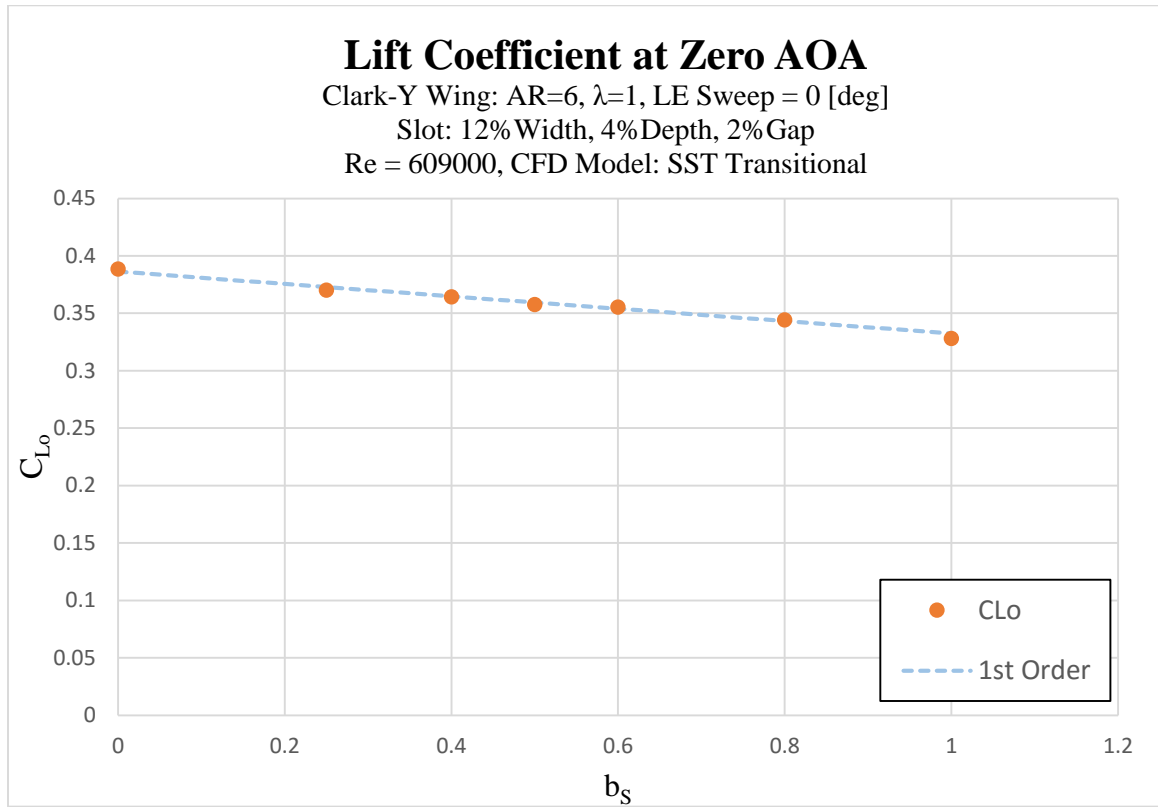


Figure 5. 11. Lift coefficient at zero angle of attack of all tested models.

$$C_{Lo} = -0.053b_s + C'_{Lo} \quad (5. 6)$$

5.3.5. Angle of Attack at Zero Lift

Figure 5. 12 shows the lift curves for all the tested models using the tendency approximations in the lift curve slope and the lift at zero AoA from equations (5. 5) and (5. 6). The only point in common between all the curves is the angle of attack where the lift is predicted to be zero. This is corroborated with the data obtained from the CFD simulations, where the lift coefficient was zero at the same angle of attack. This was calculated using equation (5. 7), obtaining a variation of $\mp .001$ between the obtained angles.

$$\alpha_{ZL} = -\frac{C_{L0}}{C_{L\alpha}} \quad (5.7)$$

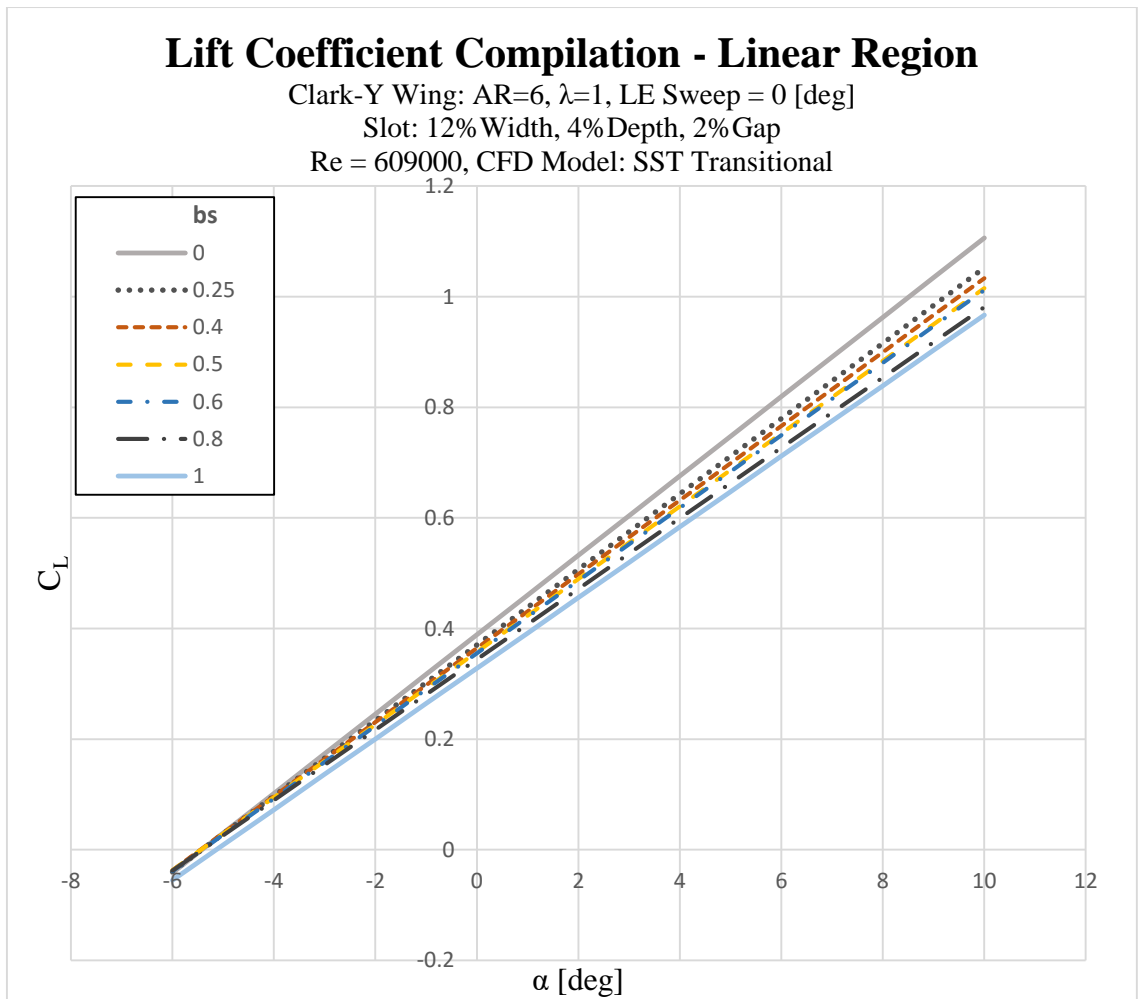


Figure 5. 12. Tendency curves for the lift coefficient versus AOA (linear region).

5.4. Drag Comparison

For the drag analysis, the drag coefficient versus AoA curve and the drag coefficient versus lift coefficient curve were compared in order to obtain their minimums. The values used in these comparison were the ones that could be approximated by a second degree polynomial. The difference between these minimums were less than 5%, and Figure 5. 13 show the average between the minimum of these two curves. As it was stated in section 5.3.3, the aspect ratio of the wing decreases as the slot-span increases, producing a larger induced drag. Due to this, the minimum drag coefficient increases as the slot-span increases. Equation (5. 8) states the linear relation between the slot-span and the minimum drag coefficient, where C_{Dmin_o} stands for the minimum drag coefficient of the plain wing.

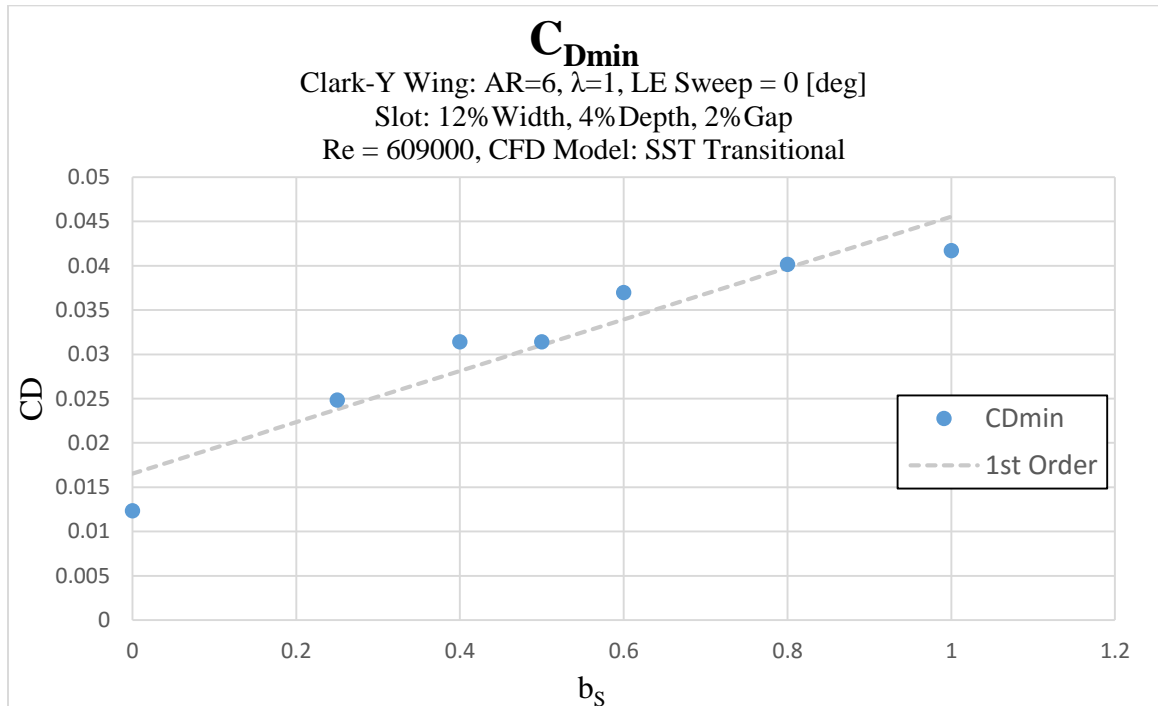


Figure 5. 13. Minimum drag coefficient of all tested models.

$$C_{Dmin} = 0.029b_s + 1.34C_{Dmin_o} \quad (5. 8)$$

VI. Validation

Once the relations were set for all the models, a new slotted-wing was analyzed in order to compare the results of this model with the defined relations. The new model had a slot span of 75% of the wing's span, and Figure 6. 1 to Figure 6. 7 show how the aerodynamic characteristics of this model compare with the previously defined relations.

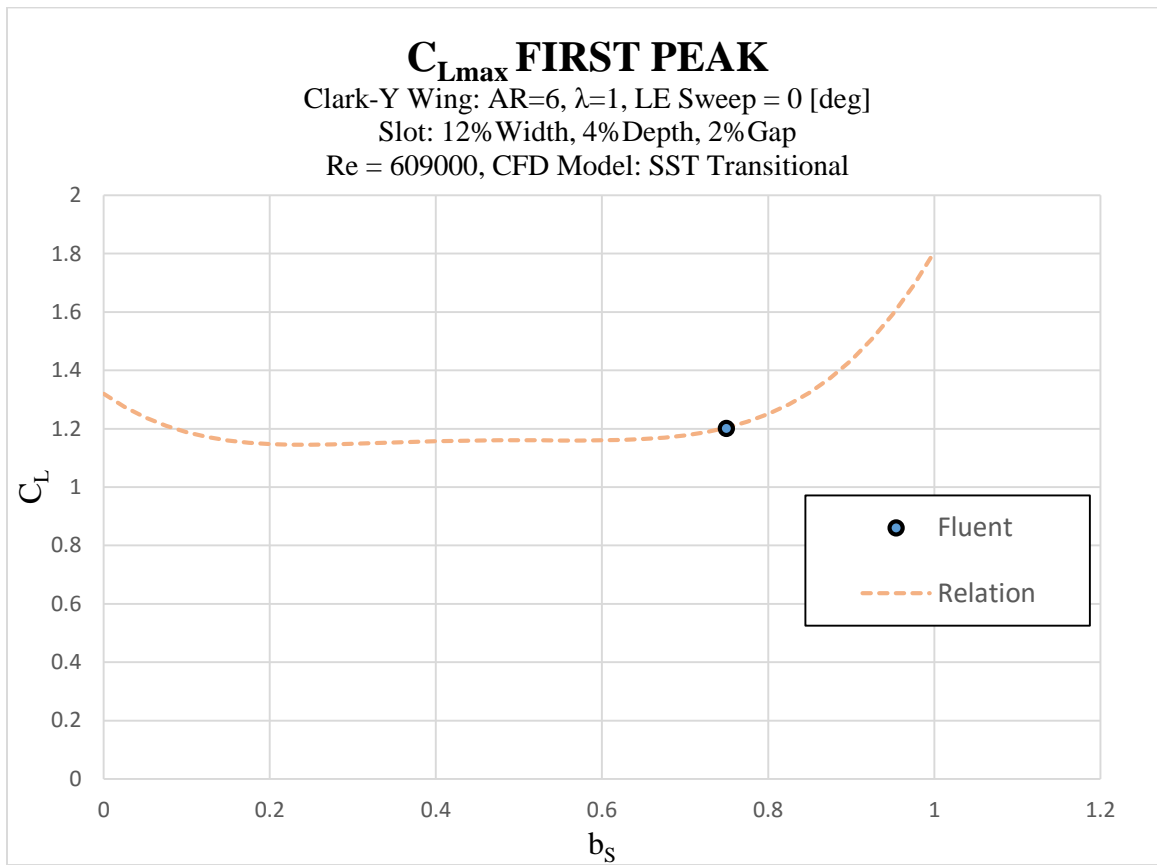


Figure 6. 1. Validation of the C_{Lmax} for the first peak relation.

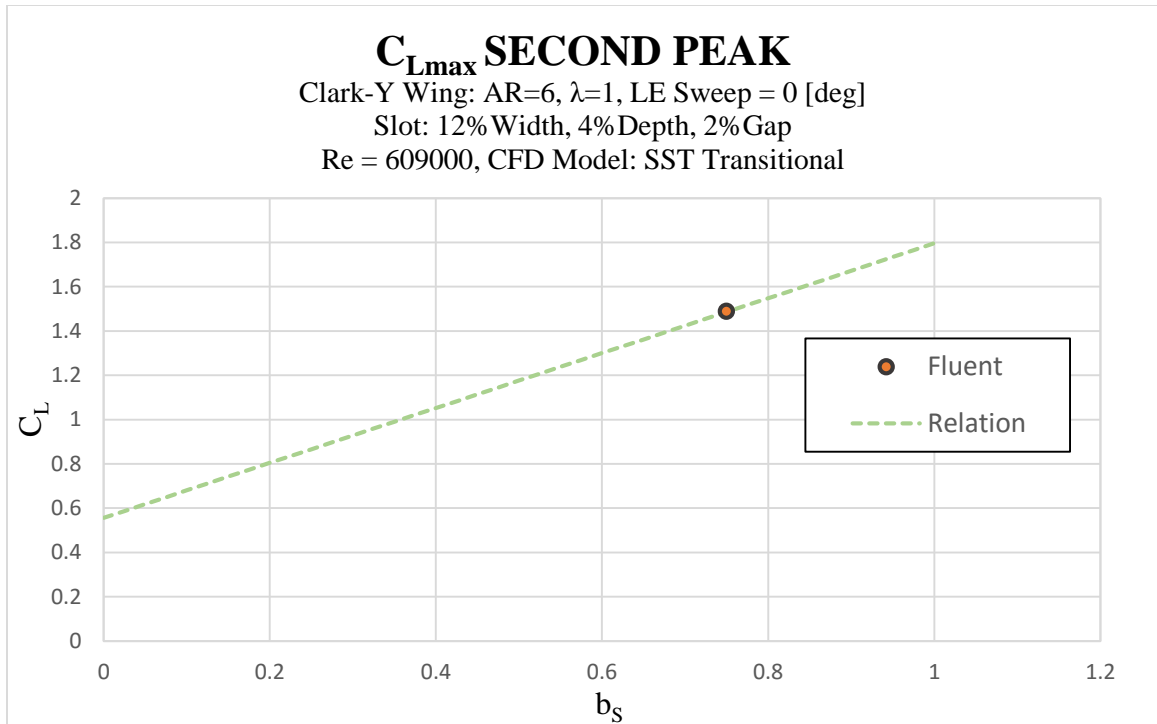


Figure 6. 2. Validation of the C_{Lmax} for the second peak relation.

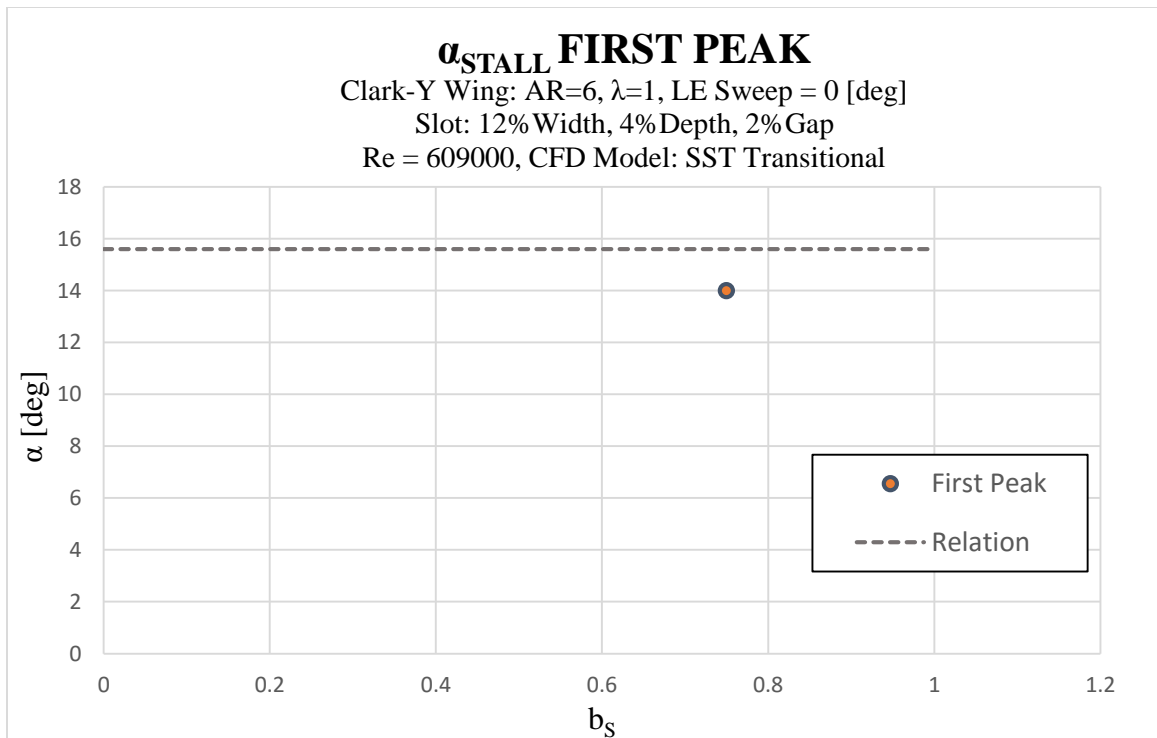


Figure 6. 3. Validation of the angle of stall for the first peak relation.

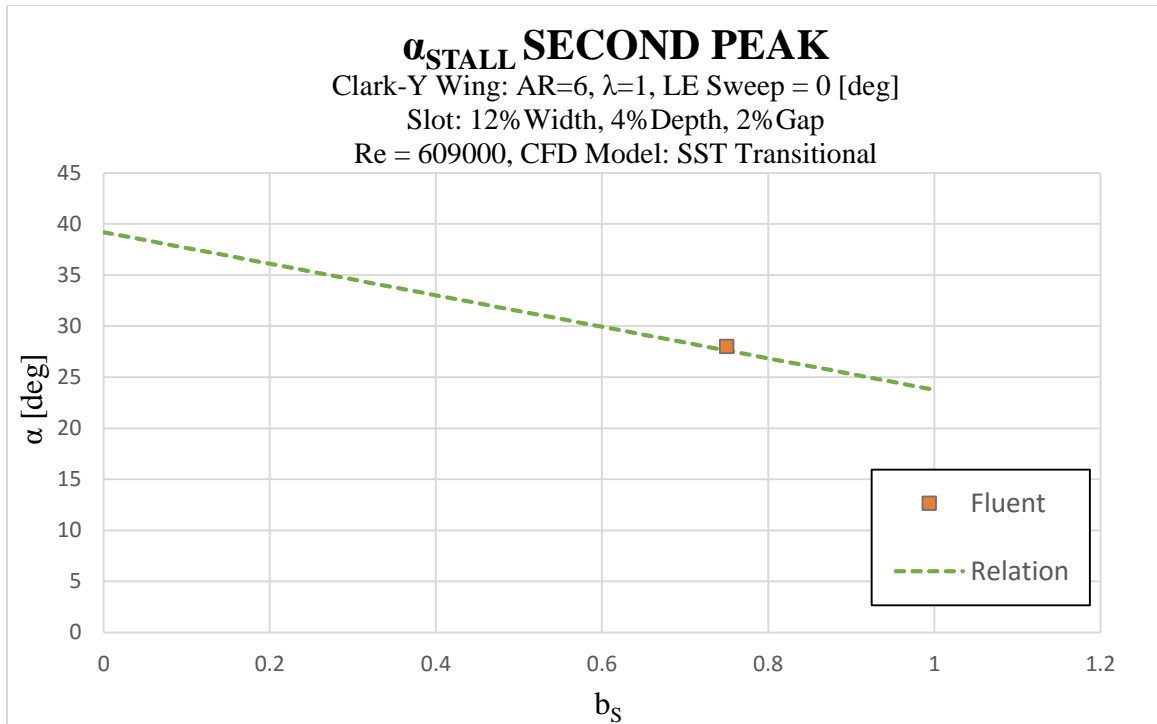


Figure 6. 4. Validation of the angle of stall for the second peak relation.

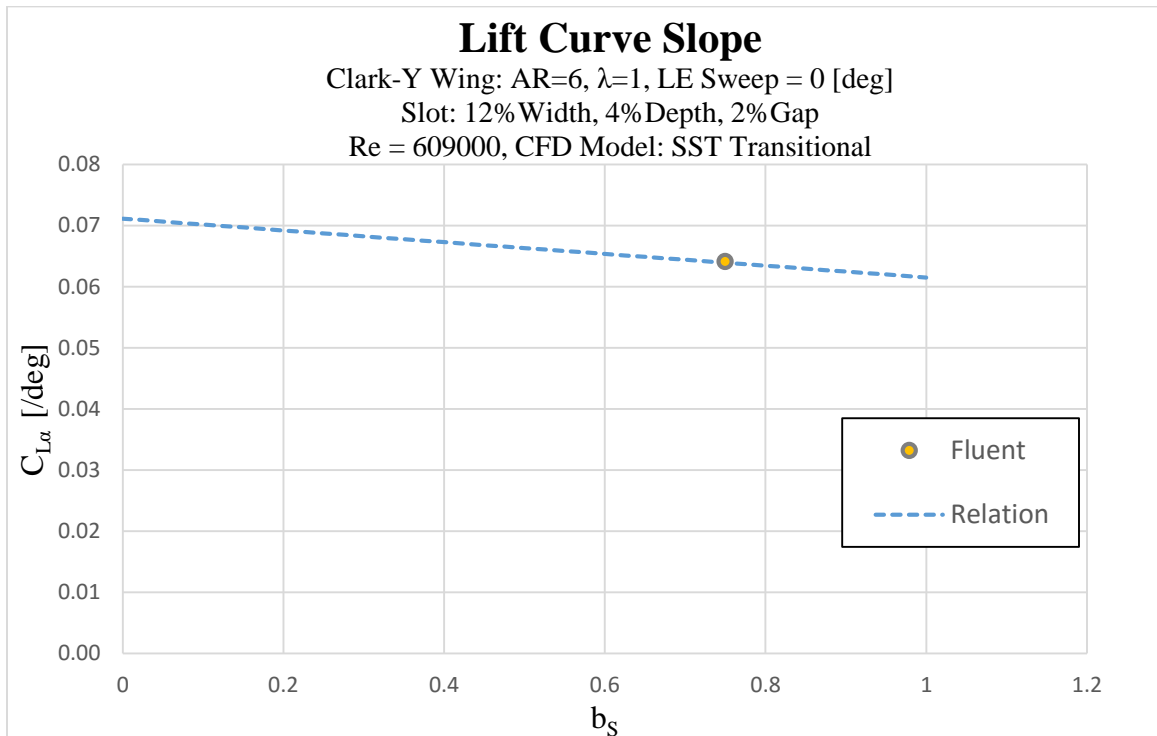


Figure 6. 5. Validation of the lift curve slope relation.

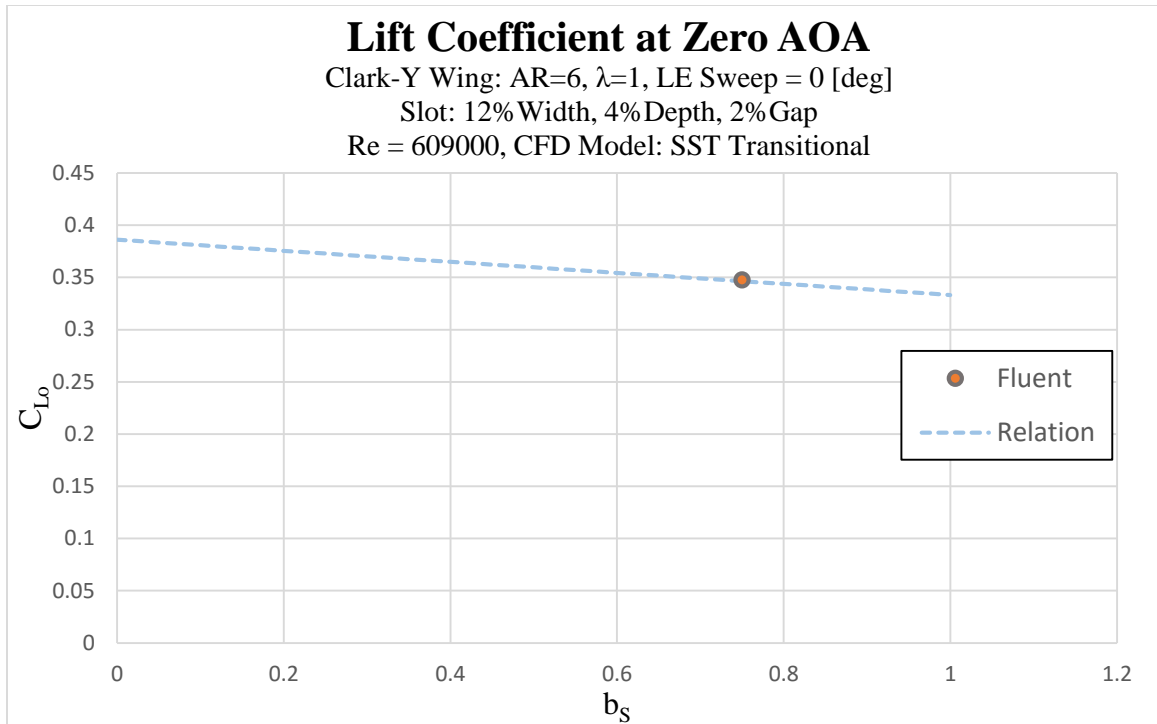


Figure 6. 6. Validation of the lift at zero AoA relation.

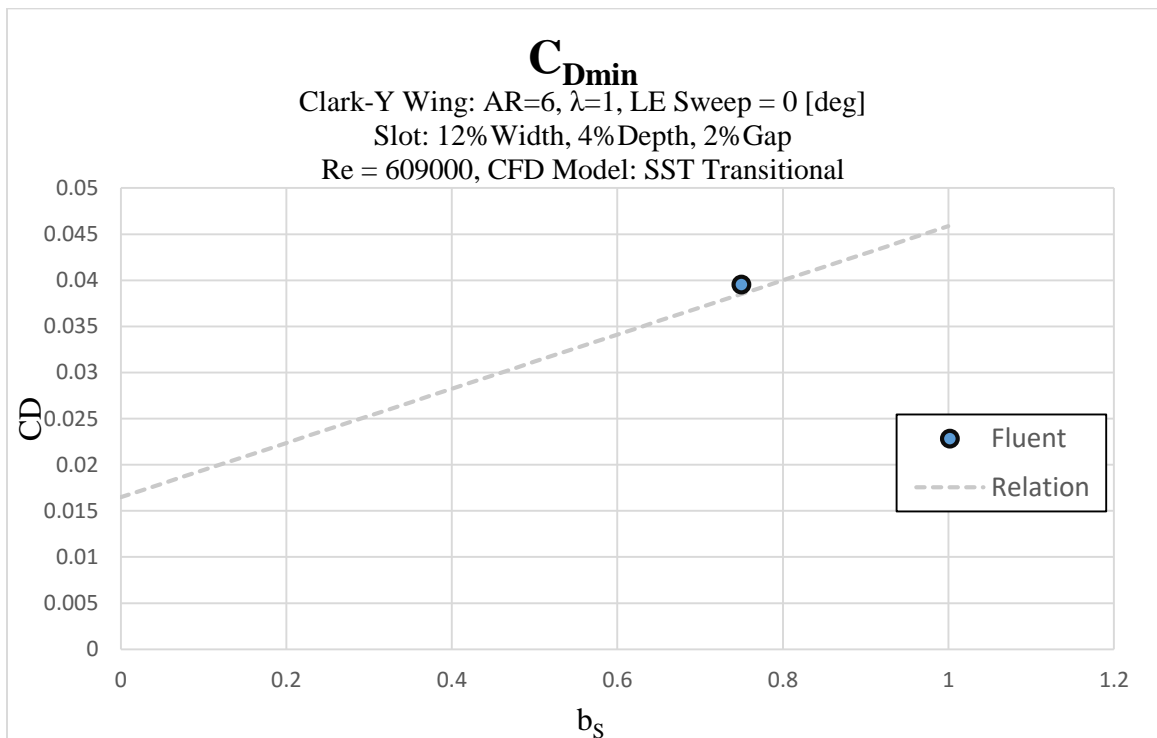


Figure 6. 7. Validation of the minimum drag coefficient relation.

VII. Conclusion

The effect of slot span on wing performance was studied to obtain relationships for aerodynamic coefficients that can be used during the design stages of aircraft with slotted wings. The relations defined in this study are limited to rectangular wings with the Clark-Y airfoil as a cross-section. By analyzing the obtained relations, it can be concluded that the span of the slot affects the aerodynamic characteristics of the wing proportionally. All the obtained relations are linear and in function of the slot span, with the exception of the first peak on the lift coefficient curve. This is because the first peak on the lift coefficient is mostly dependent on the plain section of the wing, as Weick stated [5].

Fixed slotted wings, either full-span or partially slotted-wings, have poor performance at low angles of attack. A plain wing will produce more lift and less drag than a slotted wing at low angles of attack. This is due to the abrupt change in the geometry of the slot-wing configuration, which causes flow separation when it is at low angles of attack. A slotted wing has a better performance at high angles of attack, by maintaining the flow attached over the surface of the wing at higher angles of attack than the angle of stall of the plain wing.

Having a non-fixed slot could be a solution to help the poor performance of slotted wings at small angles of attack. This can be obtained by implementing what is defined as a passive solution by Gudmundsson [23]. This means that a wing will fly with a mechanism that hold the slot closed at low angles of attack with the help of the pressure on that area. When the wing is flying at high angles of attack, the slot will open automatically. Another solution would be to implement actuators for the slots that work in the same fashion, but this would increase the weight, cost, and maintenance.

The results presented in this study show that the Transition SST viscous model predicts with high accuracy laminar-to-turbulent transitional flow effects. The benefit of this CFD model is that it will improve future airplane design by a better understanding of the behavior of bodies, and the flow at its surroundings, at transitional Reynolds number. This report also shows how the design expressions to estimate the three-dimensional characteristics of a wing from its two-dimensional coefficient also work for a slotted airfoil. This allows the designer to get a quick estimation of a full-slotted wing by performing a two-dimensional CFD analysis of a slotted airfoil.

VIII. Opportunity for Future Work

This study defined relations that only work for rectangular wings with the Clark-Y airfoil as a cross-section. This leaves an open window for further research on how the geometry of the airfoil affects these relations, and how these relations would change by modifying the geometry of the wing. In other words, how much the studied coefficients will change in the case of a swept wing, dihedral, wing twist, etc. The study of different slotted wings to obtain relations that take into consideration the geometry of the airfoil and wing could be of great interest.

Because the analyzed wing characteristics in this study correspond to the longitudinal stability of the wing, a deeper study could be performed in order to seek relationships between the slot span and the lateral stability and control of the wing, specifically how the slot span affects rolling stability. Also, the accuracy of the CFD model that was used allows for a study of slotted wings with the addition of other controls, such as ailerons, flaps, spoilers, etc; and how these combinations could be used in order to improve the performance of the wing.

All the results that were compared with experimental data show that the Transition SST model has a high accuracy for low angles of attack, where the solutions have a steady-state convergence, see Figure 3. 7. For large angles of attack, where flow starts to separate from the surface of the wing, the accuracy of the viscous model is compromised by obtaining a solution with a pseudo-steady-state convergence. A study to improve the grid design could be performed in order to avoid unsteadiness in the solution of the model.

References

1. Lyon, C., Broeren, A., Giguere, P., Gopalarathnam, A., and Slig, M.: *Summary of Low-Speed Airfoil Data. Department of Aeronautical and Astronautical Engineering, University of Illinois at Urbana-Champaign, 1997.*
2. Mark, D., and Youngren, H.: *XFOIL*. Computer software. *XFOIL - Subsonic Airfoil Development System*. Vers. 6.99. MIT, 23 Dec. 2013. Web. 20 Jan. 2016.
3. Lachmann, G.: Results of Experiments with Slotted Wings. T.M. No. 282. N.A.C.A., 1924.
4. Wenzinger, C., and Shortal, J.: *The Aerodynamic Characteristics of a Slotted Clark Y Wing as Affected by the Auxiliary Airfoil Position*. T.R. No. 400, N.A.C.A., 1931.
5. Weick, F., Wenzinger, C.: *Effect of Length of Handley Page Tip Slots on the Lateral-Stability Factor, Damping in Roll*. T.N. No. 423, N.A.C.A., 1932.
6. Weick, F., Wenzinger, C.: *Wind-Tunnel Research Comparing Lateral Control Devices, Particular at High Angles of Attack. Handley Page Tip and Full-Span Slots with Ailerons and Spoilers*. T.N. No. 443, N.A.C.A. 1933.
7. Weick, F., Shortal, J.: *The Effect of Multiple Fixed Slots and a Trailing-Edge Flap on the Lift and Drag of a Clark Y Airfoil*. Report No. 427, N.A.C.A., 1932.
8. Weick, F., and Wenzinger, C.: *The Characteristics of a Clark-Y Wing Model Equipped with Several Forms of Low-Drag Fixed Slots*. Report No. 407, N.A.C.A., 1931.

9. Schuldenfrei, Marvin, J.: *Wind-Tunnel Investigation of an NACA 23012 airfoil with a Handley Page Slat and Two Flap Arrangements*. Wartime Report No. L261, N.A.C.A., 1942.
10. Gottlieb, Stanley, M.: *Two-Dimensional Wind-Tunnel Investigation of Two NACA 6-Series Airfoils with Leading-Edge Slats*. Research Memorandum No. L8K22, N.A.C.A., 1949.
11. Weick, F., Noyes, R.: *Wind-Tunnel Research Comparing Lateral Control Devices, Particularly at High Angles of Attack*. Technical Note No. 451, N.A.C.A., 1933.
12. Weick, F., Platt, R.: *Wind-Tunnel Test on Model Wing with Flower Flap and Specially Developed Leading-Edge Slot*. Technical Note No. 459, N.A.C.A., 1933.
13. Weick, F., Wenzinger, C.: *Preliminary Investigation of Rolling Moments Obtained with Spoilers on both Slotted and Plain Wings*. Technical Note No. 415, N.A.C.A., 1932.
14. Soule, H., Wetmore, J.: *The Effect of Slots and Flaps on Lateral Control of a Low-Wing Monoplane as Determined in Flight*. Technical Note No. 478, N.A.C.A., 1933.
15. Weick, F., Flanagan, M.: *Investigation of Lateral Control Near the Stall Flight Investigation with a Light High-Wing Monoplane Tested with Various Amounts of Washout and Various Lengths of Leading-Edge Slot*. Technical Note No. 2948, N.A.C.A., 1953.

16. Fink, M., Shivers, J., and White, L.: *Wind-Tunnel tests of a Full-Scale Model of a Light Twin-Engine Airplane with Fixed Auxiliary Airfoil or Leading-Edge Slot*. T.N. D-7474, NASA, 1974.
17. Burk, S., Bowman, J., and White, W.: *Spin-Tunnel Investigation of the Spinning Characteristics of Typical Single-Engine General Aviation Airplane Designs. II-Low-Wing Model A: Tail Parachute Diameter and Canopy Distance for Emergency Spin Recovery*. Technical Paper 1076, NASA, 1977
18. Staff of Langley Research Center: *Exploratory Study of the Effects of Wing-Leading-Edge Modifications on the Stall/Spin Behavior of a Light General Aviation Airplane*. Technical Paper 1589, NASA, 1979.
19. Newsom, W., Satran, D., and Johnson, J.: *Effects of Wing-Leading-Edge Modifications on a Full-Scale, Low-Wing General Aviation Airplane*. Technical Paper 2011, NASA, 1982.
20. Withman, N., Sparks, R., Ali S., and Ashworth J.: *Experimental Investigation of Slotted Airfoil Performance with Modified Slot Configurations*. AIAA 2006-3481, Embry-Riddle Aeronautical University, 2006.
21. Sun, M., Hamdani, H.: *Separation Control by Alternating Tangential Blowing/Suction at Multiple Slots*. Technical Note – AIAA Journal Vol. 39, No. 4, Beijing University of Aeronautics and Astronautics, 2001.

22. Lynn Harmon, Robyn: *Aerodynamic Modeling of a Flapping Membrane Wing using Motion Tracking Experiments*. Thesis of the Graduate School of the University of Maryland, 2008.
23. Gudmundsson, Snorri: *General Aviation Aircraft Design – Applied Methods and Procedures*. Embry-Riddle Aeronautical University. Daytona Beach, Florida. 2013
24. Anderson Jr. J.D: *Fundamentals of Aerodynamics* (3rd Edition). Boston, MA: McGraw Hill, 2001.
25. Houghton, E.L and Carpenter, P.W: *Aerodynamics for Engineering Students* (5th Edition). Butterworth Heinemann, 2003
26. Clancy, L.J: *Aerodynamics*. Great Britain. Arnold-Heinemann Publishers, 1980.
27. Lowry, John G., and Edwards C. Polhamus: *A Method for Predicting Lift Increments due to Flap Deflection at Low Angles of Attack in Incompressible Flow*. T.R. No. 3911, N.A.C.A., 1957
28. Bono, Gustavo and Awruch, Armando: *Numerical Study between Structured and Unstructured Meshes for Euler and Navier-Stokes Equations*. Argentinian Association of Computational Mechanics, 2007
29. Heintz, Chris: *Airfoils – Official Guide to Experimental Aircraft*. Retrieved from exp-aircraft.com/library/heintz/airfoils.html [cited October 20th, 2016].
30. Aviation Safety – Boeing Commercial Airplanes: *Statistical Summary of Commercial Jet Airplane Accidents – World Wide Operations (1959-2015)*.

Retrieved from www.boeing.com/news/techissues/pdf/statsum.pdf [cited October 24th, 2016].

31. Smith A.M.O.: *High-Lift Aerodynamics. Journal of Aircraft*; Vol. 12, No. 6, 1975, pp 516-520.
32. Liebeck R. H., and Smyth D. N: *Study of Slat-Airfoil Combinations Using Computer Computer Graphics*; *Journal of Aircraft*; Vol. 20, No. 4, 1973, pp 254-256.
33. UIUI Applied Aerodynamics Group – Department of Aerospace Engineering: *Clark-Y Airfoil*. Retrieved from: <http://m-selig.ae.illinois.edu/ads/coord/clarky.dat> [cited August 2015].
34. Simons, M.: *Model Aeroplane Aerodynamics*; Model & Allied Publications; Aerofoil Sections, Ch. 7 – 9, 1978.
35. LEAP CFD Team, *Wall Functions and Y+ requirements*, URL: <http://www.computationalfluidynamics.com.au/tips-tricks-turbulence-wall-functions-and-y-requirements/> [cited May 2015].
36. LEAP CFD Team, *Overview of Scale-Resolving Simulations (SRS)*, URL: http://www.computationalfluidynamics.com.au/cfd-turbulence-part5-scale-resolving-simulations_srs/ [cited May 2015].
37. LEAP CFD Team, *Estimating the First Cell Height for Correct Y+*, URL: <http://www.computationalfluidynamics.com.au/tips-tricks-cfd-estimate-first-cell-height/> [cited May 2015].

38. LEAP CFD Team, *Reviewing how well you have Resolved the Boundary Layer*, URL: <http://www.computationalfluidynamics.com.au/tips-tricks-turbulence-part-4-reviewing-how-well-you-have-resolved-the-boundary-layer/> [cited May 2015].
39. LEAP CFD Team, *Selection of Wall Functions and Y^+ to best capture the Turbulent Boundary Layer*, URL: <http://www.computationalfluidynamics.com.au/turbulence-part-3-selection-of-wall-functions-and-y-to-best-capture-the-turbulent-boundary-layer/> [cited May 2015].
40. LEAP CFD Team, *How does the Reynolds Number affect my CFD model*, URL: <http://www.computationalfluidynamics.com.au/reynolds-number-cfd/> [cited May 2015].
41. LEAP CFD Team, *Introduction to Turbulence Modelling*, URL: <http://www.computationalfluidynamics.com.au/turbulence-modelling/> [cited May 2015].
42. LEAP CFD Team, *Convergence and Mesh Independence Study*, URL: <http://www.computationalfluidynamics.com.au/convergence-and-mesh-independent-study/> [cited May 2015].
43. Petrilli, J., Paul, R., Gopalarathnam, A., and Frink, N.: *A CFD Database for Airfoils and Wings at Post-Stall Angles of Attack*, 31st AIAA Applied Aerodynamics Conference, Fluid Dynamics and Co-located Conferences, (AIAA 2013-2916).

44. Batchelor, G.: *An Introduction to Fluid Dynamics*, Cambridge University Press, 1967.
45. FLUENT – User Guide: *Spalart – Allmaras Model Theory*, Fluent Inc, 2006.
46. Wilcox, David: *Turbulence Modeling for CFD*, Second Edition, Anaheim, 1998.